T2R2 東京科学大学 リサーチリポジトリ
Science Tokyo Research Repository

論文 / 著書情報
Article / Book Information

題目(和文)	Weck ’ s試液を用いたカラーメタログラフィーによるA356アルミニウム合金のミクロ組織解析
Title(English)	Microstructure analysis of A356 aluminum alloy by color metallography using Weck ’ s reagent
著者(和文)	雷 斯敏
Author(English)	Simin Lei
出典(和文)	学位:博士（工学）, 学位授与機関:東京工業大学, 報告番号:甲第12087号, 授与年月日:2021年9月24日, 学位の種別:課程博士, 審査員:熊井 真次,村右 信二,中村 吉男,史 蹟,小林 郁夫
Citation(English)	Degree:Doctor (Engineering), Conferring organization: Tokyo Institute of Technology, Report number:甲第12087号, Conferred date:2021/9/24, Degree Type:Course doctor, Examiner:,,,,
学位種別(和文)	博士論文
Type(English)	Doctoral Thesis

Powered by T2R2 (Science Tokyo Research Repository)

Tokyo Institute of Technology

Microstructure analysis of A356 aluminum alloy by color metallography using Weck's reagent

A Dissertation for the Degree of

Doctor of Engineering

Field of Materials Science and Engineering

By

Simin Lei

Contents

Chapter 1 General introduction **1**

1.1. Color etching metallography 1

1.2. Weck's reagent 4

1.3. Previous studies concerning the application of Weck's reagent to color metallography of A356 aluminum alloy 6

1.4. Motivation and purpose of the present study 9

References 11

Chapter 2 Coloring behavior in the eutectic solidified region of semi-solid die-cast A356 aluminum alloy etched by Weck's reagent **31**

2.1. Introduction 31

2.2. Experimental 32

2.2.1. Material and introduction of pre-plastic strain 32

2.2.2. Fabrication of semi-solid slurry and die-casting 33

2.2.3. Solution treatment 33

2.2.4. Microstructure observation by optical microscopy 34

2.2.5. Surface characterization by scanning electron microscopy 34

2.2.6. Microstructure analysis of the film by scanning transmission electron microscopy 34

2.2.7. Chemical composition analysis by EPMA 35

2.3. Results 36

2.3.1. Microstructural features of as-cast specimen 36

2.3.2. Microstructural features of solution-treated specimen 36

2.3.3. Surface topography observation by SEI for the etched specimen before and after solution treatment 37

2.3.4. Cross-sectional observation and compositional analysis of the manganese dioxide film by STEM and EDS 38

2.3.5. Chemical analysis of solution treated specimen by EPMA 39

2.4. Discussion 40

2.4.1. Microstructure characteristics revealed by Weck's reagent 40

2.4.2. Peculiar network structure revealed by Weck's reagent 42
2.4.3. Characterization of manganese dioxide film in eutectic solidified region . 44
2.5. Conclusions 45
References 47
Chapter 3 Effect of etching time and temperature on coloration by Weck's reagent 77
3.1. Introduction 77
3.2. Experimental 78
3.2.1. Material and preparation of semi-solid slurry 78
3.2.2. Microstructure observation 79
3.2.3. Characterization of the surface morphology by scanning electron microscopy 79
3.3. Results 80
3.3.1. Influence of the etchant temperature on the coloration of as-cast specimen etched for 8 s 80
3.3.2. Influence of the etchant temperature on the coloration of as-cast specimen etched for 12 s 81
3.3.3. Influence of the etchant temperature on the coloration of as-cast specimen etched for 16 s 82
3.3.4. Influence of the etchant temperature on the coloration of the solution-treated specimen 82
3.3.5. Comparison of the coloration of the as-cast and solution-treated specimen etched with different etching conditions 84
3.4. Discussion 84
3.4.1. Chemical reactions during etching process and its relationship with the etching conditions 84
3.4.2. Origin of different color contrast in the as-cast specimen and the effect of etching condition 85
3.4.3. Origin of different color contrast in the solution-treated specimen and the effect of etching condition 89
3.5. Conclusions 91
References 93

Chapter 4 Applicability of Weck's reagent for accurate evaluation of solid fractions with different cooling rates **127**
4.1. Introduction 127
4.2. Experimental 129
4.2.1. Material and introduction of pre-plastic strain 129
4.2.2. Fabrication of semi-solid slurry with different volume 130
4.2.3. Microstructure observation 131
4.2.4. Chemical composition analysis by EPMA 131
4.3. Results 132
4.3.1. Microstructural features of large and small specimens revealed by Weck's reagent 132
4.3.2. Chemical analysis of large specimen by EPMA 134
4.4. Discussion 134
4.4.1. Micro-segregation and grain growth in large specimen during water quenching 134
4.4.2. Correct evaluation of solid fraction at semi-solid state 136
4.4.3. Effect of cooling rates on the amount of solid growth during quenching 139
4.5. Conclusions 141
References 143
Chapter 5 Summary and general conclusions **157**
Acknowledgements **162**

Chapter 1

General introduction

1.1. Color etching metallography

As an effective microstructure analysis technique, color etching metallography was used for characterizing the microstructural features of alloys. This technique has a very long history. The first color micrographs were published more than a hundred years ago [1]. When observing the black-and-white micrographs, the naked eyes can only distinguish about sixty levels of gray shades from black to white. But when observing the color micrographs, the naked eyes can distinguish a large number of colors. For this reason, the color etchants for color etching metallography can reveal much more features in the microstructure compared to conventional black-and-white etchants. However, the application of color etching metallography was still limited. The first reason is that the cost was very high to print the color micrograph in the past, making reproducing the color micrograph very difficult. The second reason is the insufficient understanding of this technique. Many kinds of color etchants have been used. They are considered to be sensitive to chemical composition or crystallographic orientation. However, most of their characteristics or mechanisms have not been examined yet. This is the

reason why the color micrographs are still rare in recent research even though the digital image technique has made the reproduction of color micrographs much easier. The third reason is that many alternative techniques have emerged. The chemical composition can be analyzed by electron probe micro-analysis (EPMA) and the crystallographic orientation can be quantitatively characterized by electron backscattered diffraction (EBSD). Color etching metallography doesn't show any obvious advantages compared to these advanced techniques.

Nevertheless, the research on the color etching metallography method is still going on. Recently, there have been several studies on the application of the color etching metallography method [2-7]. Some studies tried to explain the coloration mechanisms, and the correlation of the color differences to the materials properties was also investigated [4, 6 and 7]. The color difference was found that reveals the micro-segregations of chemical compositions [4] and the crystallographic orientations [6, 7]. There are three well-known coloring mechanisms summarized by Maltais et al. [8], as shown in Fig. 1-1. Generally, specimen etched by color etchant forms a thin film with several hundred micrometers on the top surface of the specimen which can cause light interference. The difference of the film thickness from location to location exhibits the difference in color when observing by using optical microscope (Fig. 1-1 (a)). An example of color etched austenite showing

different color reference to Zhou [9] is given, as shown in Fig. 1-2. Zhou suggests that the color difference in austenite comes from the Si micro-segregation. Etched by alkaline solution, the micro-segregation causes the film to form with different thickness. In addition, the film's anisotropy would also cause the color difference although the film thickness is homogeneous (Fig. 1-1 (b)). Owing to the correlation of the film and the orientation of the granular substrate, the color difference was considered to reveal the difference in the crystallographic orientation of the grains by Szabo and Kardos [7], as shown in Fig. 1-3. Furthermore, the etch pitting would be also caused by anisotropy. An example of wrought aluminum alloy anodized by Barker's reagent (1.8% HBF_4 in distilled water) revealing the grain structure is given [1], as shown in Fig. 1-4. Anodizing usually forms a film on the specimen's surface. But anodizing by using Barker's reagent will not form the film on the aluminum alloys specimen's surface. As shown in Fig. 1-1 (c), two sets of parallel faces are furrowed on the specimen surface, which exhibits the difference in color under the polarized light [1]. In this case, the color difference comes from the different furrowed face orientation, and it is correlated to the grain orientation. However, these three coloring mechanisms mentioned above couldn't explain all the colorations. A novel color etching method called "line etching" was developed by Maltais et al. to etch magnesium alloys [10]. This etching method

provides a way to observe the color by the birefringence of linearly crackled surface under the polarized light.

The history and recent researches of color etching metallography mentioned above suggest that the understanding of coloring mechanism is an important thing to use the color etchant effectively. Etched by different color etchant, the coloring mechanism is different, and the difference in color is also represents different properties from etchant to etchant.

1.2. Weck's reagent

Weck's reagent was developed by Weck and Leistner in the 1980s [11]. This reagent is a kind of color etchant and can be used to investigate the solute segregation in aluminum alloys. Weck's reagent provides a sharp color contrast in the microstructure of cast and welded aluminum alloys. Weck's reagent consists of 4% $KMnO_4$, 1% NaOH and 95% H_2O. An example is shown in Fig. 1-5 from Ref. [1]. The material is the as-cast aluminum alloy with the chemical composition of Al, 4.4%Cu, 0.3%Mg and 0.3%Mn. Etched by Weck's reagent, the dendritic aluminum phase exhibited different color. The color difference is correlated with the micro-segregation of the solute elements. Based on the researches of the chemical activity of aluminum [12, 13] and the permanganate conversion coating on aluminum alloy [14], Suárez-Peña et al. explained the etching

mechanism of Weck's reagent in detail [15] as follows;

(1) The activity of aluminum is very high. In the aqueous environment, the initial product of the aluminum corrosion is the aluminum hydroxide. Subsequently, the hydrated oxides ($Al_2O_3 \cdot H_2O$) will be produced.

(2) Immersed in Weck's reagent, the oxide layer becomes unstable due to the high pH value of the alkaline solution of potassium permanganate. Subsequently, the oxide layer formed by corrosion is dissolved and the fresh aluminum is exposed.

(3) A colored film is formed via the reaction of the exposed aluminum with the potassium permanganate. The overall formation reaction is given as:

$$Al + MnO_4^- + 2\ H_2O \rightarrow Al(OH)_4^- + MnO_2$$

During the solidification process, the segregation was occurred in dendrite due to the different electrochemical potentials from center to edge, exhibited the difference in color [15].

1.3. Previous studies concerning the application of Weck's reagent to color metallography of A356 aluminum alloy

Weck's reagent developed by Weck and Leistner could be recognized as a sensitive color etchant for aluminum alloys. However, the explanation of the coloring mechanism by the researcher mentioned above was insufficient, and there was no detailed investigation on the relationship between micro-segregation and the color difference after etching. In order to understand the coloring mechanism by Weck's reagent, Gao et al. carried out many experimental studies [16, 17]. The solute distribution was characterized by EPMA analysis and compared to the optical micrograph etched by Weck's reagent, as shown in Fig. 1-6. The detailed relationship between micro-segregation in A356 aluminum alloys and the color difference revealed by Weck's reagent was investigated.

In addition, Gao et al. applied the Weck's reagent to detect the micro-segregation of the semi-solid processed A356 aluminum alloy and applied for the correct evaluation of the solid fraction in the semi-solid slurry. The grain growth during water quenching was distinguished from the original solid phase at semi-solid state as shown in Fig. 1-7. The evaluated solid fraction with the help of Weck's reagent is exhibited in Fig. 1-8. In this figure, the solid fraction obtained from the non-etched

microstructure analysis and the solid fraction estimated from the Al-Si binary phase diagram are also given. The obtained solid fraction with a help of Weck's reagent etching showed a good agreement with that of phase diagram. This is due to the part of grain growth during the quenching which is done to freeze the semi-solid state can be visualized differently from the original spherical solid grains. Therefore the original sold fraction in the semi-solid state at a solid-liquid co-existing temperature can be obtained correctly.

The condition of etched surface was investigated by using various advanced characterization methods. A careful microstructure analysis by using scanning electron microscopy (SEM) revealed that the relative height and roughness of the etched surface change from location to location as shown in Fig. 1-9. The etched surface condition was also investigated quantitatively by using a laser microscopy and atomic force microscopy (AFM). Fig. 1-10 shows the color, laser intensity and surface profile obtained by laser microscopy. The etched surface shows a different reflection of laser from location to location. The surface profile also reveals that the surface condition is not constant, and some places are rough and some places are flat. Fig. 1-11 shows an optical micrograph of the spheroidal grain which was supplied for the characterization by AFM. The three regions with different colors were selected for the AFM observation. The surface topographies of these regions in both 2D and 3D

are displayed in Fig. 1-12. The AFM measurements found that three regions are flat in an atomic scale with the average roughness of 3 or 4 nm. Considering form these analytical results, it was confirmed that the top surface of the film is flat in an atomic. In contrast, the bottom surface of the film, that is the top surface of the metallic base is not flat and shows a variety of local height and roughness. The cross-section of the film was also examined by scanning transmission electron microscopy (STEM). It was revealed that the thickness of the film changed from location to location as shown in Fig. 1-13. Compositional analysis by dispersive X-ray spectroscopy (EDS) (Fig. 1-14) and secondary ion mass spectrometry (SIMS) (Fig. 1-15 and Fig. 1-16) found that the film consists of manganese dioxide.

Based on the various kinds of microstructure analysis results, the coloring mechanism of Weck's reagent was proposed by Gao et al. [17] as shown below.

The top surface of the film is flat, while the bottom surface of the film and the substrate surface are rough. The schematic illustration of the cross-section of the specimen after etching with Weck's reagent is shown in Fig. 1-17. The incident light can be reflected by the top surface of the film and the rough interface between the bottom surface of the film and the substrate surface, which leads to the light interference. The diffraction of the light may also happen. The light with the certain wavelength

absorbed by the manganese dioxide film also influences the coloration. The difference in color revealed by Weck's reagent may result from the combination of interference, diffraction and absorption of the light.

1.4. Motivation and purpose of the present study

The previous researches provided a lot of important information about of color etching of A356 aluminum alloy with Weck's reagent. However, it should be mentioned that several critical subjects are left untouched. They are;

(1) The relationship between the color contrast and micro-solute-segregation was intensively studied for inside of the large primary α-Al spheroidal grains in semi-solid slurry of A356 alloy. However, the origin of color contrast and the effect of microstructure have not been examined for the eutectic solidified region surrounding the spheroidal grains.

(2) It is known that the etching condition depends not only etching time but also etching temperature. However, in the previous studies [17], the suitable etching condition of Weck's reagent for aluminum alloys was investigated only from the point of etching time. The effect of etching temperature has not been investigated.

(3) The color etching with Weck's reagent has been applied for small size specimens to evaluate the solid fraction solid fraction. In this case, the residual liquid in the semi-solid slurry is considered to be cooled rapidly at a relatively even cooling rate during the quenching. Therefore, grain growth from the surface of each original spheroidal grain should be even in the volume of specimen. In contrast, in the case of relatively large specimens in the semi-solid state, the local cooling rate is considered to be different from location to location. The influence of the cooling rate on the growth behavior of the solid layer around the pre-existing spheroidal primary α-Al during water quenching is of interest, however, it has not been examined yet.

Taking these situations into account, it is worth to challenge these unsolved subjects in this research field. The purpose of this study is to investigate the unsolved subjects mentioned above and establish the color metallography by using Weck's reagent as a useful tool for microstructure analysis of semi-solid processed A356 aluminum alloy.

References

[1] G.F Vander Voort, Metallography and Microstructures, ASM Handbook. Ohio: ASM International, 2004.

[2] S.M.A Boutorabi and J. Campbell, An etching technique for primary austenite dendrites in ductile cast iron, Mater. Charact. 31(1993) 127-132.

[3] A. Ray and S. Dhua, Microstructural manifestations in color: some applications for steels, Mater. Charact. 37(1996) 1-8.

[4] C.F Yeung, H. Zhao and W.B. Lee, The morphology of solidification of thin-section ductile iron castings, Mater. Charact. 40(1998) 201-208.

[5] J. Zhou, Colour metallography of cast iron, Chapter 1, China Foundry 9(2009) 152-157.

[6] P.J Szabó and A. Bonyár, Effect of grain orientation on chemical etching, Micron 43(2012) 349-351.

[7] P.J. Szabó and I. Kardos, Correlation between grain orientation and the shade of color etching, Mater. Charact. 61(2010) 814-817.

[8] A. Maltais, D. Dubé, F. Roy, M. Fiset, Optical anisotropy of a color-etched AZ91 magnesium alloy, Mater. Charact. 54 (2005) 315-326.

[9] J. Zhou, Colour metallography of cast iron, China Foundry 6 (2009):

152-157.

[10] A. Maltais, M. Fiset, G. Laroche, S. Turgeon, D. Dubé, Improvement in metallography of As-Cast AZ91 alloy, Mater. Charact. 52 (2004) 103-119.

[11] E. Weck, E. Leistner, Metallographic instructions for colour etching by immersion, part iii: non-ferrous metals, cemented carbides and ferrous metals, nickel-base and cobalt-base alloys. DVS GmbH, Düsseldorf, 1986.

[12] H.P. Godard, W.P. Jepson, M.R. Bothwell, R.L. Kane, The corrosion of light metals. John Wiley and Sons, New York, 1967.

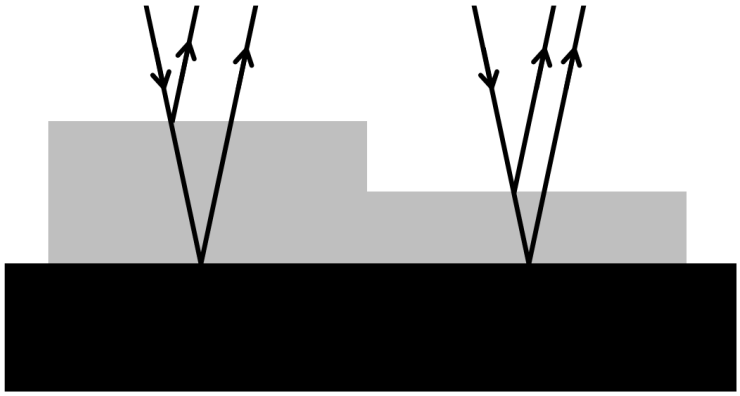
[13] M. Pourbaix, Aluminium atlas of electrochemical equilibrium in aqueous solutions. Pergamon, Oxford, 1966.

[14] S.A. Kulinich, A.S Akhtar, P.C. Wong, K.C. Wong, K.A.R. Mitchell, Growth Of Permanganate Conversion Coating On 2024-Al Alloy. Thin Solid Films 515 (2007) 8386-8392.

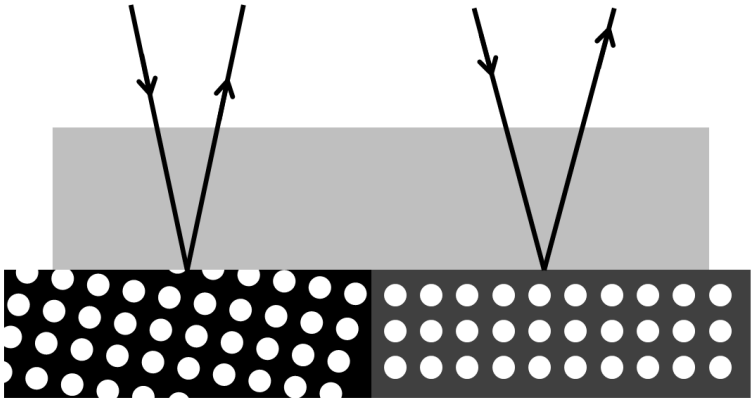
[15] B. Suárez-Peña, J. Asensio-Lozano, G.F. Vander-Voort, Colour metallography in commercial Al-Si alloys. Optimization of the microstructural characterization techniques in light optical microscopy. Rev. Metal 46(2010) 469-476.

[16] L. Gao, Y. Harada, S. Kumai, Microstructural characterization of aluminum alloys using Weck's reagent, part I: Applications. Mater Charact. 107 (2015) 426-433.

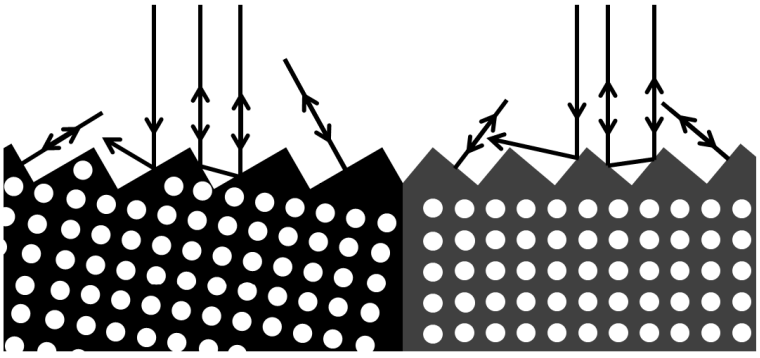
[17] L. Gao, Y. Harada, S. Kumai, Microstructural characterization of aluminum alloys using Weck's reagent, part II: Coloring mechanism. Mater Charact. 107 (2015) 434-452.



(a)



(b)



(c)

Fig. 1-1. Schematics of surfaces producing color after etching summarized by Maltais et al. [8]: (a) Interference film with different thickness. (b) Anisotropic film with the same thickness. (c) Etching pitting after anodizing of Al alloy.

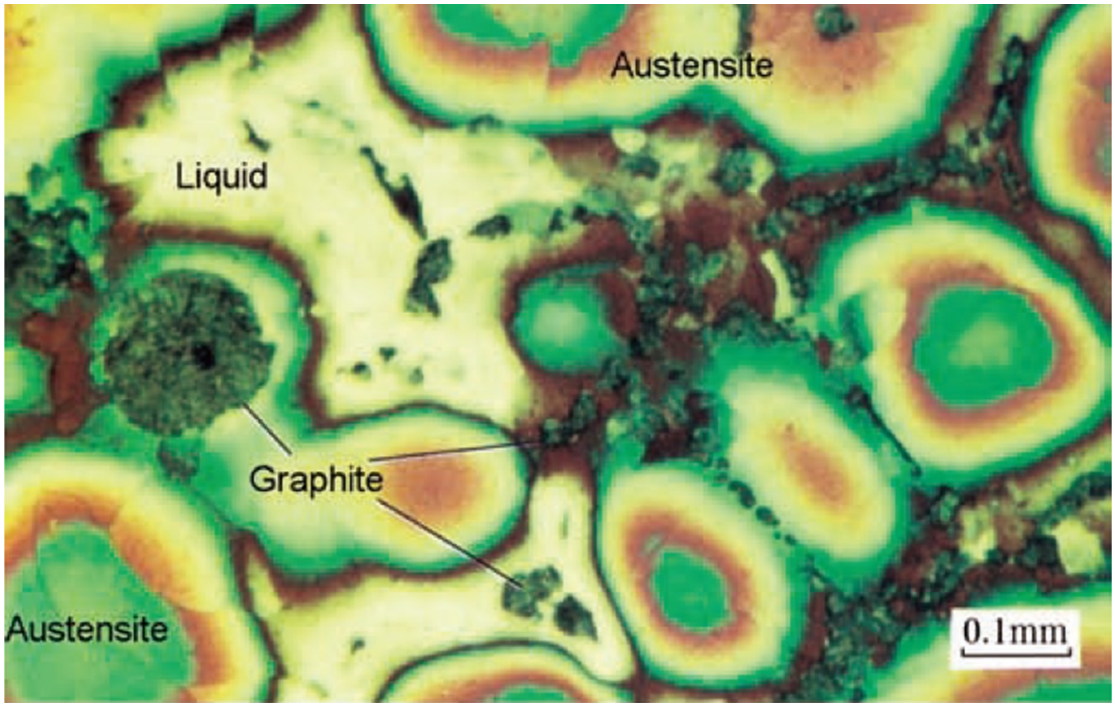
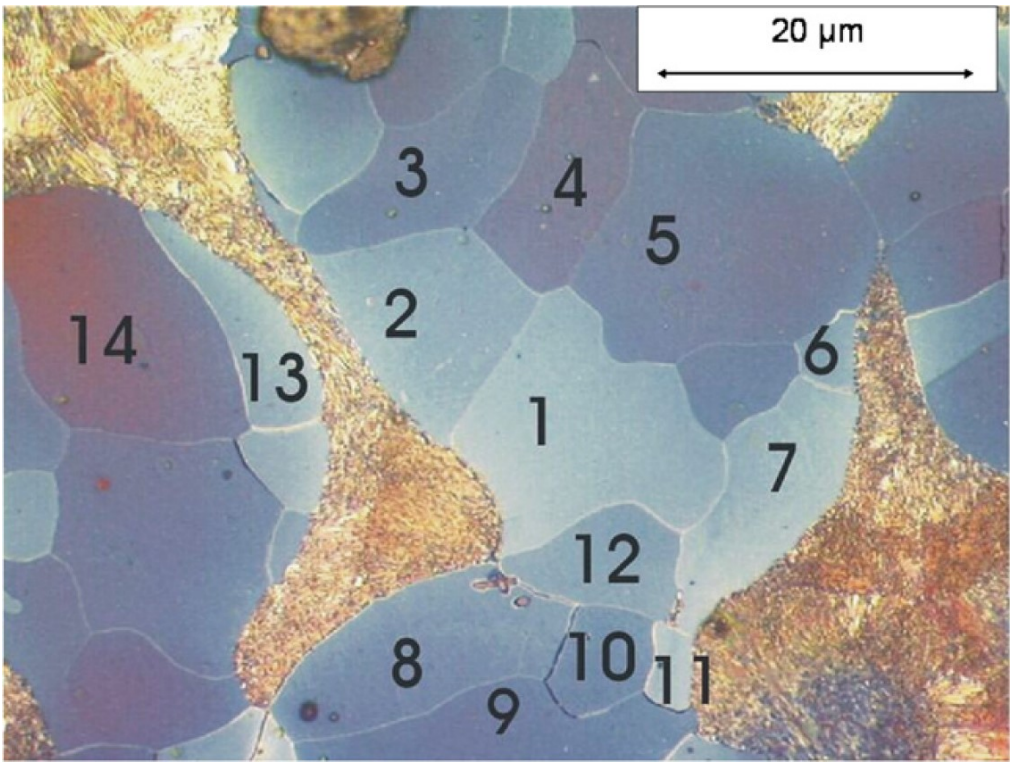
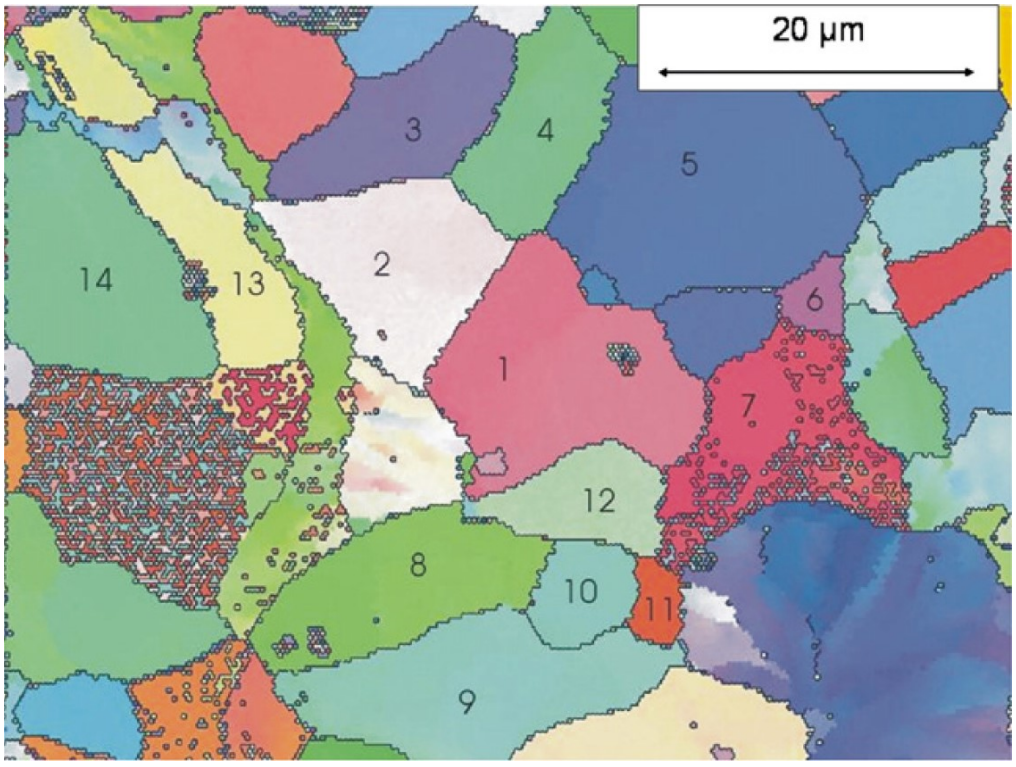


Fig. 1-2. An example of color etched austenite showing different color which is caused by Si micro-segregation [9].



(a)



(b)

Fig. 1-3. An example showing the correlation between the (a) shade of color etching obtained by etching a cast iron specimen and (b) grain orientation by EBSD analysis [7].

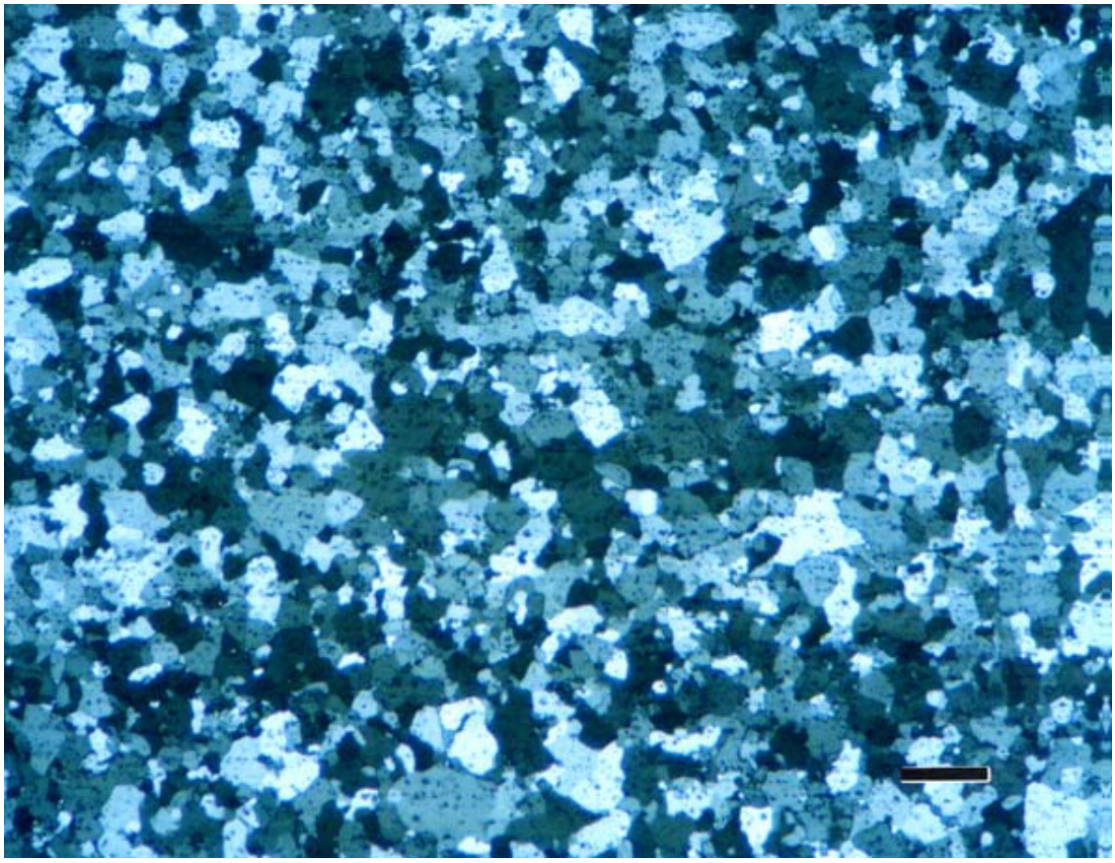


Fig. 1-4. An example showing the grain structure of wrought aluminum alloy after anodizing [1]. The microstructure was observed under polarized light and the magnification bar is 100 μm long

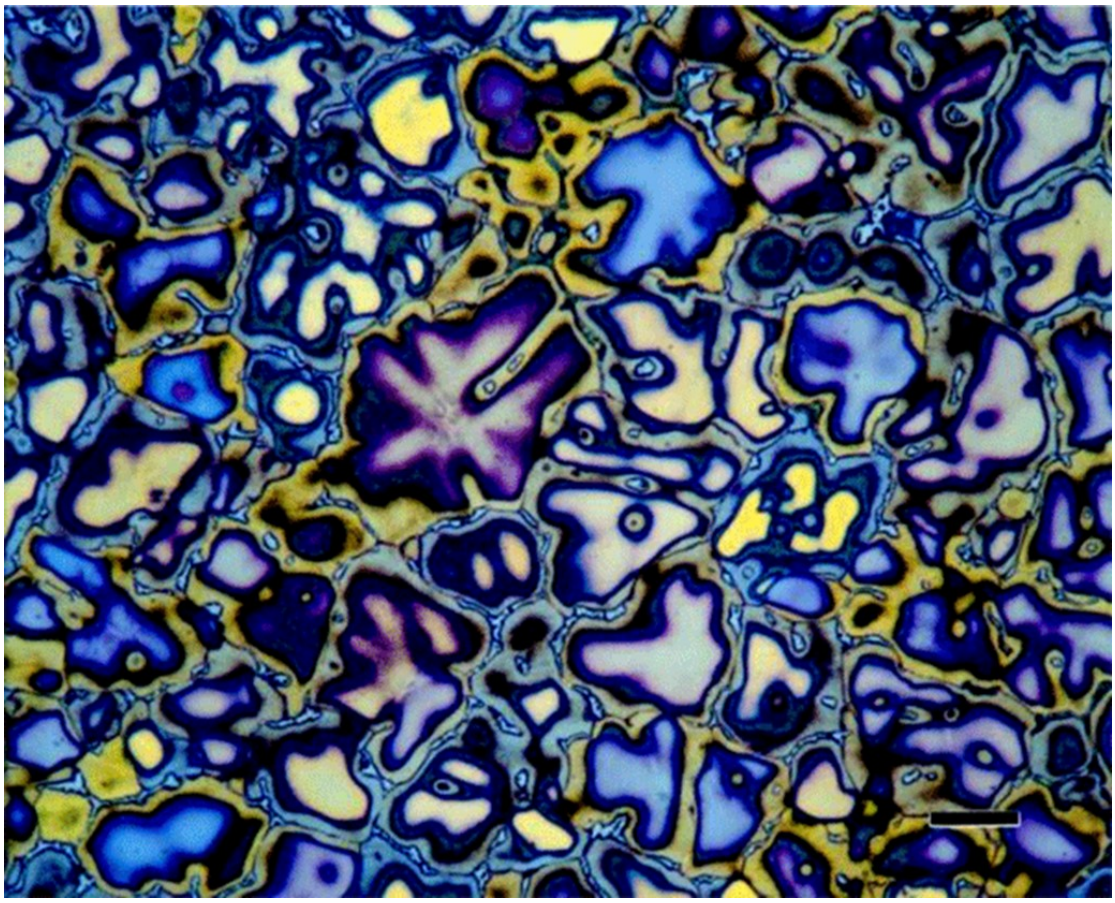
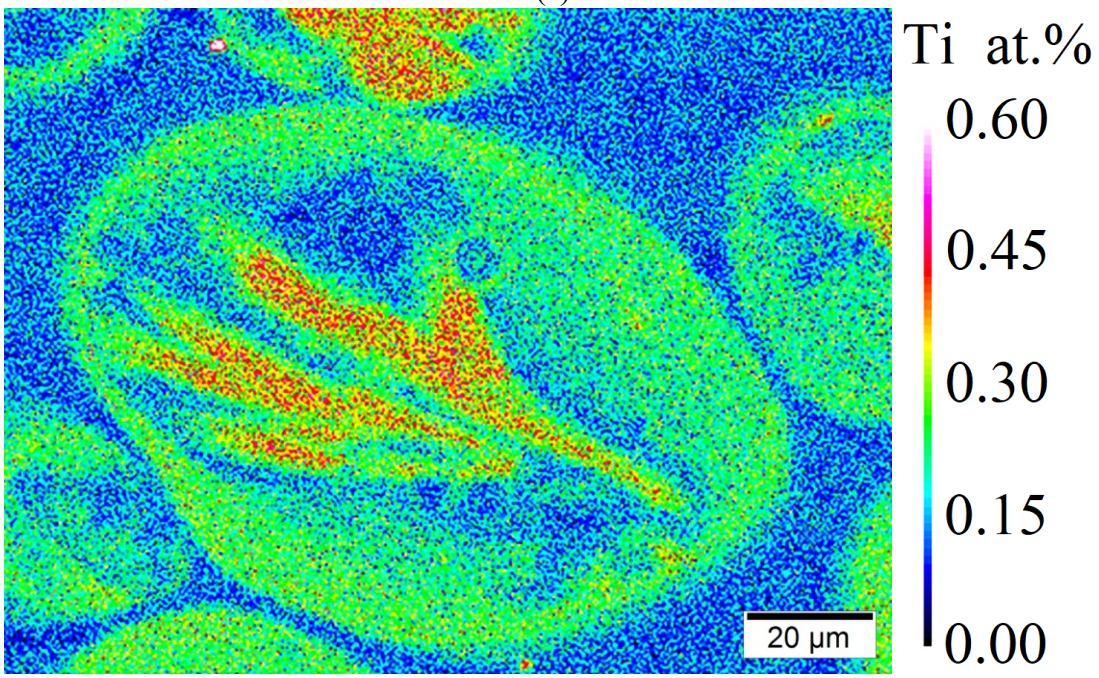


Fig. 1-5. An example of color etching provided in [1]. The micrograph is observed with crossed polarized light and sensitive tint so the color contrast is strengthened. Magnification bar is 50 μm long.

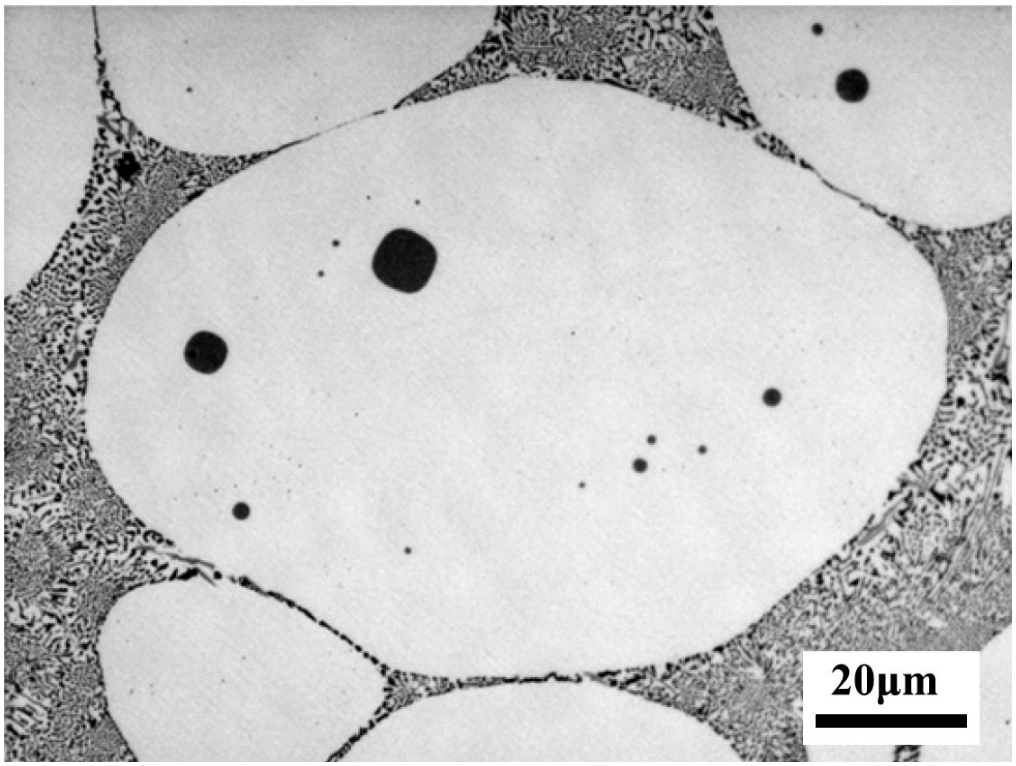


(a)

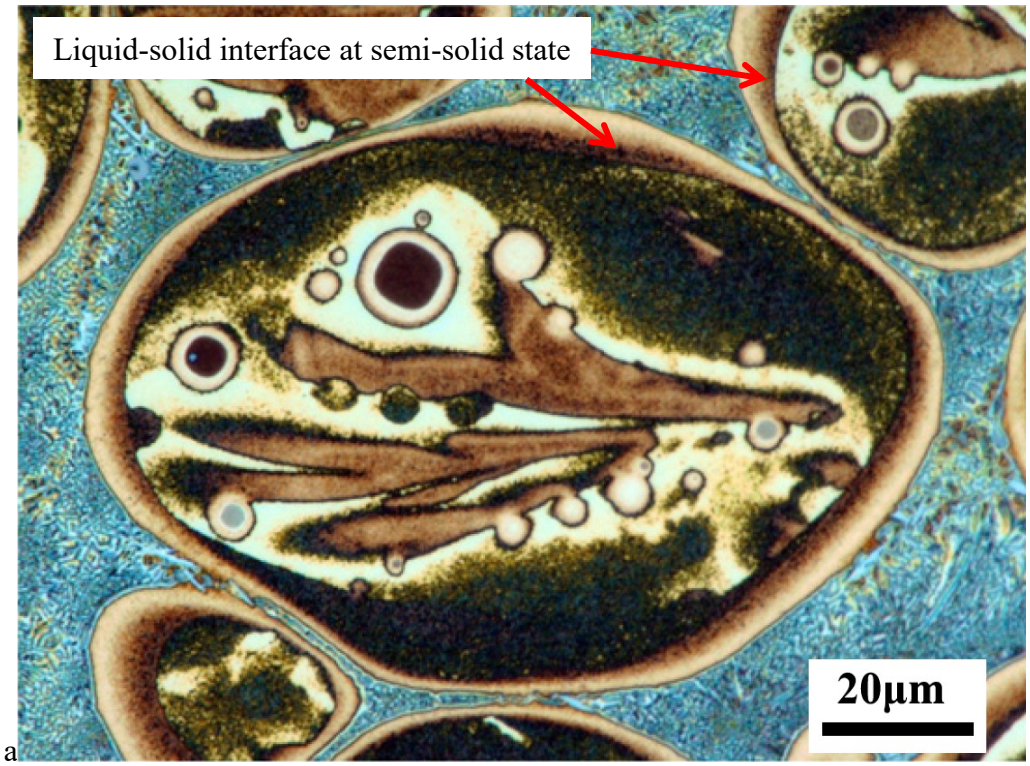


(b)

Fig. 1-6. Optical micrograph of the semi-solid A356 specimen etched by Weck's reagent (a) as well as the Ti micro-segregation detected by EPMA mapping (b) [16].



(a)



a

(b)

Fig. 1-7. Microstructures of specimens before (a) and after (b) etched by Weck's reagent [16]. The original solid-liquid interface is indicated by arrows in the figure.

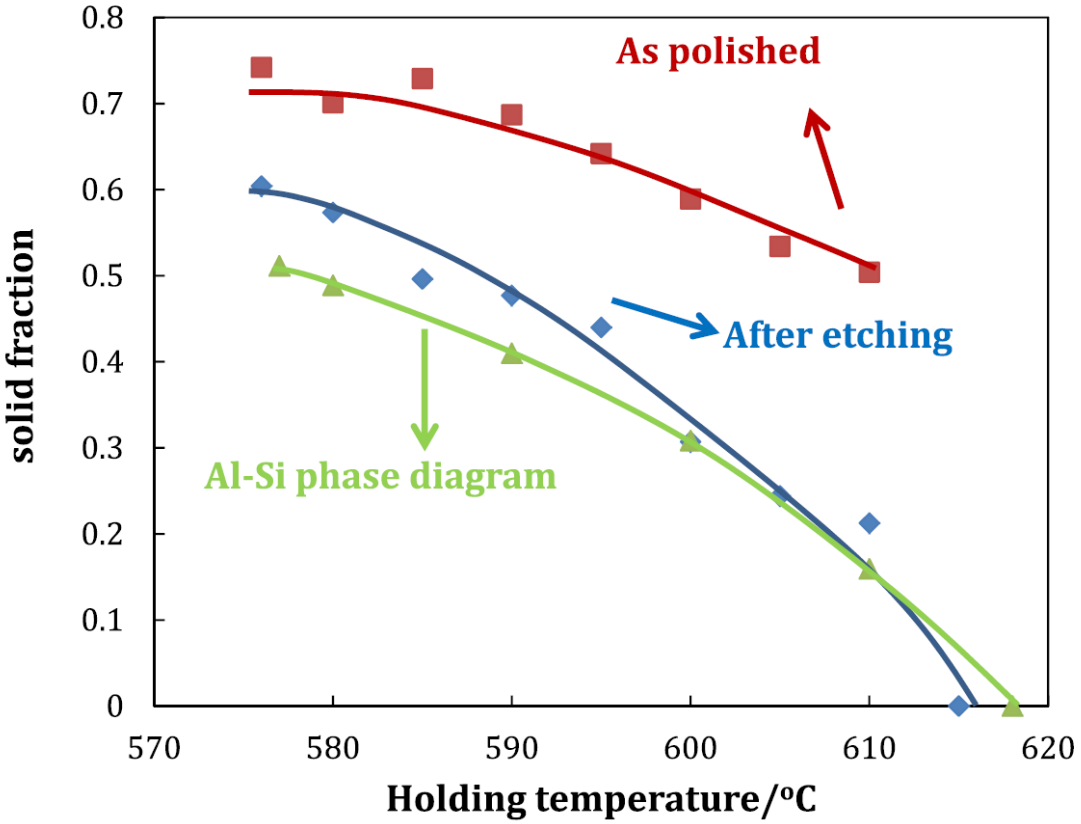


Fig. 1-8. Solid fractions of A356 aluminum alloy measured from as polished and as etched specimens, as well as the calculation using Al-Si binary phase diagram [16].

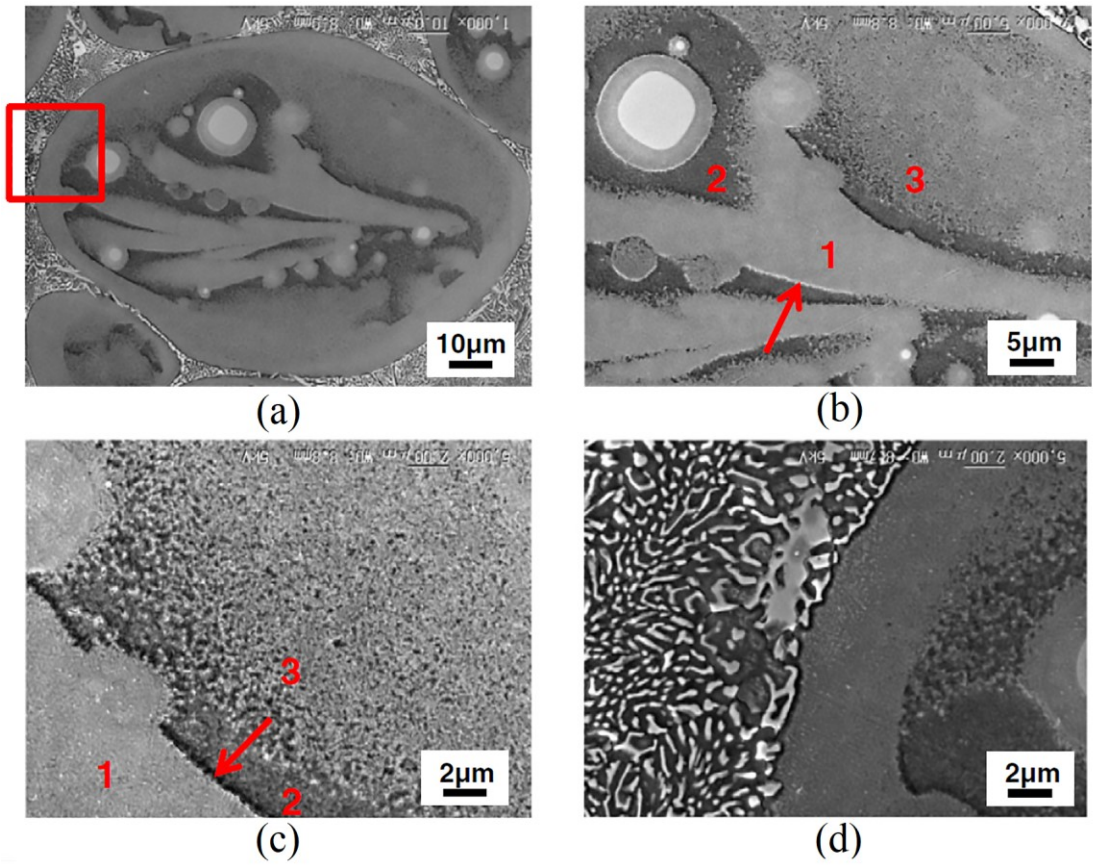
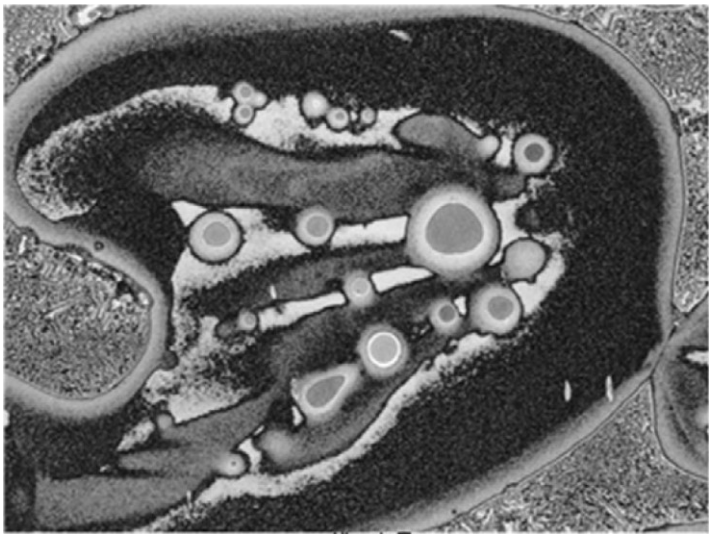


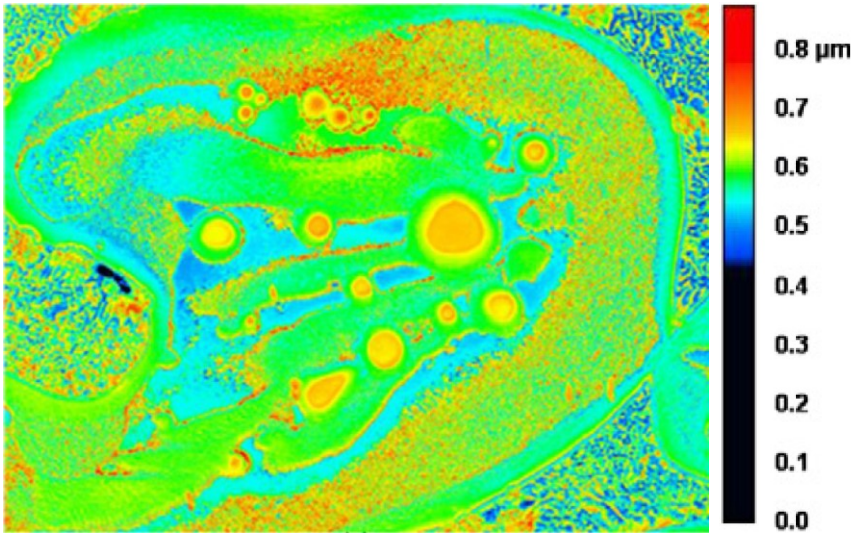
Fig. 1-9. SEM observation of the etched surface whose optical microstructure is shown in Fig. 1-6 (a) [17].



(a)



(b)



(c)

Fig. 1-10. Results obtained by Laser microscopy: (a) color, (b) laser intensity and (c) surface profile [17].

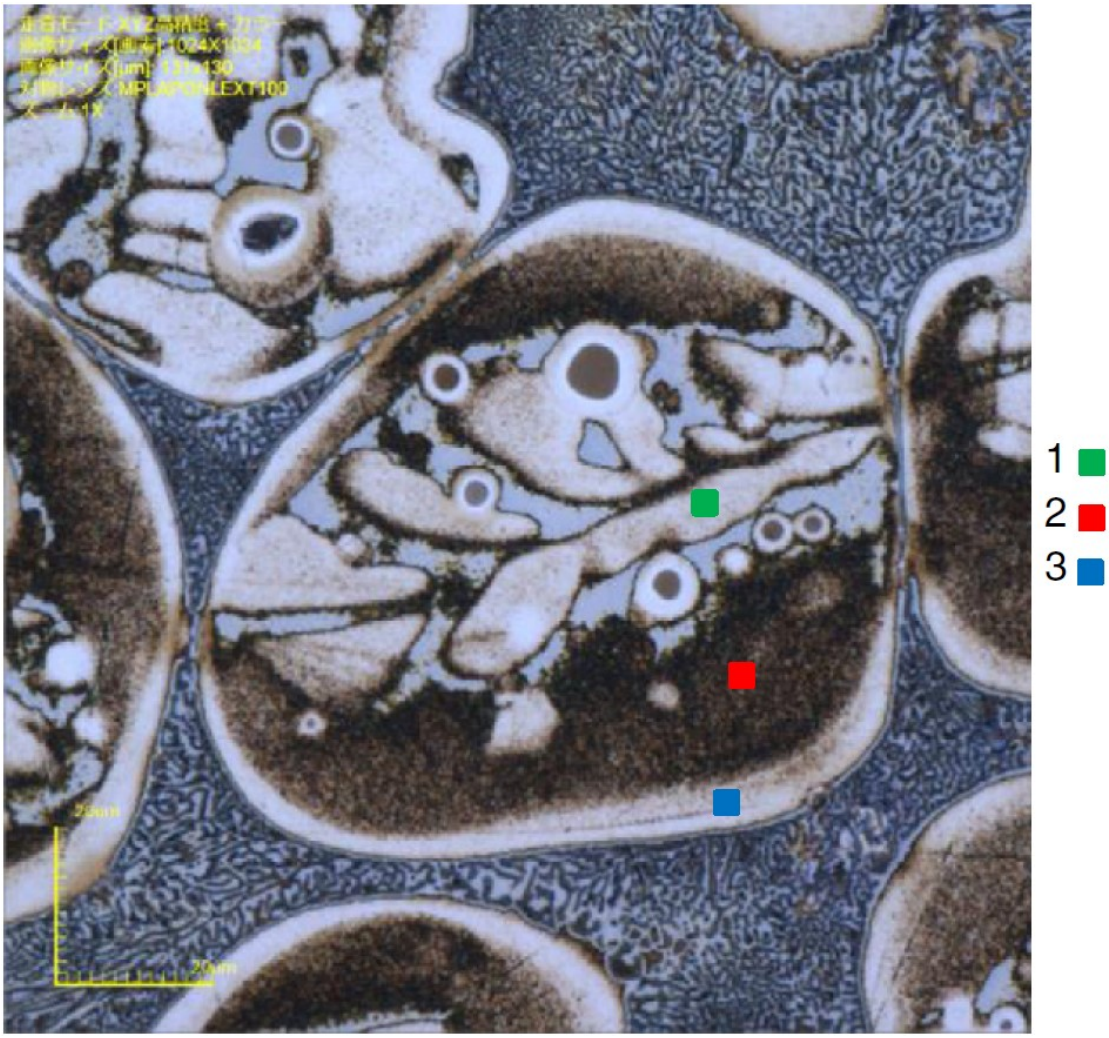
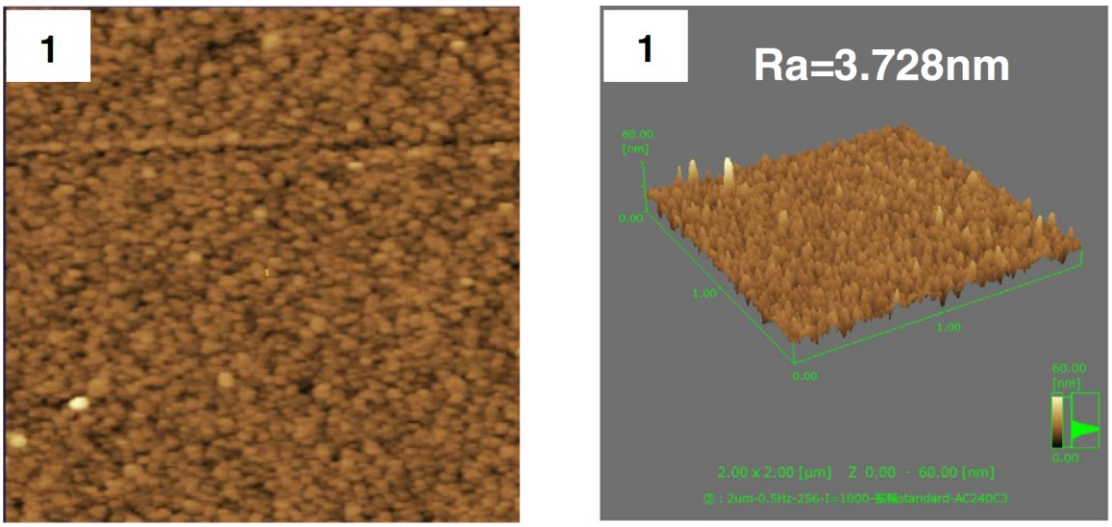
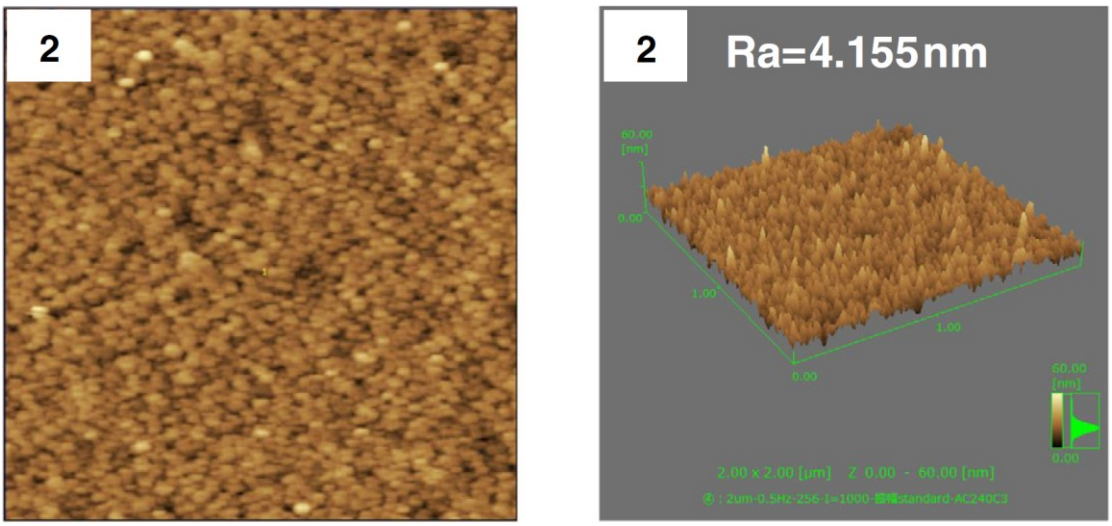


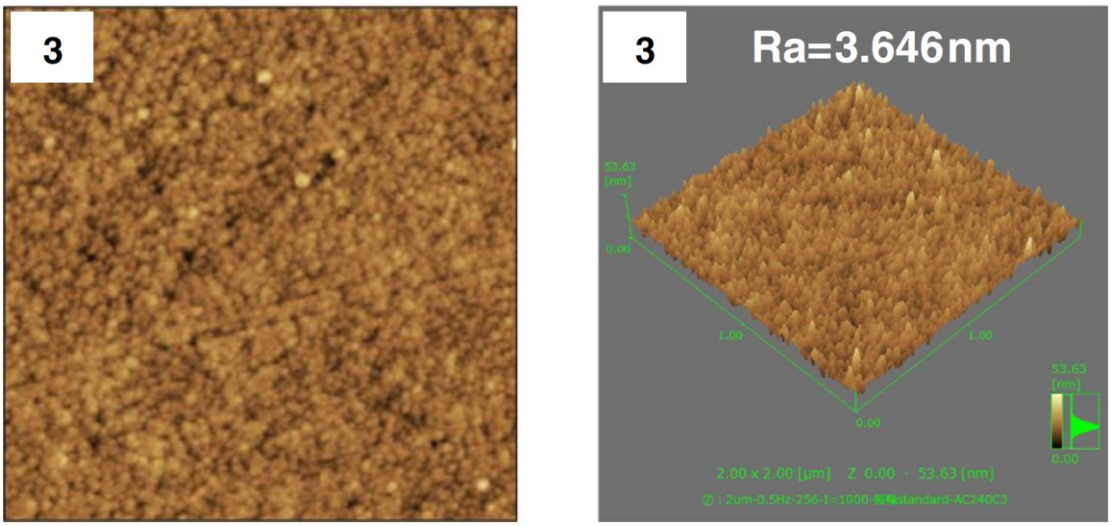
Fig. 1-11. Optical micrograph of the spheroidal grain which was characterized by AFM. The three analysis locations are indicated by three points [17].



(a)

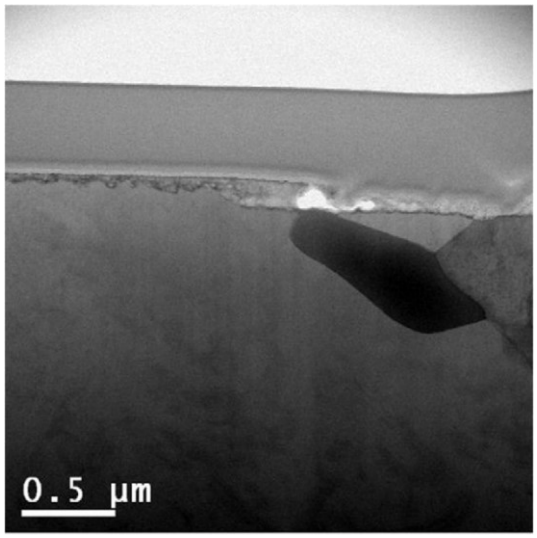


(b)

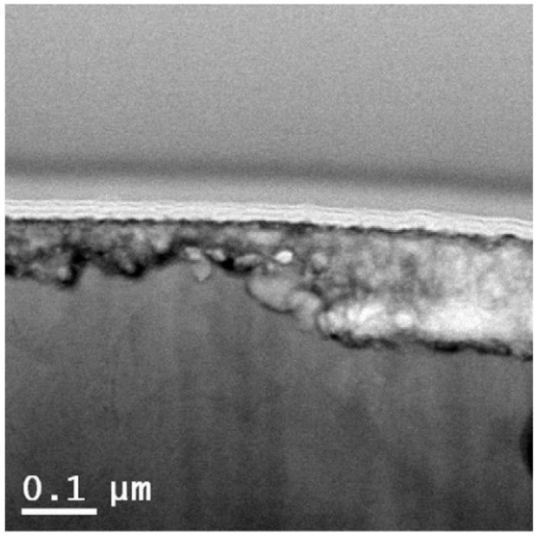


(c)

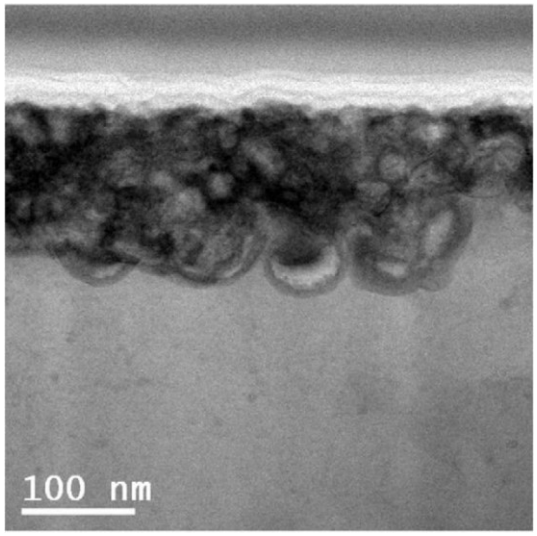
Fig. 1-12. Both 2D and 3D surface profile made by AFM, the number indicates the analyzed location in Fig. 1-11 [17].



(a)



(b)



(c)

Fig. 1-13. Cross section of the film observed by STEM [17].

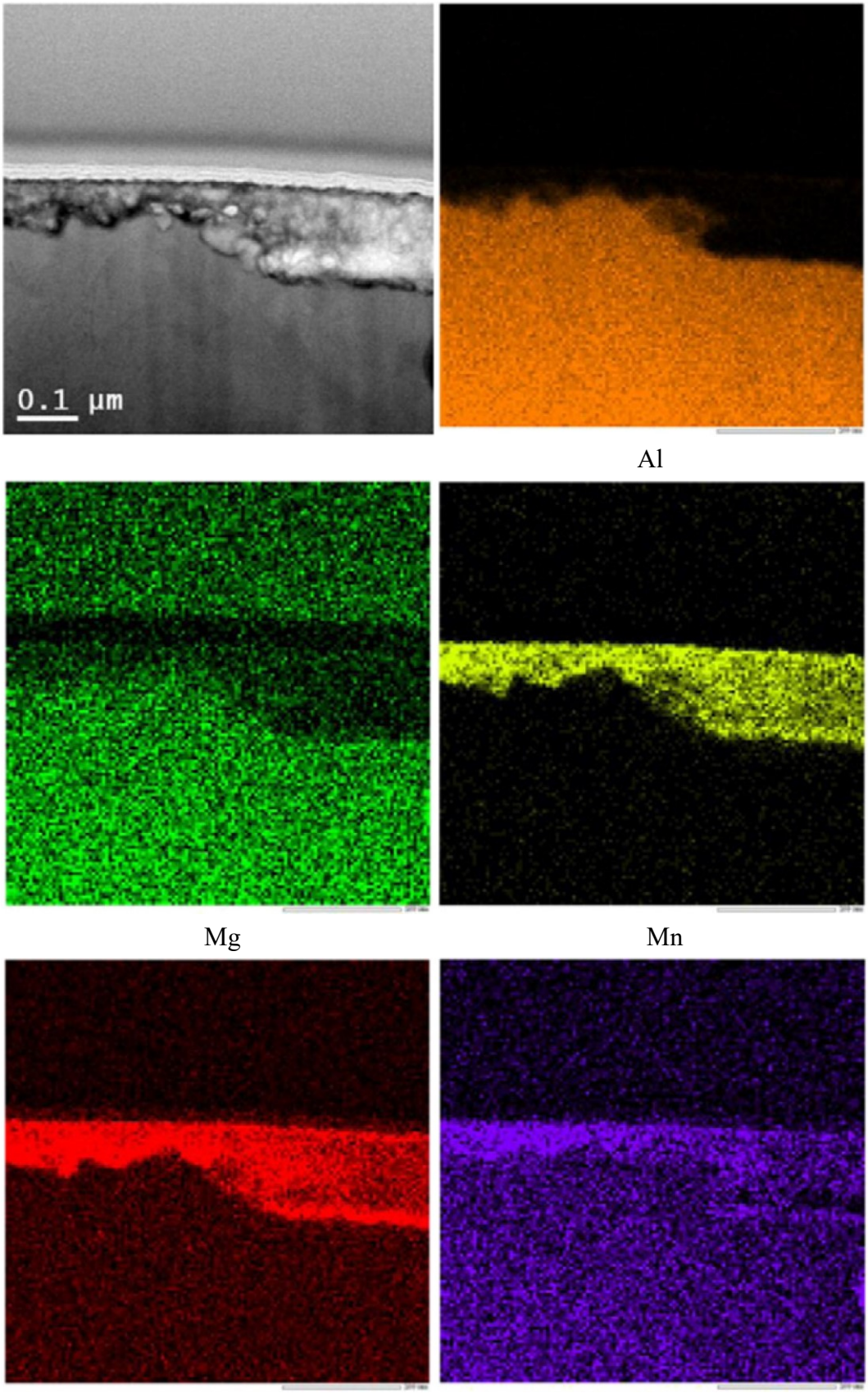


Fig. 1-14. Composition analysis of the film by STEM equipped with EDS [17].

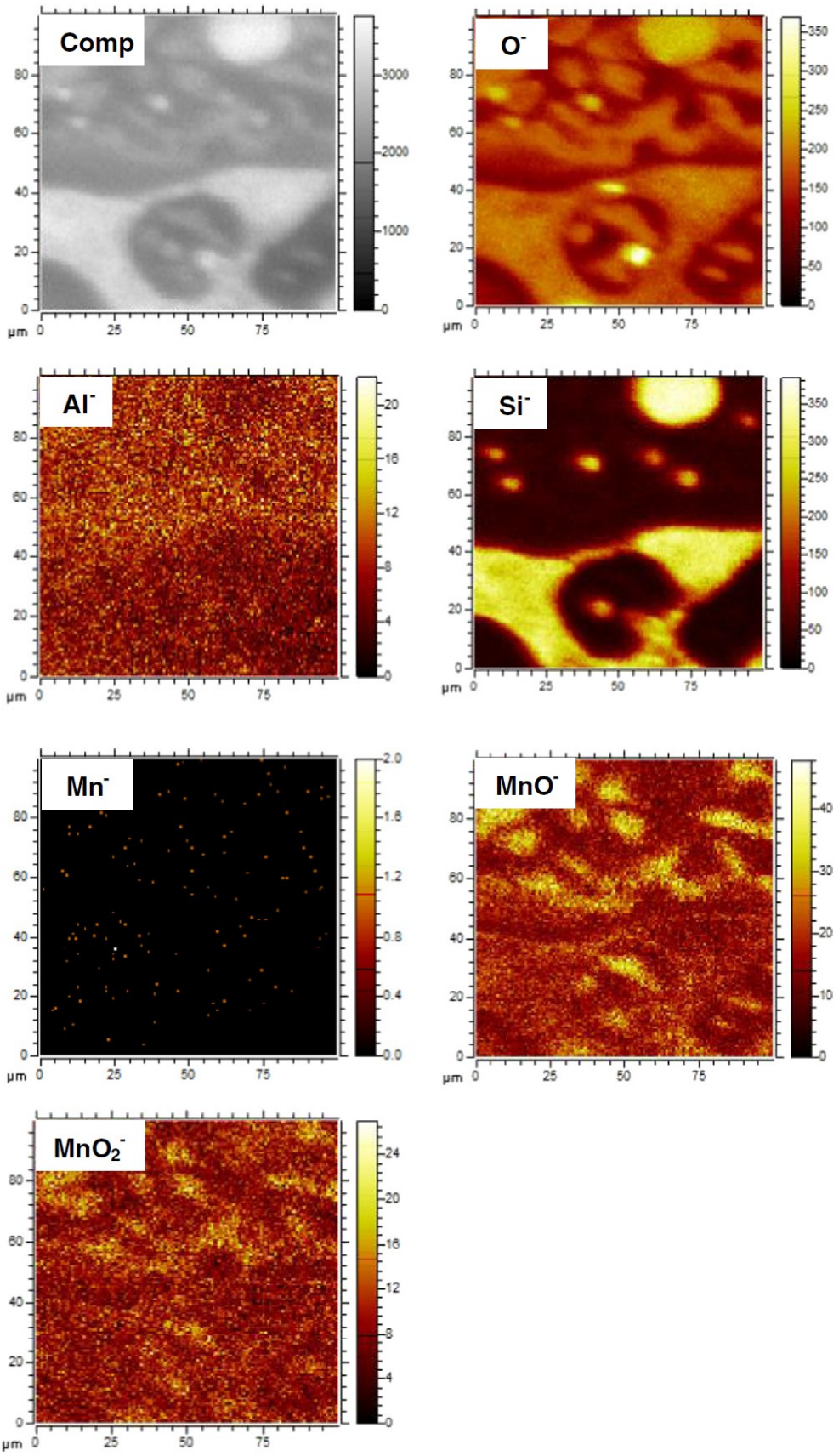


Fig. 1-15. Mapping of negative irons from the film analyzed by TOF-SIMS [17].

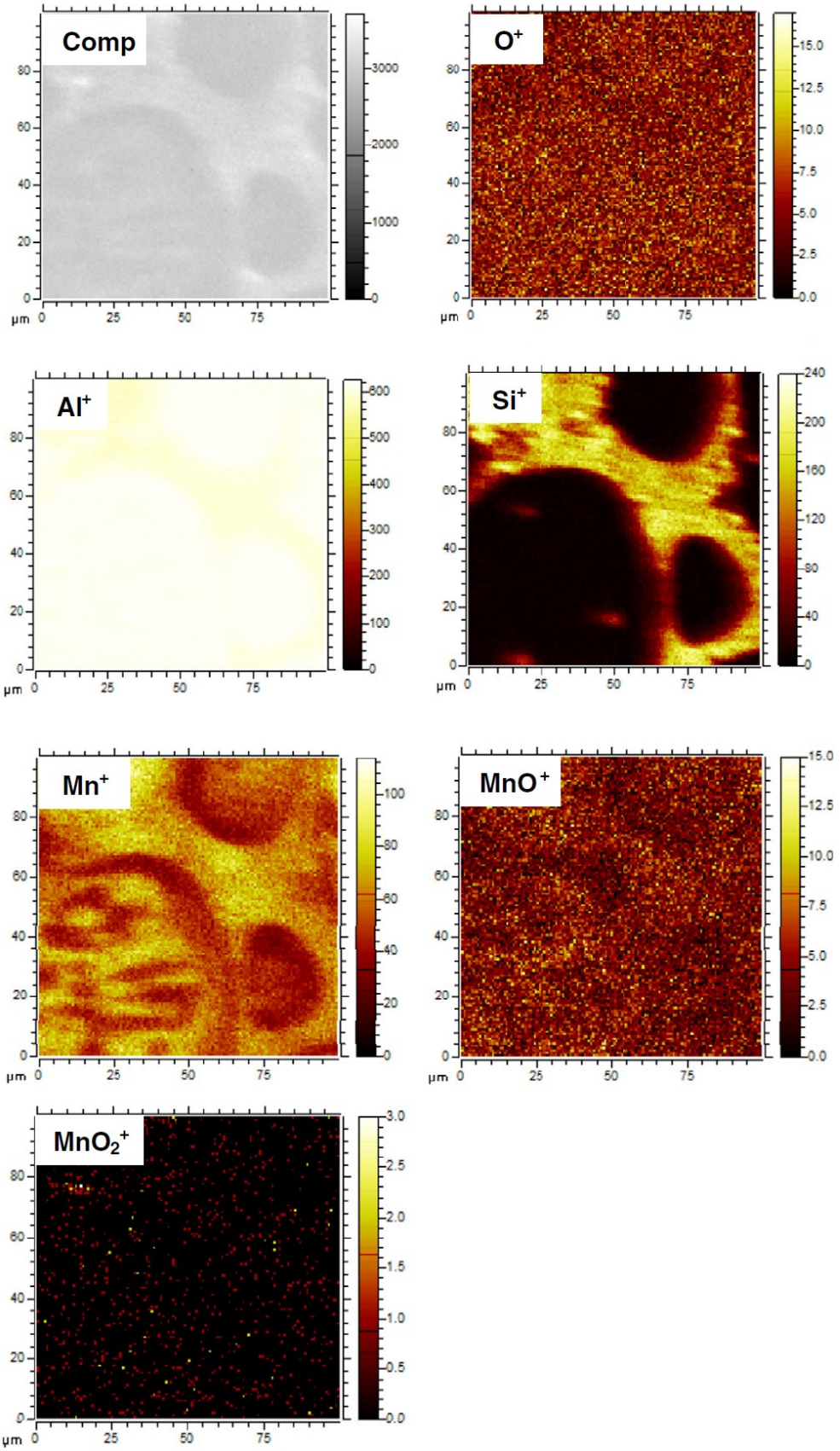


Fig. 1-16. Mapping of positive irons from the film analyzed by TOF-SIMS [17].

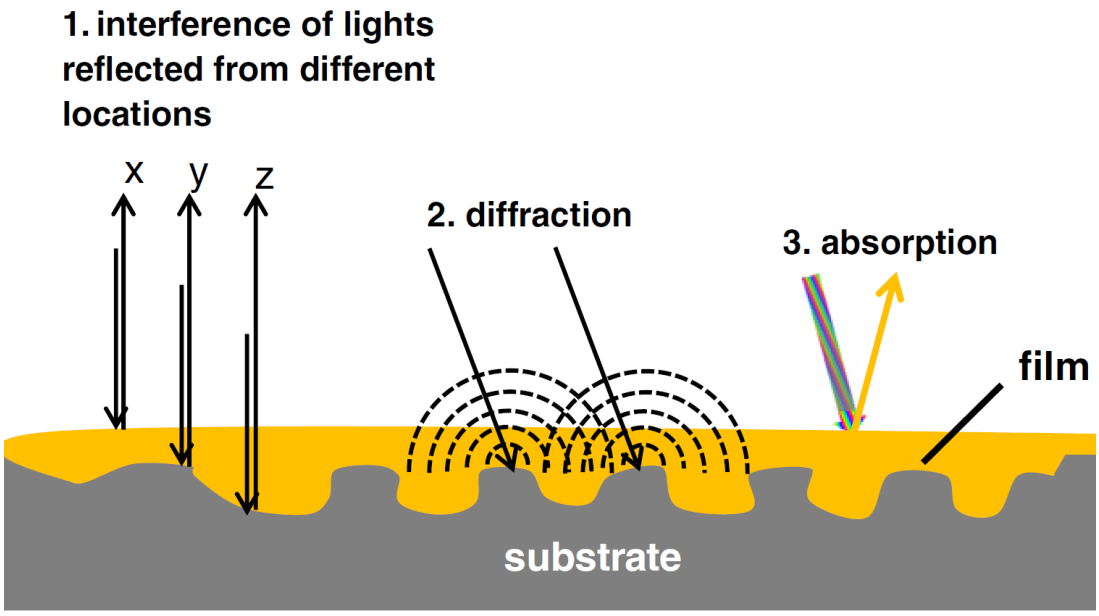


Fig. 1-17. Schematic illustration showing the cross section of the specimen after etching as well as three proposed coloring mechanisms [17].

Chapter 2

Coloring behavior in the eutectic solidified region of semi-solid die-cast A356 aluminum alloy etched by Weck's reagent

2.1. Introduction

In the chapter 1, the characteristics and the advantages of color etching metallography and the role of Weck's reagent as a color etchant were introduced [1-5]. Many applications of Weck's reagent were shown, such as the detection of the grain boundaries in cast aluminum alloy or the micro-segregation in aluminum phase, and the correct evaluation of solid fraction of the semi-solid aluminum alloy slurry. Understanding of coloring mechanism by Weck's reagent is important. Suárez-Peña et al. [2] suggested that aluminum reacts with Weck's reagent and produces a film of manganese dioxide on the specimen's surface during etching. Gao et al. [4, 5] confirmed the existence of the manganese dioxide film. They did the characterization of the film, such as the surface morphology and the thickness of the film which can affect the optical properties. It was revealed that the color contrast after etching was influenced by film's thickness and surface morphology. In particular the brightness of the color contrast is influenced by the roughness of the interface between the bottom surface of manganese dioxide film and aluminum substrate.

Although Gao et al. examined the color contrast in the large primary α-grains, they did not examine the color contrast in the eutectic solidified region surrounding the spheroidal grains. The characterization of manganese dioxide film in the eutectic solidified region and the factors influence the morphology of the manganese dioxide film in the eutectic solidified region are of interest in order to reveal the overall coloring behavior of the A356 aluminum alloy. In this chapter, the etched surface observation in the eutectic region was carried out for the semi-solid die-cast A356 aluminum alloy.

2.2. Experimental

2.2.1. Material and introduction of pre-plastic strain

The material used in this research is A356 cast aluminum alloy. The chemical composition of the alloy is shown in Table 2-1. Ti and Sr were added to refine the α-Al phase and eutectic phase, respectively. The reason for choosing this alloy is that A356 Al alloy is the most frequently used commercial alloy for the semi-solid processing. The material was supplied as a cylindrical-shape billet with 30 mm in diameter and 100 mm in height.

In order to obtain spheroidal grains in the semi-solid state, a pre-plastic strain was introduced to the billet by cold compression before

heating to the semi-solid temperature, as shown in Fig. 2-1. The cold compression to the billet was made by using a 500 ton compressing machine at Nissan Motor Co., Ltd. The compressing rate was 0.2mm/sec. The temperature increase of the billet during the deformation to the target height (66 mm, 33% reduction in height) was about 20 °C.

2.2.2. Fabrication of semi-solid slurry and die-casting

The compressed billet was provided for the fabrication of semi-solid slurry. In order to measure the temperature of the billet, a small hole was machined at the side of the billet and a thermocouple was inserted into it, as shown in Fig. 2-2. The billet was held in the electric furnace and heated up to 595 °C, which corresponds to the semi-solid temperature at which the solid fraction is approximately 50% according to the Al-Si binary phase diagram. The heating rate was about 24 °C/min. At the target temperature (595 °C), the billet was isothermally held for 5 min. Then the billet was rapidly cooled by die-casting, as shown in Fig. 2-3.

2.2.3. Solution treatment

A number of cubic specimens with 8×8×5 mm^3 were collected from the die-cast product. Some of the cubic specimens were provided for the heat treatments. They were held in the electric furnace and heated up to 535 °C and isothermally held for 8 h. After the isothermal holding, the

specimens were quenched into water. The quenched specimens were kept at room temperature for 24 h and then put into the 155 °C-oil bath for 6 h, then quickly quenched into water, as shown in Fig. 2-4.

2.2.4. Microstructure observation by optical microscopy

The as-cast cubic specimens and heat-treated cubic specimens were used for the microstructural analysis. The specimens were ground using 120, 600, 1000, 2000 and 4000 grit paper, polished using 3, 1 μm diamond paste and OPS colloidal silica. After that, the polished specimens were etched by Weck's reagent for 12 s and carefully washed by distilled water. The etched specimens were observed by an optical microscopy (OM) without filters, and the optical micrographs were directly taken.

2.2.5. Surface characterization by scanning electron microscopy

The secondary electron image (SEI) of etched specimen was taken by scanning electron microscopy (SEM) to characterize the topography of the etched surface. The accelerating voltage was set to 5 kV.

2.2.6. Microstructure analysis of the film by scanning transmission electron microscopy

The morphology of the manganese dioxide film formed in the

eutectic solidified region was observed by a scanning transmission electron microscopy (STEM). The carbon coating was coated on the etched surface to protect the surface. A small thin specimen vertical to the surface was sliced by focused ion beam (FIB) for STEM observation. The cross-section of the manganese dioxide film was observed by STEM and the thickness and the roughness of the film from location to location was evaluated. The composition of the film was analyzed by Energy Dispersive X-ray Spectroscopy (EDS) qualitatively, and concentration mappings of Al, Si, Mn and O were obtained.

2.2.7. Chemical composition analysis by EPMA

The micro-segregations of Mg, Si and Ti of the solution-treated specimens were evaluated by EPMA analysis using X-ray Wavelength Dispersive Spectroscopy (WDS). The location for the chemical analysis was controlled to be the same as the location where the optical micrographs taken by the optical microscopy. The acceleration voltage was set to 15 kV and the electron beam current was set to 185 nA. The solute elements distribution of the solution-treated specimen was evaluated by the intensities of characteristic X-rays and the distribution mappings of these solute elements were obtained. Based on the calibration standards, the intensity of each element was converted into atomic percentage and labeled in the distribution mappings.

2.3. Results

2.3.1. Microstructural features of as-cast specimen

Fig. 2-5 and Fig. 2-6 show the optical micrographs of the as-polished and the etched semi-solid die-cast specimen at different magnification. The microstructural feature consists of large primary α-Al grains, eutectic solidified region surrounding them, and fine secondary α-Al particles in it. These features are labeled in Fig. 2-5 (a) and Fig. 2-6 (a). The specimen etched by Weck's reagent shows the characteristic color differences inside the large primary α-Al grains as shown in Fig. 2-6 (b). As discussed in Gao et al.'s research [4, 5], these characteristic color differences come from the differences of the roughness of the interface between manganese dioxide film and substrate. The roughness of the interface between the bottom surface of manganese dioxide film and α-Al substrate was controlled by the concentration of the elements in aluminum alloys. The eutectic solidified region exhibits the lamellar structures as shown in Fig. 2-6 (c).

2.3.2. Microstructural features of solution-treated specimen

Fig. 2-7 and Fig. 2-8 show the optical micrographs of the as-polished and the etched solution-treated specimen at different magnification. The microstructure consists of large primary α-Al grains

and eutectic solidified region surrounding them. These features are labeled in Fig. 2-7 (a) and Fig. 2-8 (a). The morphology of eutectic silicon at the solidified liquid phase was transferred to spheroidal in solution-treated specimen. The specimen etched by Weck's reagent also shows the characteristic color differences inside the large primary α-Al grains. The eutectic region also revealed color differences of eutectic silicon and aluminum. In addition, a peculiar network structure can be observed in the eutectic region.

2.3.3. Surface topography observation by SEI for the etched specimen before and after solution treatment

Fig. 2-9 shows the optical microstructures of the as-cast specimen before and after etching. Fig. 2-10 shows the SEI images of the as-cast specimen etched by Weck's reagent. The local difference in surface topography in the large primary α-Al grains was clearly exhibited with the help of Weck's reagent. In the eutectic solidified region, the lamellar structure of the eutectic silicon and aluminum was also clearly exhibited with the help of Weck's reagent.

Fig. 2-11 shows the optical microstructures of the solution-treated specimen before and after etching. Fig. 2-12 shows the SEI image of the solution-treated specimen etched by Weck's reagent. The differences of the surface topography in the large primary α-Al grains were also clearly

exhibited with the help of Weck's reagent. In the eutectic solidified region, the spheroidal eutectic silicon particles in the aluminum matrix were clearly shown. In addition, a peculiar network structure was revealed in the eutectic solidified region. This network structure is considered to be the sub-grain boundaries due to the solution treatment.

2.3.4. Cross-sectional observation and compositional analysis of the manganese dioxide film by STEM and EDS

The cross-section of the eutectic etched surface in the solidified region of the as-cast specimen was observed by STEM, as shown in Fig. 2-13. The eutectic silicon phase with the needle-like morphology was disorderly distributed in the aluminum matrix of the eutectic solidified region. The manganese dioxide film is observed only on the top surface of aluminum phase. The film's thickness is around 100 nm. Fig. 2-14 shows the results of composition analysis for aluminum, silicon and the film by EDS. The results indicate that the film does not contain Al and Si and mainly consist of Mn and O. This result confirms that manganese dioxide film is formed in the eutectic solidified region as well as in the large primary α-Al grains.

The cross-section of the surface of the etched eutectic solidified region of the solution-treated specimen was observed by STEM, as shown in Fig. 2-15. By the solution treatment, the morphology of the

eutectic silicon changed from needle-like to spheroidal morphology, the manganese dioxide film is also formed only on the aluminum phase. The thickness of the film is around 200 nm. Fig. 2-16 shows the results of composition analysis by EDS. The high concentration of the aluminum indicates the aluminum matrix, the high concentration of the silicon indicates the eutectic silicon and the high concentration of the manganese and oxygen indicates the film formed on the surface. They were clearly distinguished by the composition analysis.

2.3.5. Chemical analysis of solution-treated specimen by EPMA

EPMA analysis was performed to examine the origin of color difference in the solution-treated semi-solid die-cast A356 aluminum alloys. Fig. 2-17 (a) shows the optical micrograph of the large primary α-Al grain of solution-treated specimen etched by Weck's reagent. Fig. 2-17 (b) to (d) shows the solute distribution in the structure for Mg, Si and Ti, respectively. The attached color bars show the level of composition for each element. Fig. 2-17 (b) shows the solute distribution of Mg was homogenously in the Al matrix. Si was difficult to observe in the large spheroidal primary α-Al grain, instead, high concentration of Si was observed in the eutectic solidified region (Fig. 2-17 (c)). Segregation of Mg and Si could not be observed in the large spheroidal primary α-Al grain, except for sporadic entrapped eutectic solidified region. Fig. 2-17

(d) shows the characteristic solute distribution of Ti in the large spheroidal primary α-Al grain. The Ti is the heavy segregated at the center of the large spheroidal primary α-Al grain and the ring-shaped region at the edge of the large spheroidal primary α-Al grain.

Fig. 2-18 (a) shows the optical micrograph of the eutectic solidified region of solution-treated specimen etched by Weck's reagent. Fig. 2-18 (b) to (d) shows the solute distribution in the structure for Mg, Si and Ti, respectively. The attached color bars show the level of composition for each element. In the eutectic solidified region, the solute distribution of Mg was also homogenously in the Al matrix (Fig. 2-18 (b)). Many locations with the high concentration of Si were observed (Fig. 2-18 (c)) as mentioned before. The characteristic solute distribution of Ti was also observed, as shown in Fig. 2-18 (d). The segregation also could be observed in eutectic solidified region, but it is not heavy as in large spheroidal primary α-Al grain. The peculiar network structure distribution of elements couldn't be observed in the eutectic solidified region by using EPMA analysis.

2.4. Discussion

2.4.1. Microstructure characteristics revealed by Weck's reagent

In this chapter, the microstructure characteristic of semi-solid

die-cast A356 aluminum alloy revealed by Weck's reagent is discussed. As shown in Fig. 2-9 (c), the characteristic color differences were revealed by Weck's reagent in the large primary α-Al grains in as-cast semi-solid die-cast A356 aluminum alloy. According to the proposed coloring mechanism of Weck's reagent by Gao et al. [4, 5], the aluminum substrate reacts with Weck's reagent and produces a manganese dioxide. The color differences come from the difference in film thickness and roughness of the interface between the bottom surface of manganese dioxide film and substrate. The SEI image of the large primary α-Al grains, as shown in Fig. 2-10 (a) supported this idea. In the eutectic solidified region, eutectic silicon and aluminum matrix has a different color, as shown in Fig. 2-9 (d). This suggests that only aluminum phase in the eutectic structure reacted with Weck's reagent. This idea is supported by the facts obtained by the cross-sectional observation and the compositional analysis by STEM and EDS, as shown in Fig. 2-13 and Fig. 2-14. The SEI image of the eutectic solidified region of the as-cast specimen found that the surface topography of eutectic silicon and aluminum matrix is different, as shown in Fig. 2-10 (b).

In order to investigate the etching behavior in the eutectic solidified region much more, the effect of solution treatment on the solute elements distribution and morphological change of the eutectic silicon and aluminum matrix at the eutectic solidified region was examined. Fig. 2-11

(c) shows the characteristic color difference in the large primary α-Al grain of the solution-treated specimen. The colors in the large primary α-Al grain were not as colorful as those of the as-cast specimens. The local difference in surface topography was not so obvious, as shown in Fig. 2-12 (a). It is considered that the diffusion of the solute elements during the solution treatment homogenized the micro-segregation of the solute elements in the large primary α-Al grains. This shows a good agreement with the EPMA results, as shown in Fig. 2-17. The eutectic region also showed a characteristic color difference by the solution treatment. This is considered to result from the change in the eutectic aluminum phase which reacted with Weck's reagent. This shows a good agreement with the morphological change of the film and compositional change detected by STEM and EDS analysis, as shown in Fig. 2-15 and Fig. 2-16. The SEI image of in the eutectic solidified region of the solution-treated specimen also exhibited the different surface topography of eutectic silicon and aluminum matrix, as shown in Fig. 2-12 (b). Comparing the SEI images with the optical micrographs found that the surface topography has a strong correlation with the color difference revealed by Weck's reagent.

2.4.2. Peculiar network structure revealed by Weck's reagent

As shown in Fig. 2-11 (d), a peculiar network structure was

observed in the eutectic solidified region in the solution-treated specimen etched by Weck's reagent. This structure was not observed in the as-polished specimen, as shown in Fig. 2-11 (b). The EPMA analysis results, as shown in Fig. 2-18 did not show any peculiar of Mg, Si and Ti solute distribution corresponding to the network structure in the eutectic solidified region. The results show that the peculiar color revealed by Weck's reagent dose not comes from the micro-segregation of the solute elements in the eutectic solidified region. The SEI image of the surface topography of this kind of peculiar network structure is shown in Fig. 2-12 (b). The results show that the aluminum matrix in the eutectic solidified region is separated to many small blocks. The morphology of the small blocks coincides with the peculiar network structure observed by optical microscopy. There are considered to be the sub-grain boundaries of aluminum matrix formed by the solution treatment.

In order to investigate the origin of the peculiar network structure in the solution-treated specimen, the etched specimen surface was polished by 1 μm diamond paste for 60 s, 180 s and 300 s. The original optical micrographs of the etched surface are shown in Fig. 2-19. As shown in Fig. 2-19 (c), in the specimen surface polished by 180 s, the peculiar network structure remained although characteristic color contrasts completely disappeared. Additional EPMA analysis was carried out to examine the existence of manganese in the specimen surface of Fig. 2-19

(c). Fig. 2-20 (a) shows the optical micrograph of the eutectic region of specimen polished by 180 s. Fig. 2-20 (b) to (e) shows the solute distribution in the structure for Mg, Si, Ti and Mn, respectively. As shown in Fig. 2-20 (e), high manganese concentration tracing the network morphology is observed. This result suggests the manganese dioxide film formed by Weck's reagent etching remains in the sub-grain boundaries.

2.4.3. Characterization of manganese dioxide film in eutectic solidified region

In this chapter, the etching behavior in the eutectic solidified region of semi-solid die-cast A356 aluminum alloy by Weck's reagent was examined and the morphology of the manganese dioxide film formed by the etching was investigated. It is obvious that the morphology of the manganese dioxide film has a strong effect on the coloring behavior.

The schematic illustration of the cross section of the manganese dioxide film is shown in Fig. 2-21. Cross-sectional observation by STEM and compositional analysis by EDS revealed that the morphology of manganese dioxide film in the eutectic solidified region is like this for the as-cast condition (Fig. 2-21(a)). The top surface of the film is flat in atomic scale, but the thickness and the bottom surface morphology change location to location depending on the solute distribution in the aluminum matrix. The solution treatment caused a big morphological

change in the thickness of the manganese dioxide film in the eutectic solidified region because of the spheroidization and coarsening of eutectic silicon phase and homogenization of solute elements in the aluminum matrix. Additional change of the film morphology may occur due to the recrystallization of the aluminum in the eutectic solidified region, as shown in Fig. 2-21(b).

2.5. Conclusions

In this chapter, the color etching behavior in the eutectic solidified region of semi-solid die-cast A356 aluminum alloy by using Weck's reagent was examined. Various characterization methods were applied to understand more about the manganese dioxide film formed during etching process in terms of the topography of interface between manganese dioxide film and substrate.

Eutectic aluminum and silicon in the eutectic solidified region exhibited different color in as-cast condition. SEI observation found that they exhibited different height. The cross-sectional observation and compositional analysis by using STEM and EDS revealed that only aluminum matrix reacted with Weck's reagent and the film was formed by the conversion coating mechanism proposed by Gao et al. The top surface of the manganese dioxide film was flat in atomic scale, but the

thickness of the film and the roughness of the bottom surface of the film changed location to location. No film formation was observed on the silicon phase. Difference in color contrast is considered to depend on the lamellar morphology of the eutectic solidified region. Therefore, the morphological change of silicon phase in the eutectic solidified region, from needle-like morphology to spheroidal morphology, caused the change in color contrast in the solution-treated condition. The morphological change of the film was confirmed by STEM observation.

A peculiar network structure was observed in the microstructure etched by Weck's reagent in solution-treated condition. Cross-sectional observation of the film in the solution-treated specimen revealed that the peculiar network morphology may result from local morphological change of the film tracing the boundaries or sub-boundaries of the recrystallized grains due to the solution treatment.

References

[1] E. Weck, E. Leistner, Metallographic instructions for colour etching by immersion, part iii: non-ferrous metals, cemented carbides and ferrous metals, nickel-base and cobalt-base alloys, DVS GmbH, Düsseldorf, 1986.

[2] B. Suárez-Peña, J. Asensio-Lozano, G.F. Vander-Voort, Colour metallography in commercial Al-Si alloys. Optimization of the microstructural characterization techniques in light optical microscopy, Rev. Metal 46(2010) 469-476.

[3] S.A. Kulinich, A.S Akhtar, P.C. Wong, K.C. Wong, K.A.R. Mitchell, Growth Of Permanganate Conversion Coating On 2024-Al Alloy, Thin Solid Films 515 (2007) 8386-8392.

[4] L. Gao, Y. Harada, S. Kumai, Microstructural characterization of aluminum alloys using Weck's reagent, part I: Applications, Mater Charact. 107 (2015) 426-433.

[5] L. Gao, Y. Harada, S. Kumai, Microstructural characterization of aluminum alloys using Weck's reagent, part II: Coloring mechanism, Mater Charact. 107 (2015) 434-452.

Table 2-1 Chemical compositions of A356 alloy used in this chapter (mass%).

Si	Mg	Fe	Ti	Sr	Mn	Al
6.90	0.39	0.10	0.14	0.025	<0.10	Bal.

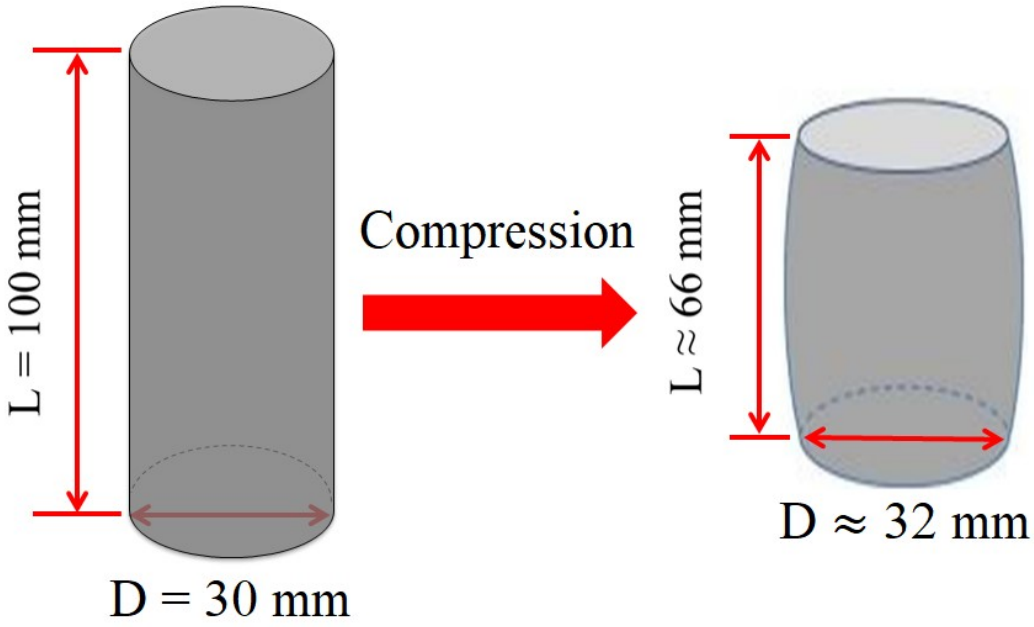


Fig. 2-1. Schematic of the A356 cast aluminum alloy billet before and after compression.

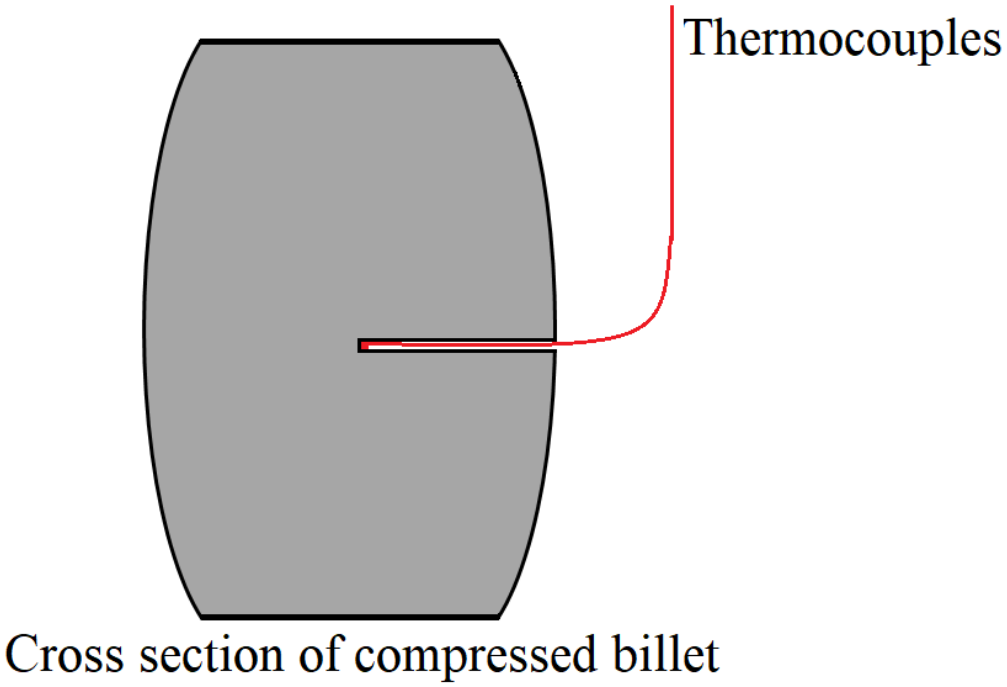


Fig. 2-2. Schematic of thermocouple insert in the compressed billet.

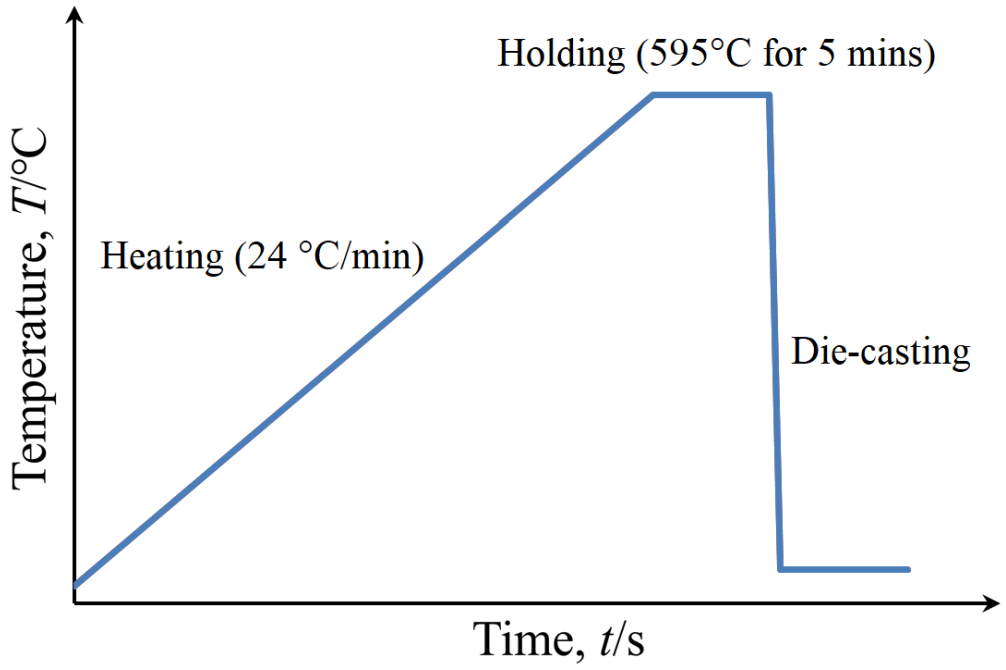


Fig. 2-3. Schematic temperature-time curve for heating, holding and die-casting process in this chapter.

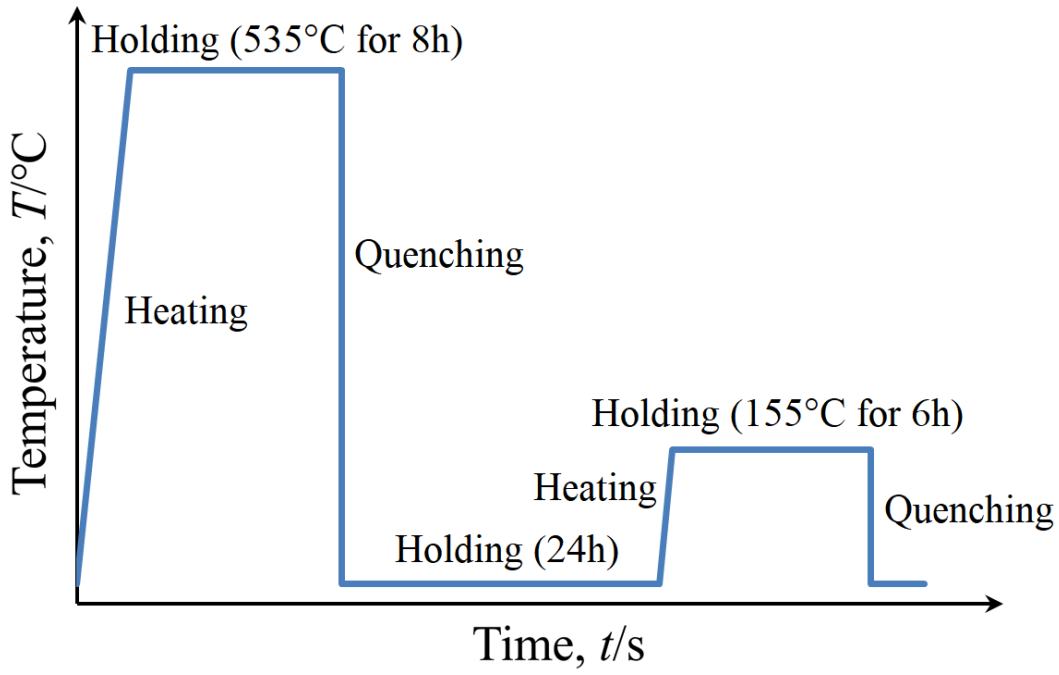
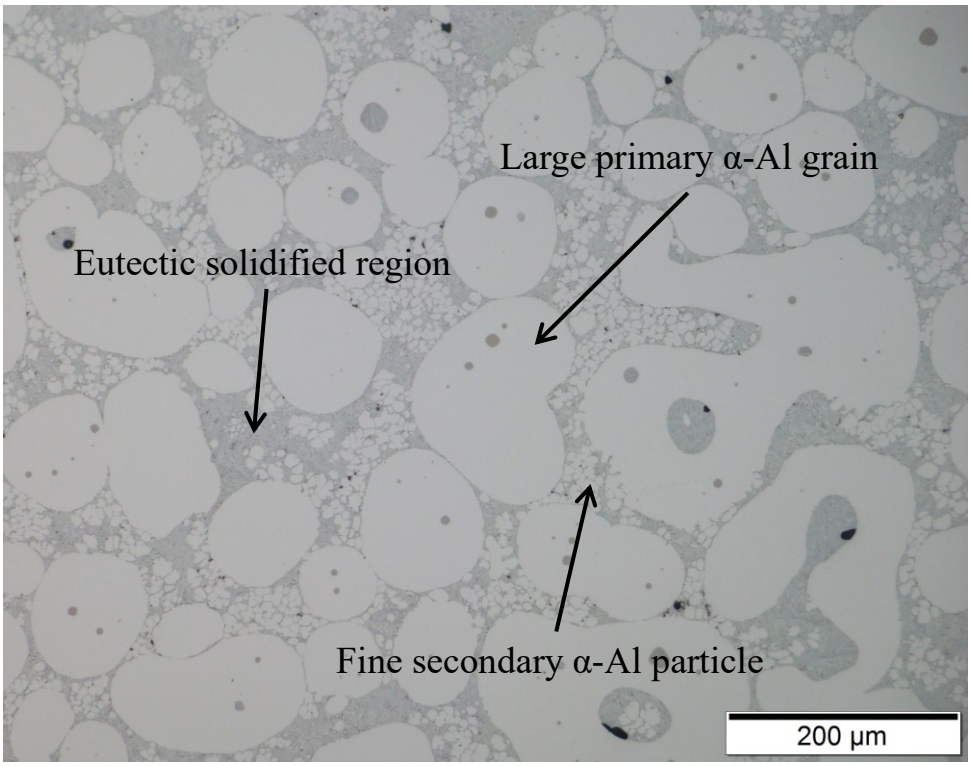
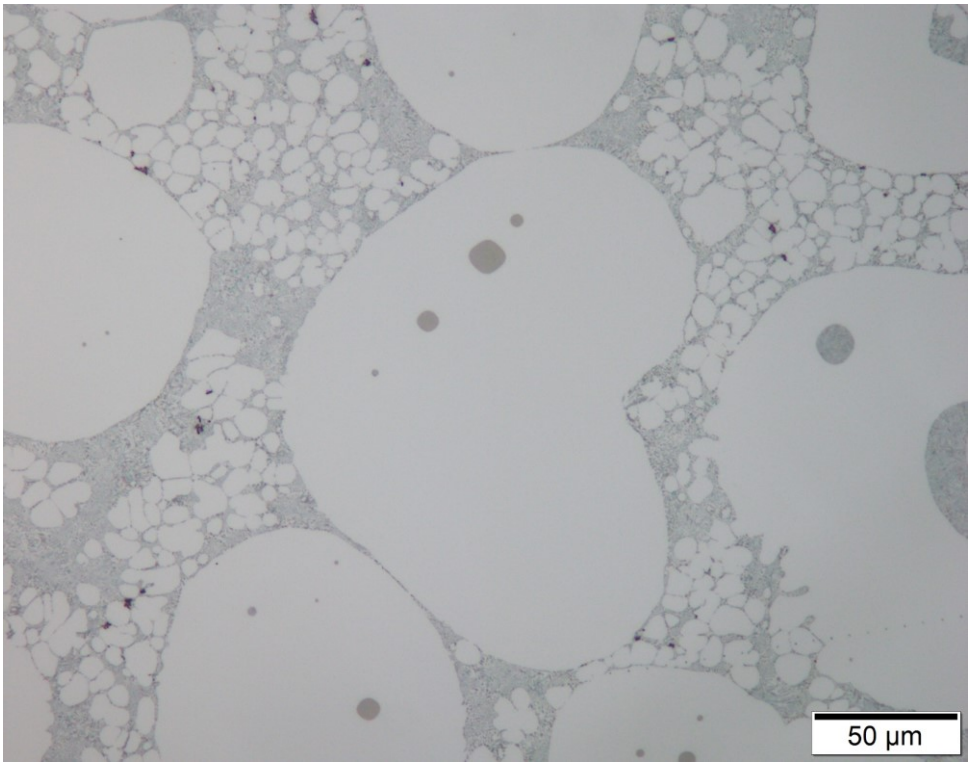


Fig. 2-4. Schematic temperature-time curve for solution treatment process in this chapter.

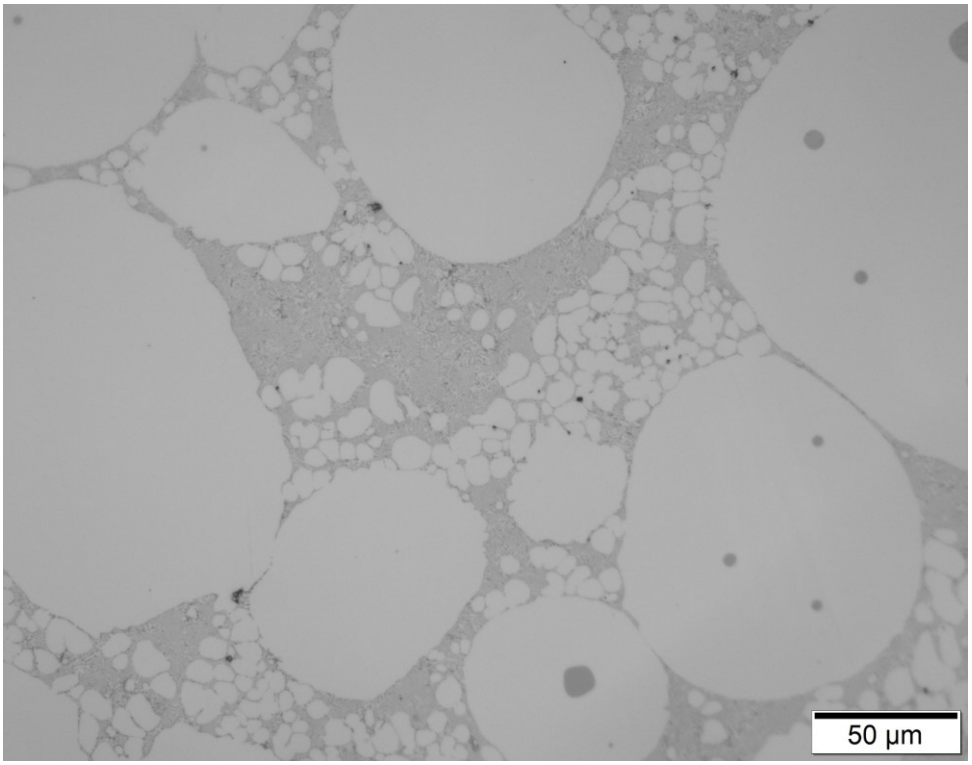


(a)

Fig. 2-5. Microstructure of the as-cast specimen without etching for different magnifications and locations

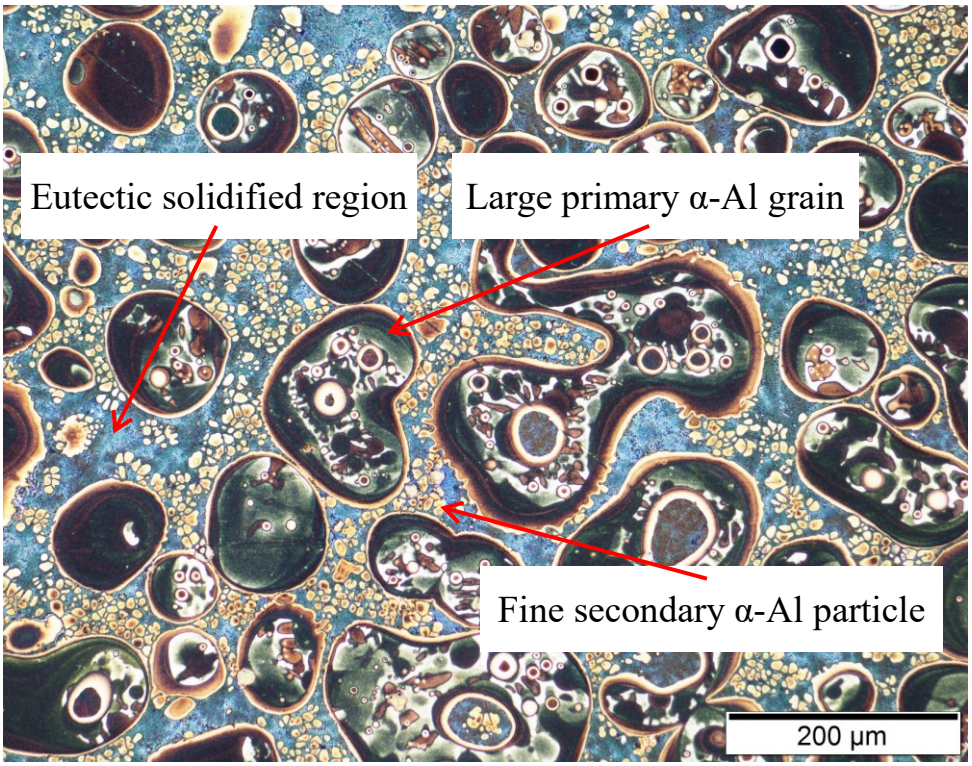


(b)



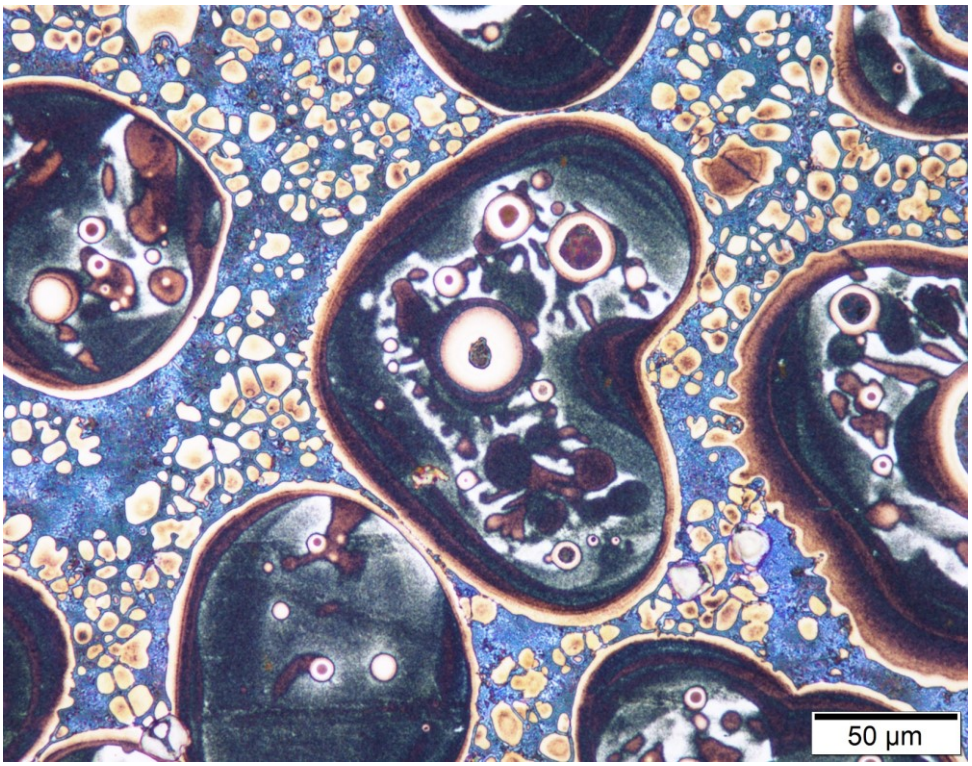
(c)

Continued

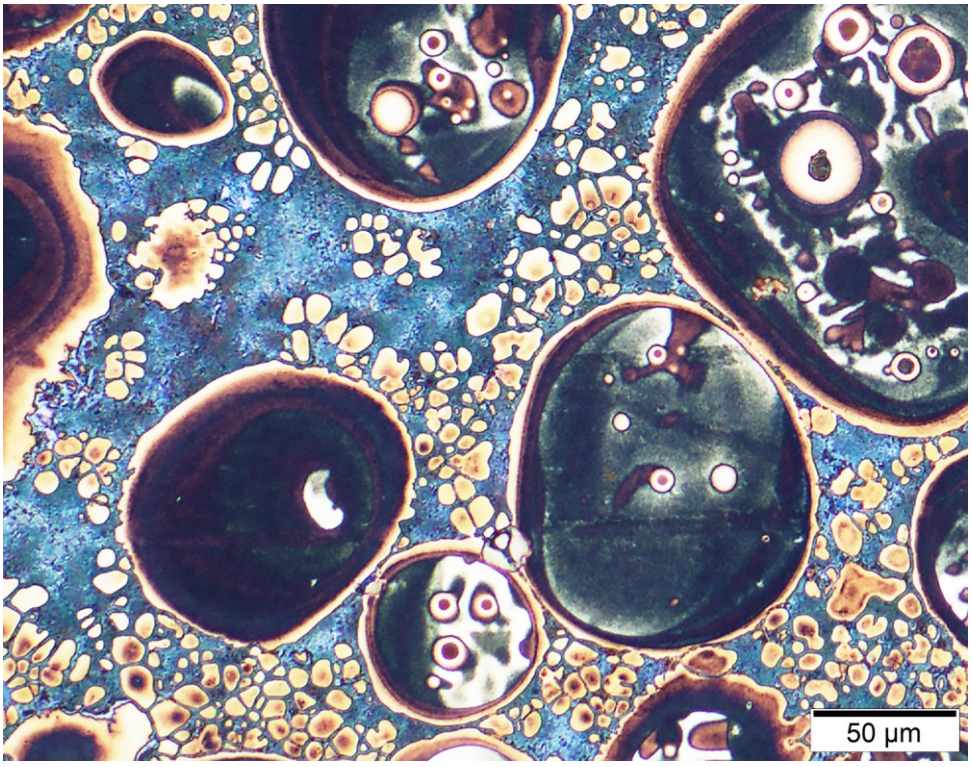


(a)

Fig. 2-6. Microstructure of the as-cast specimen etched by Weck's reagent for different magnifications and locations.

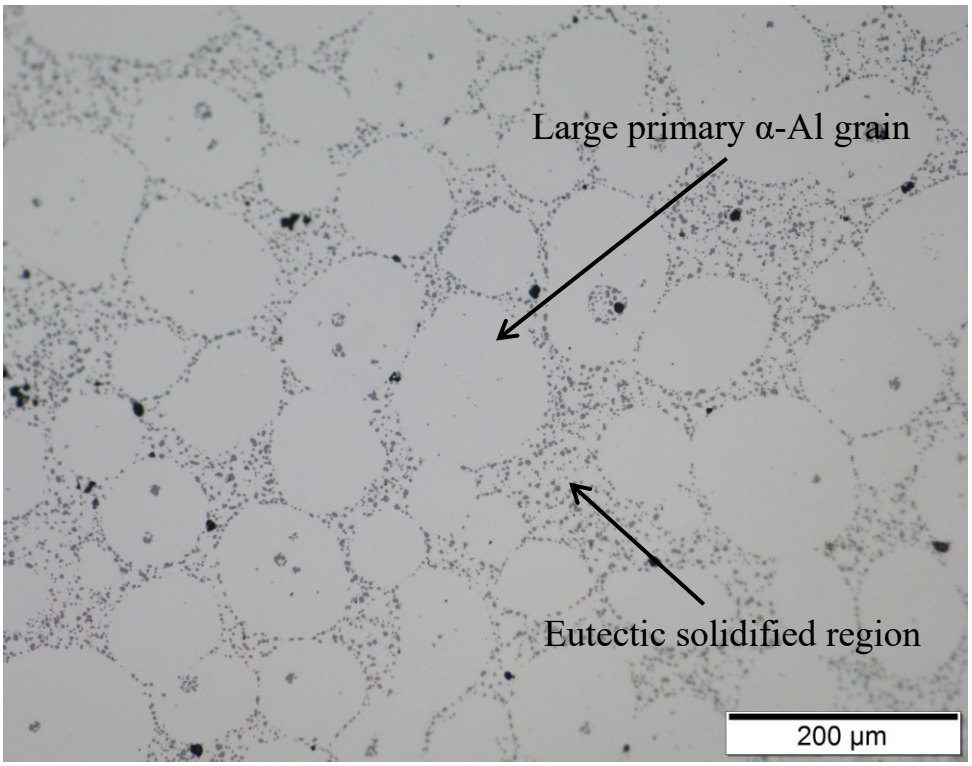


(b)



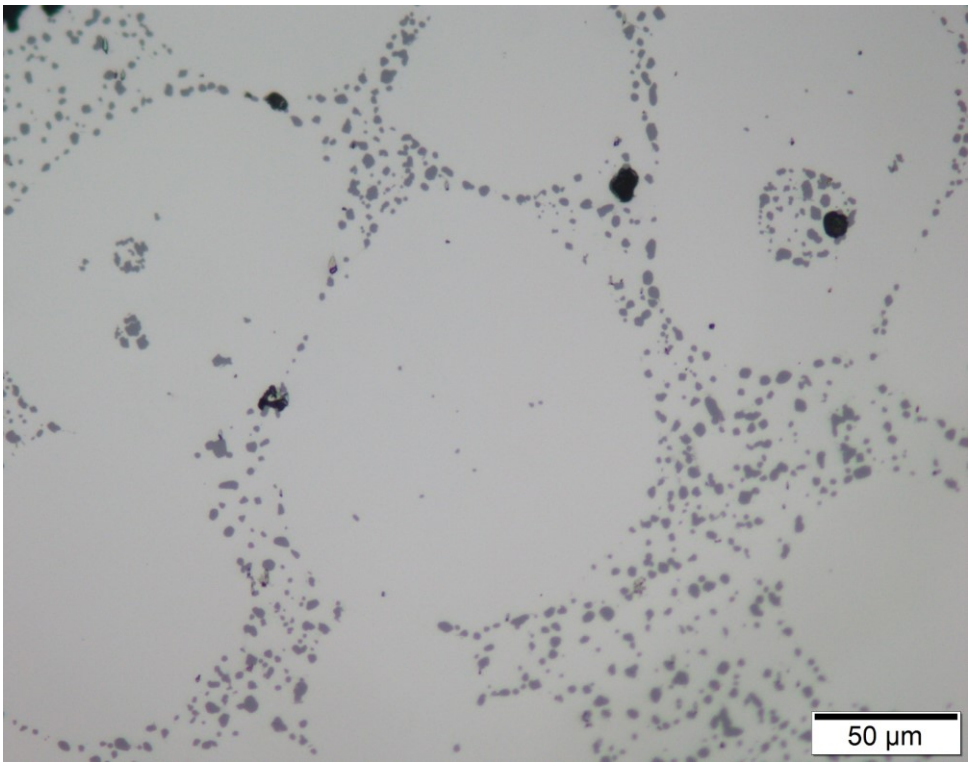
(c)

Continued

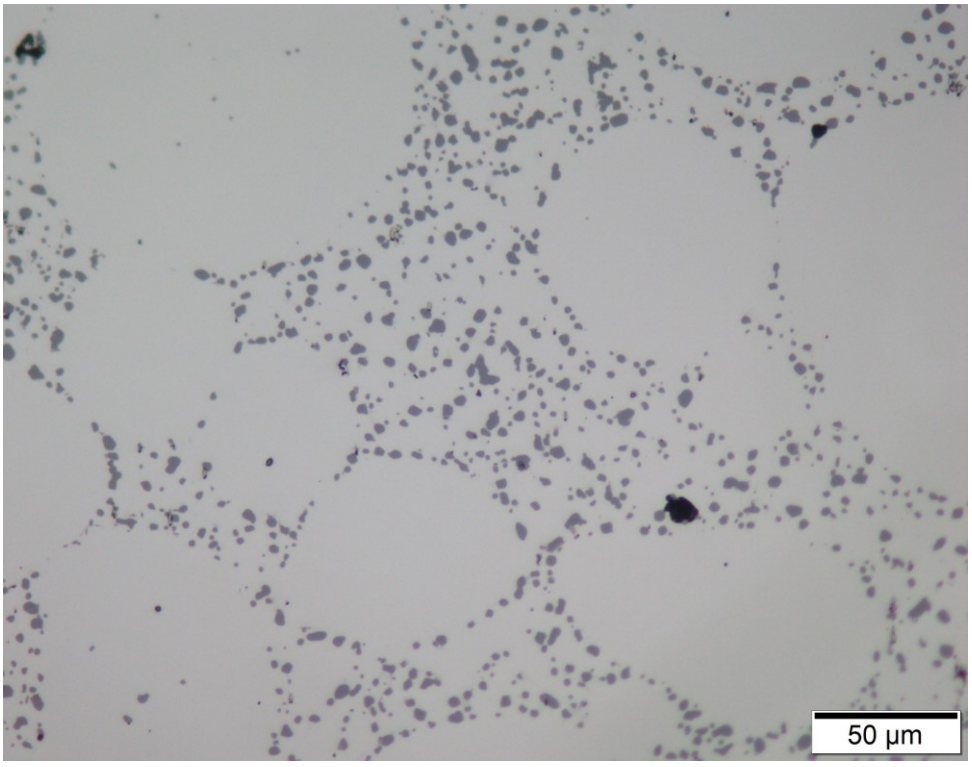


(a)

Fig. 2-7. Microstructure of the solution-treated specimen without etching for different magnifications and locations.

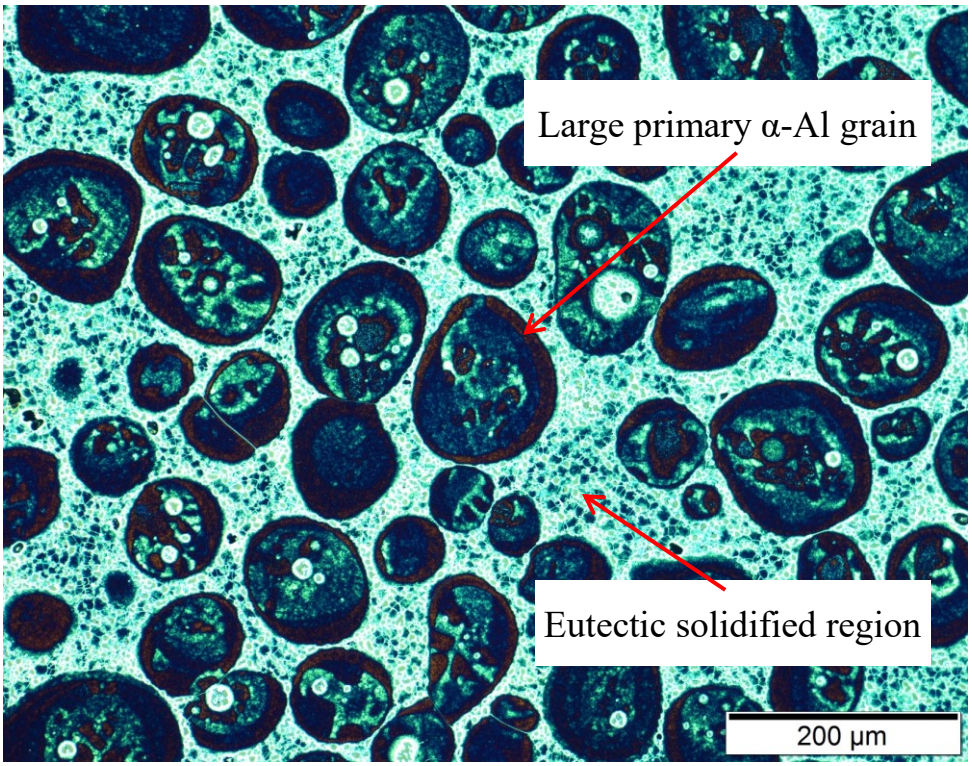


(b)



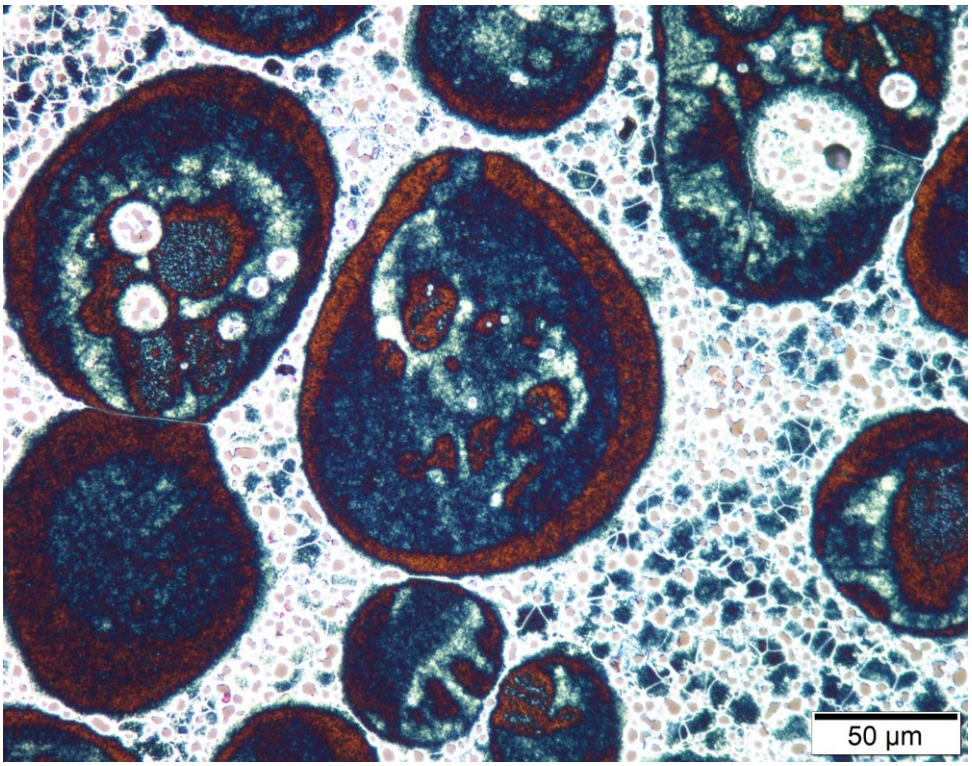
(c)

Continued

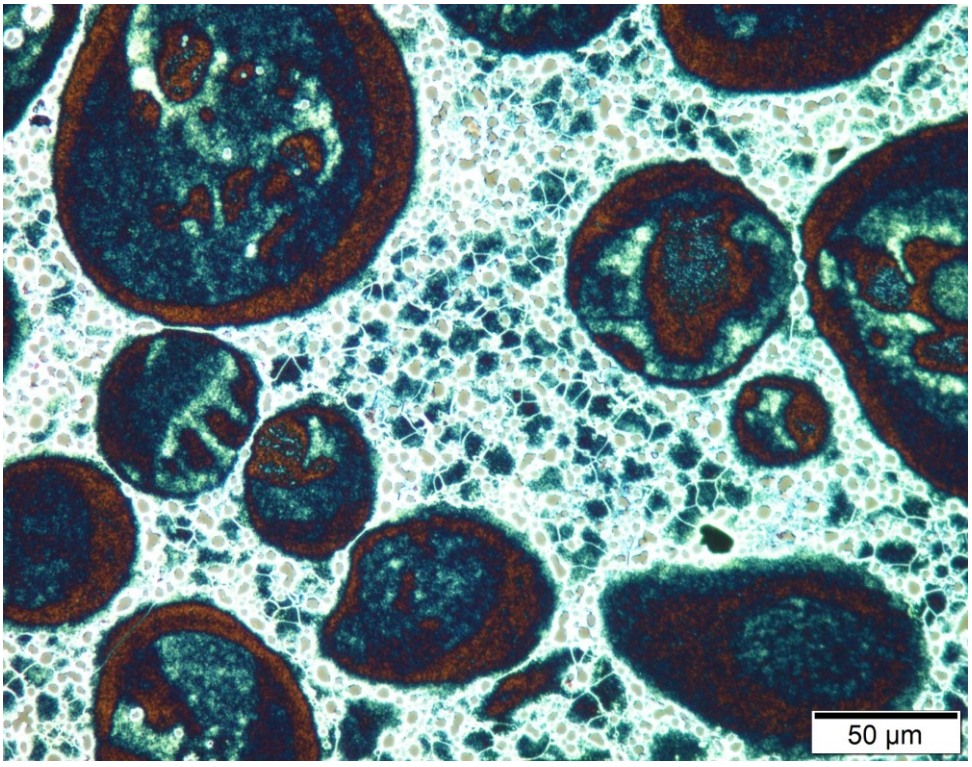


(a)

Fig. 2-8. Microstructure of the solution-treated specimen etched by Weck's reagent for different magnifications and locations.

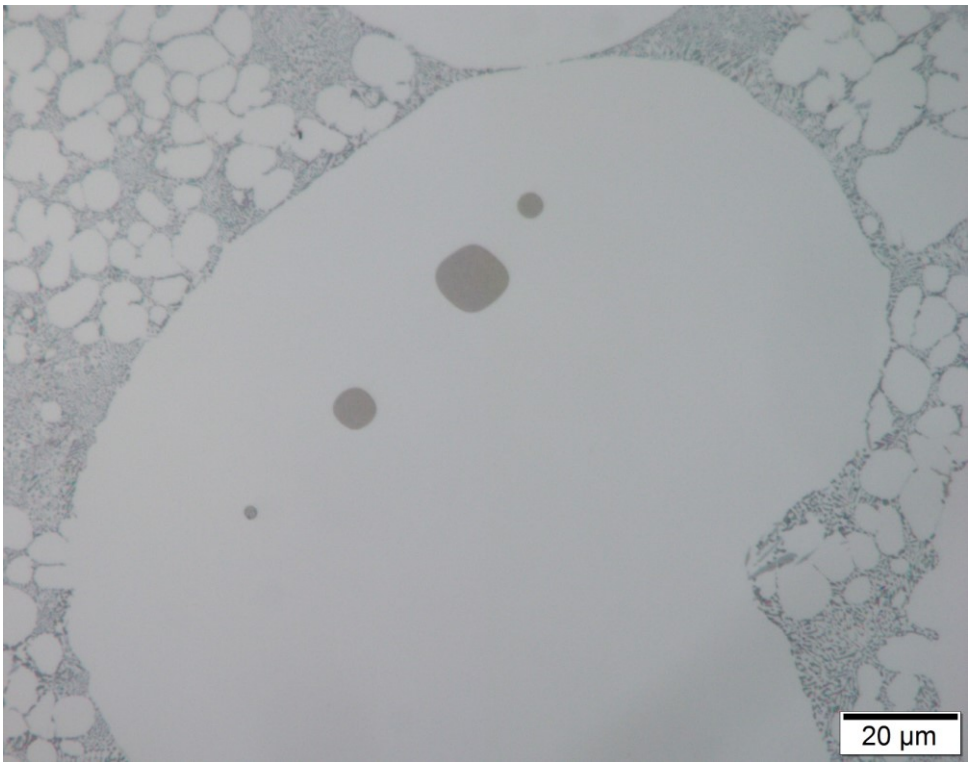


(b)

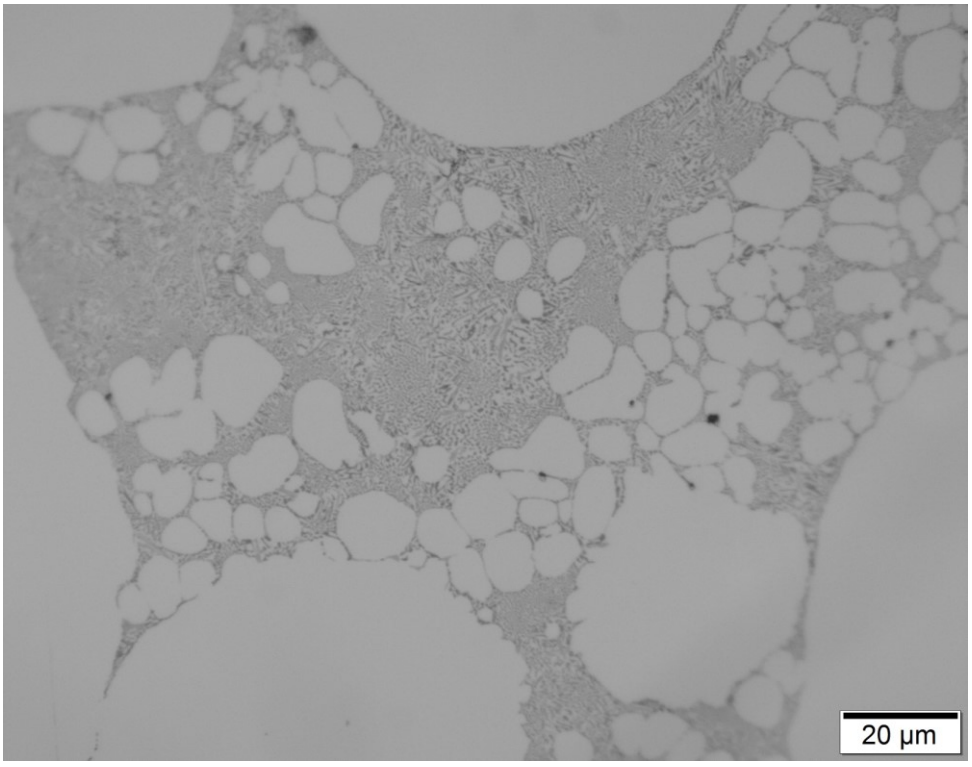


(c)

Continued

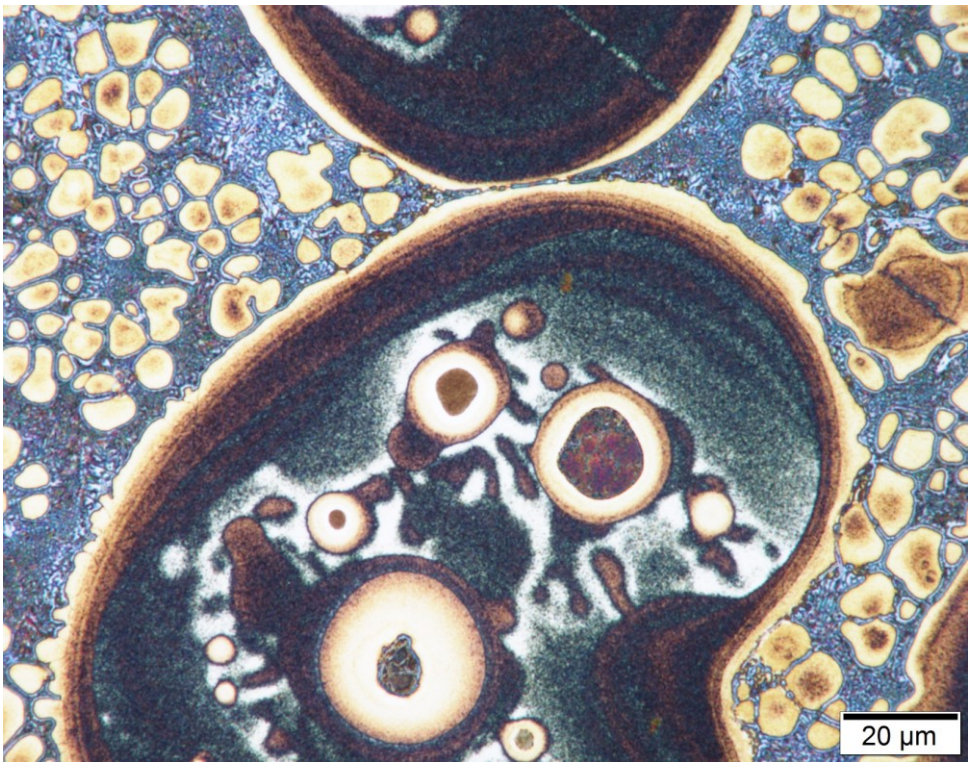


(a)

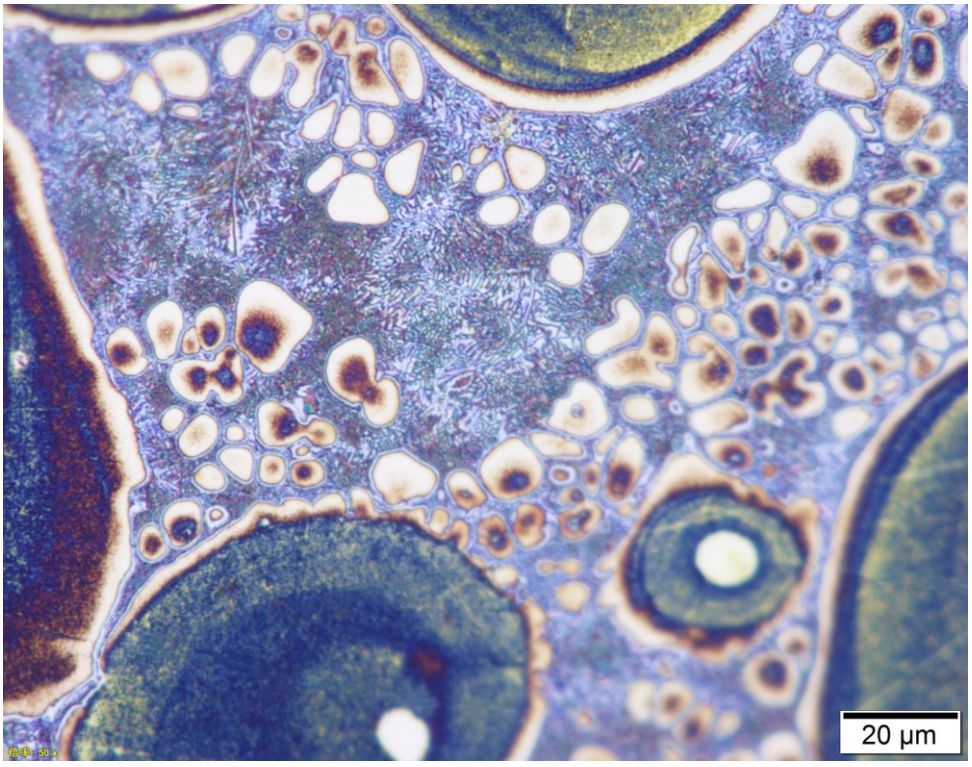


(b)

Fig. 2-9. Optical micrographs of the as-cast specimen (a) and (b): without etching, (c) and (d): etched by Weck's reagent.

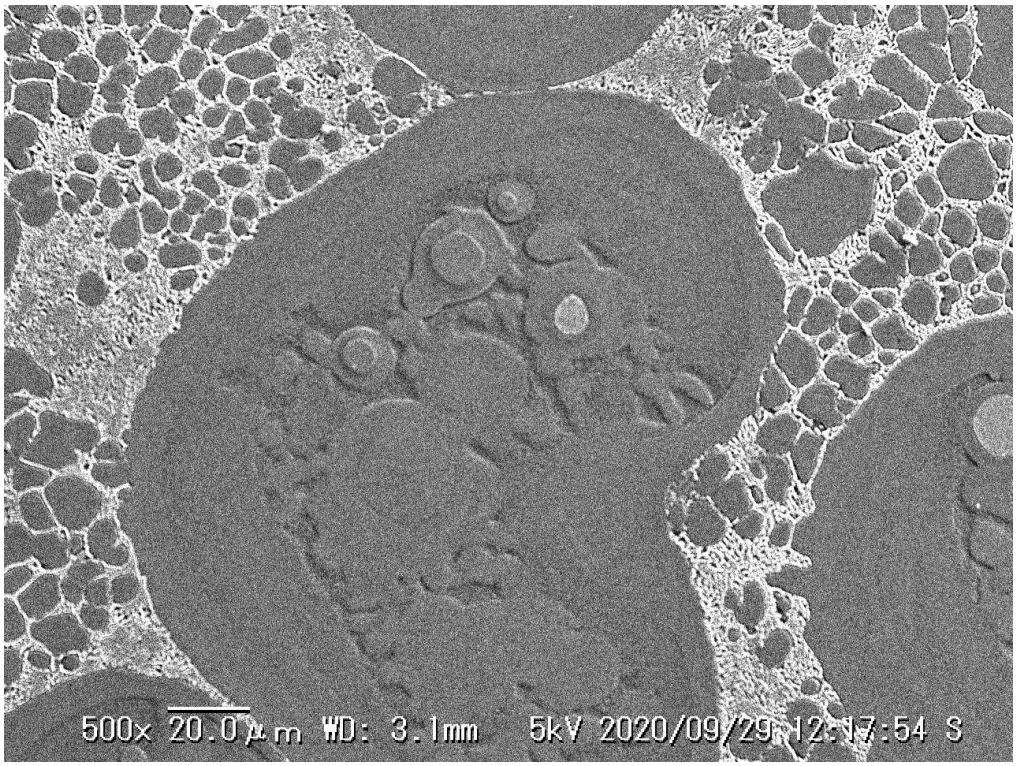


(c)

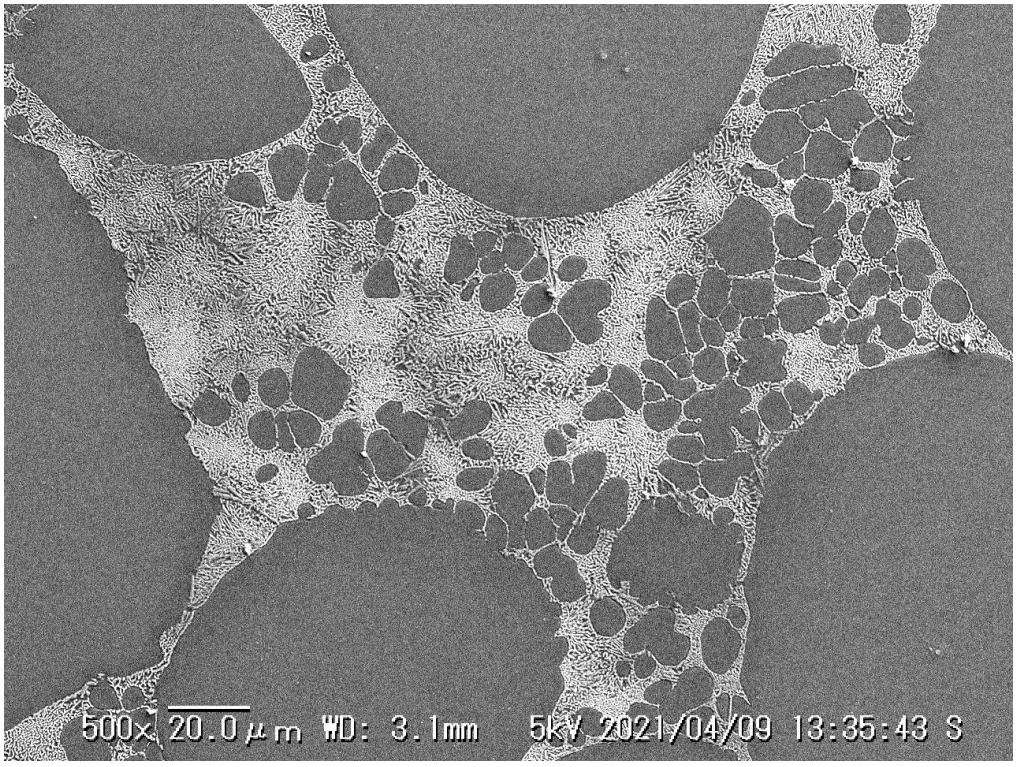


(d)

Continued

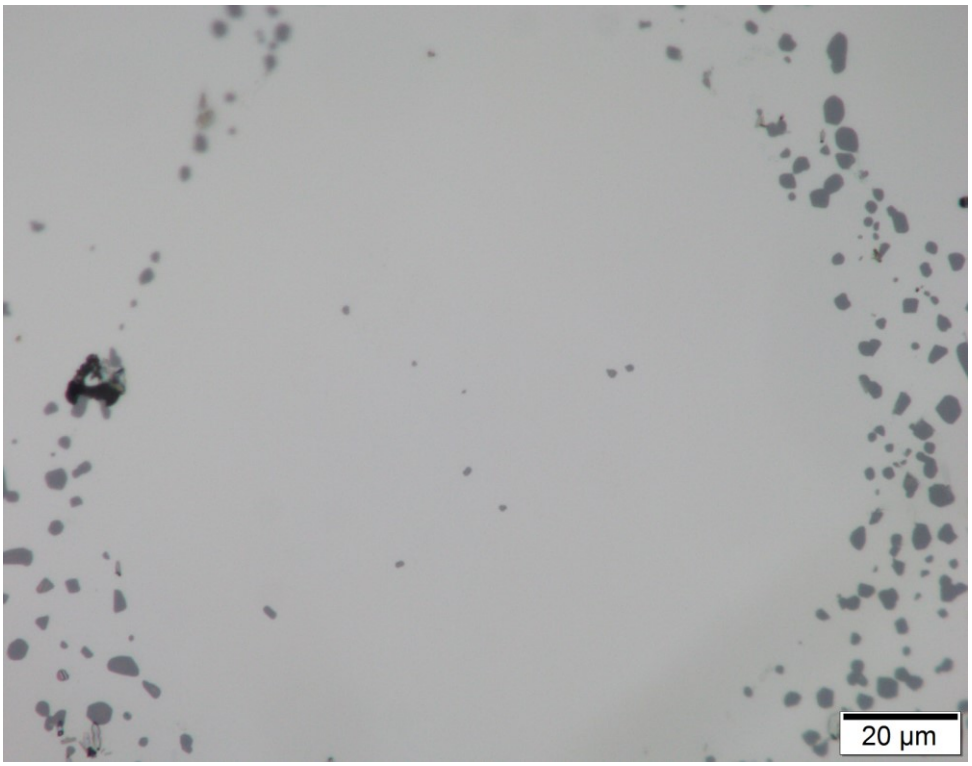


(a)

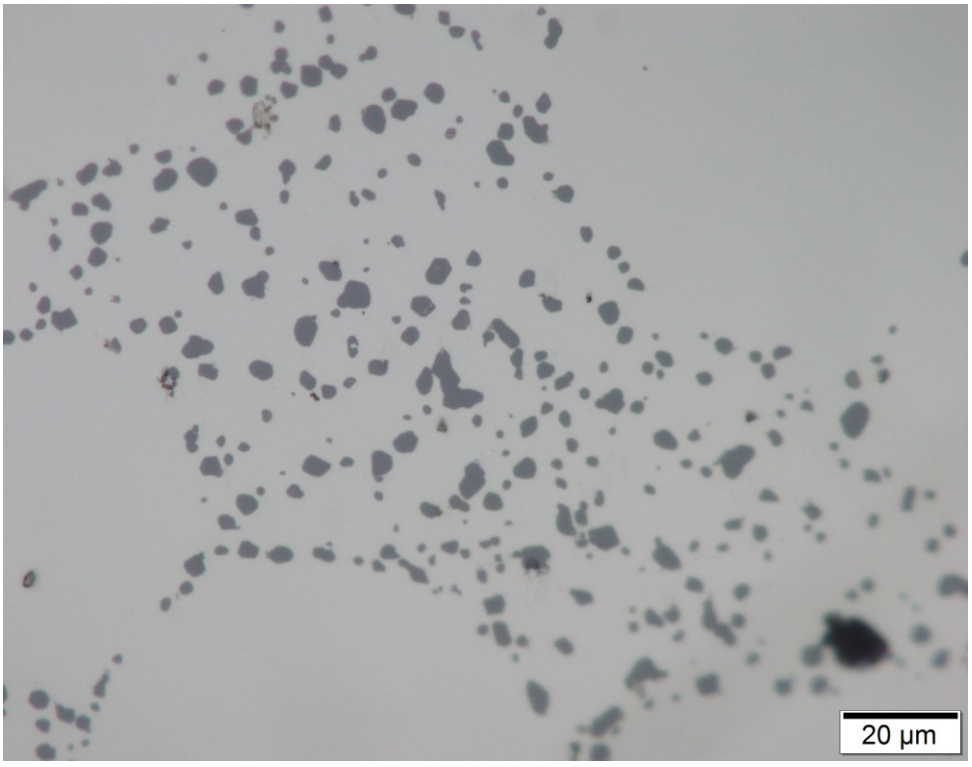


(b)

Fig. 2-10. SEI observation of the as-cast specimen etched by Weck's reagent.

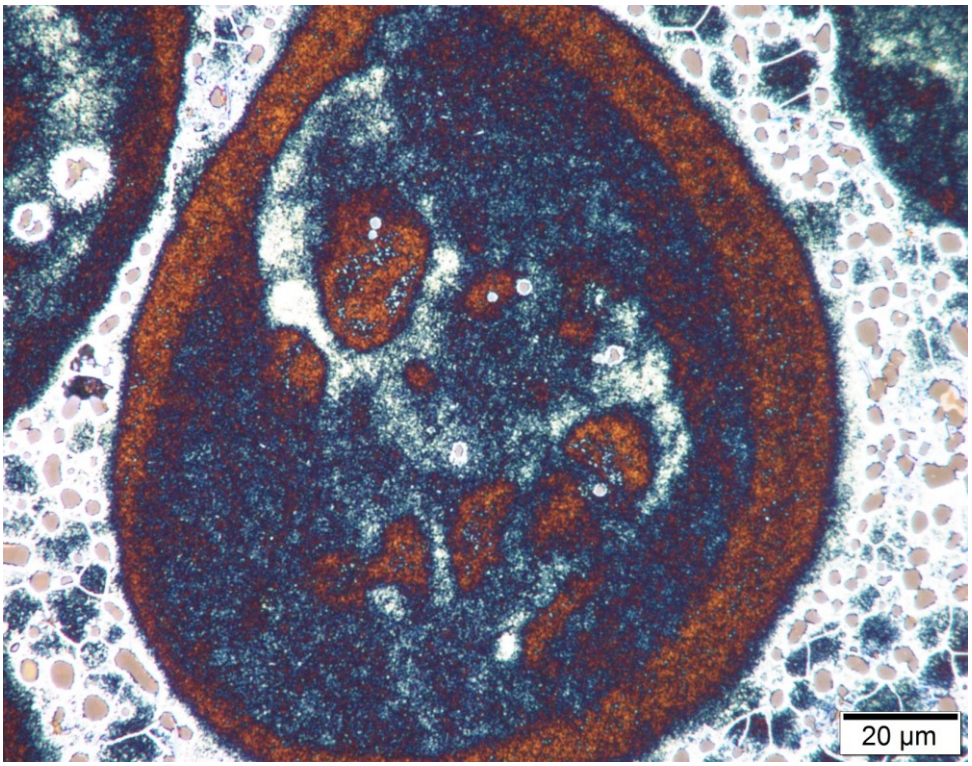


(a)



(b)

Fig. 2-11. Optical micrographs of the solution-treated specimen (a) and (b): without etching, (c) and (d): etched by Weck's reagent.

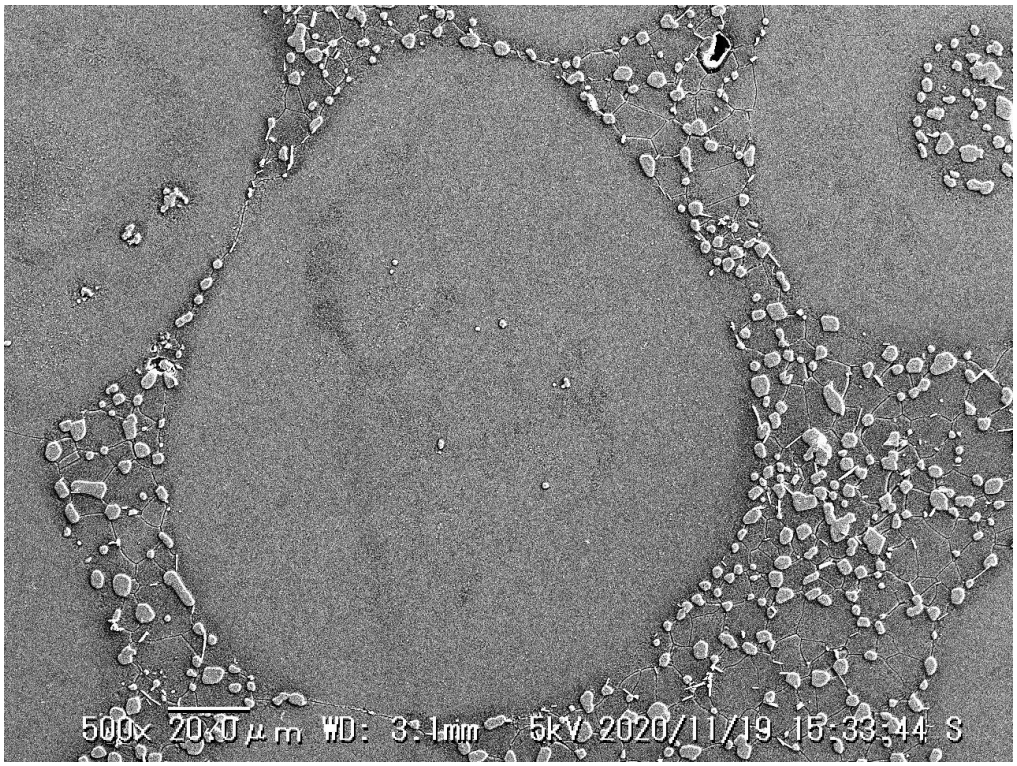


(c)

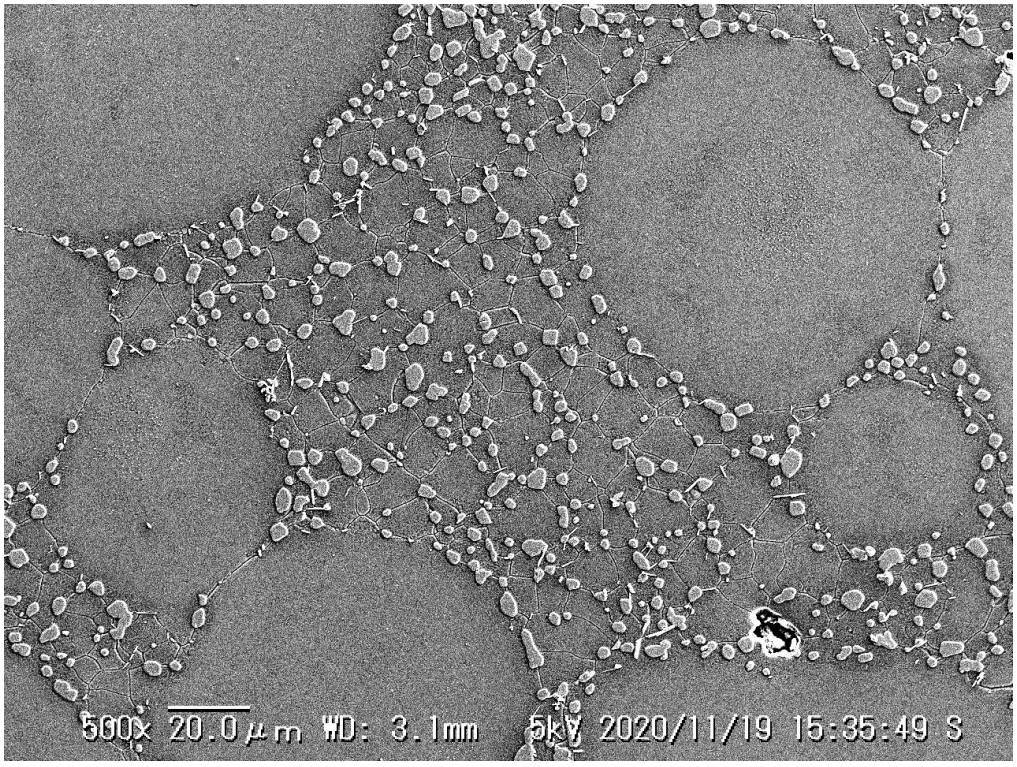


(d)

Continued



(a)



(b)

Fig. 2-12. SEI observation of the solution-treated specimen etched by Weck's reagent.

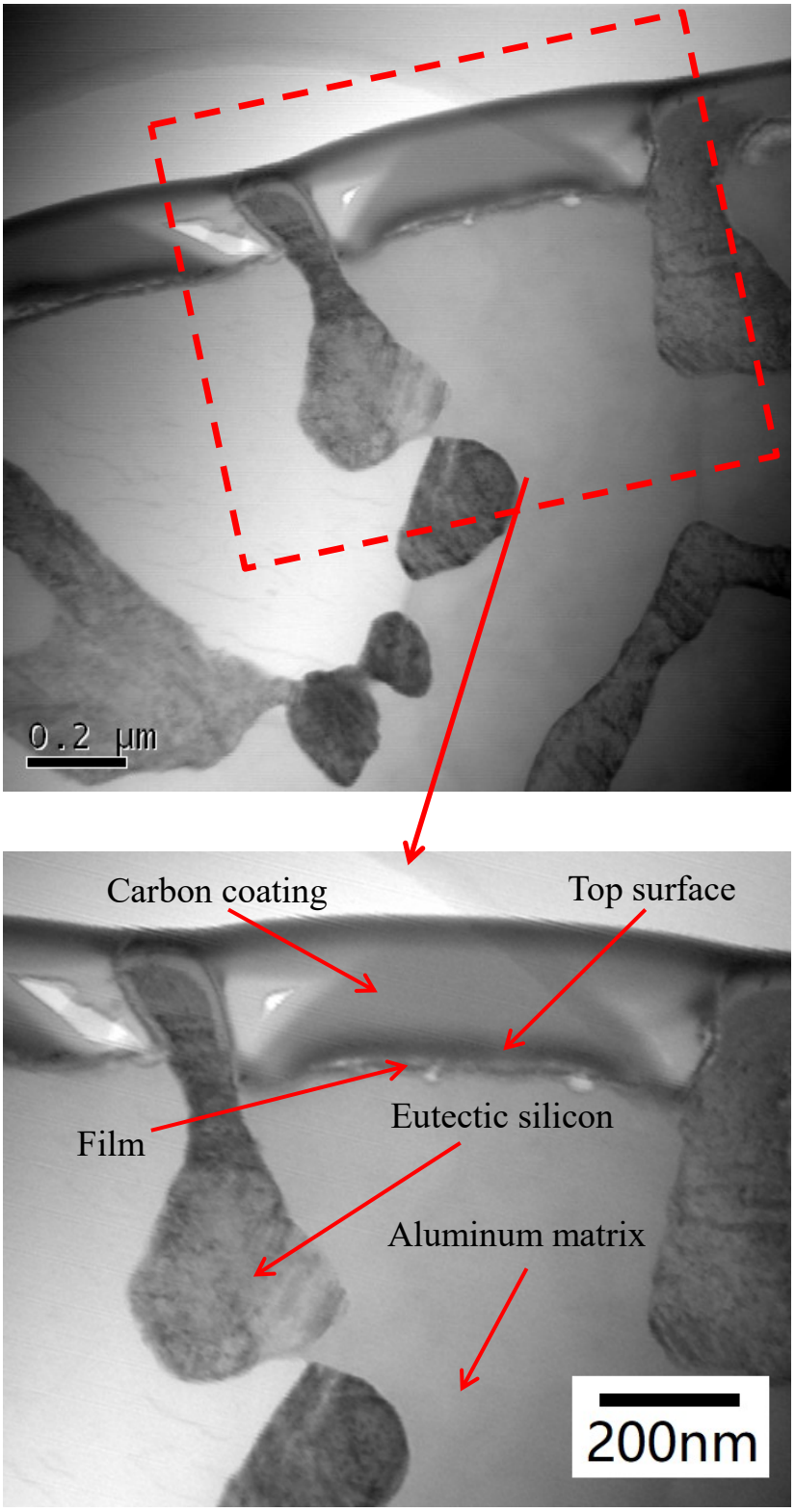


Fig. 2-13. Cross-section of the eutectic solidified region of as-cast specimen observed by STEM.

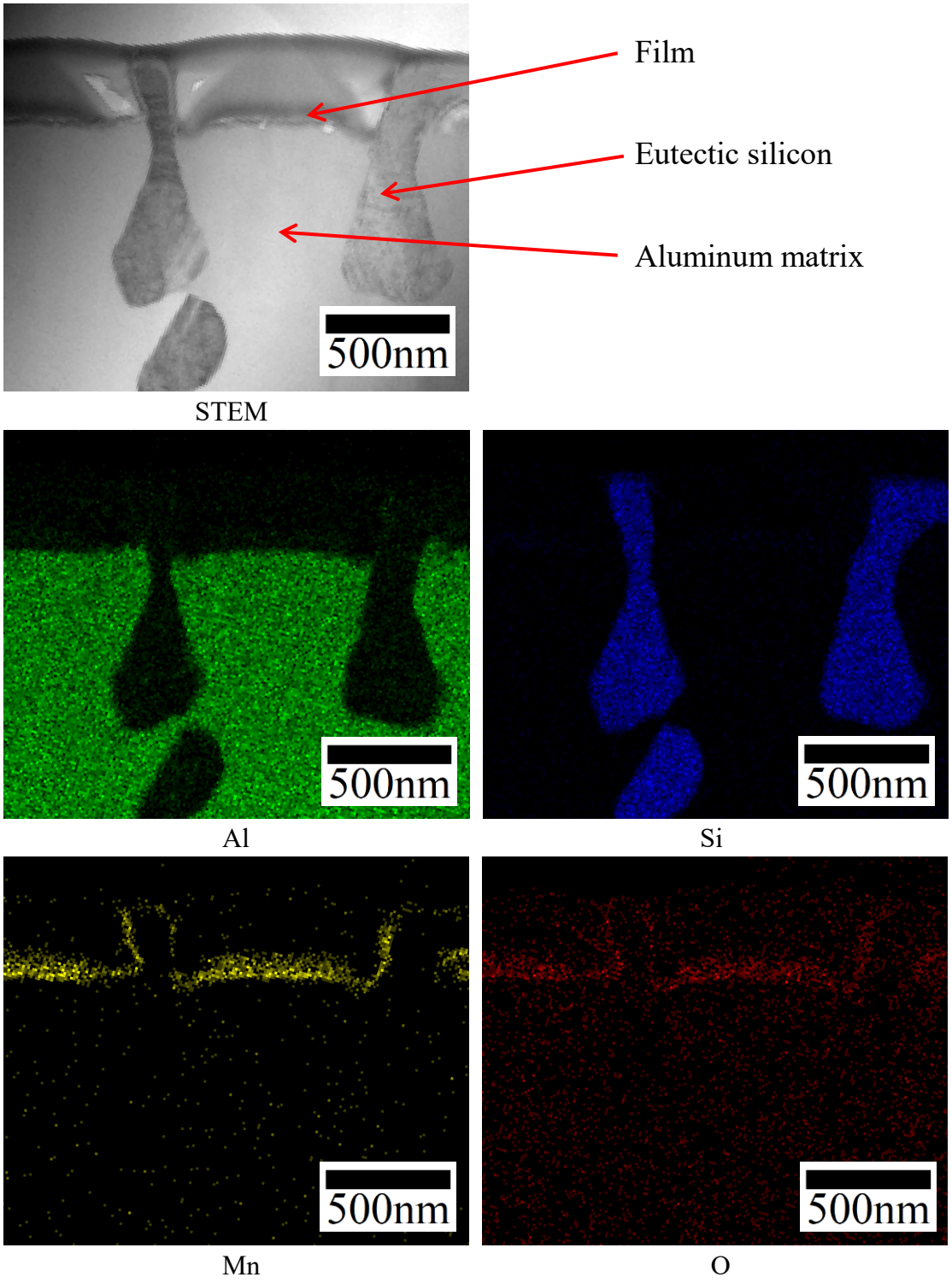


Fig. 2-14. Composition analysis of as-cast specimen by STEM equipped with EDS.

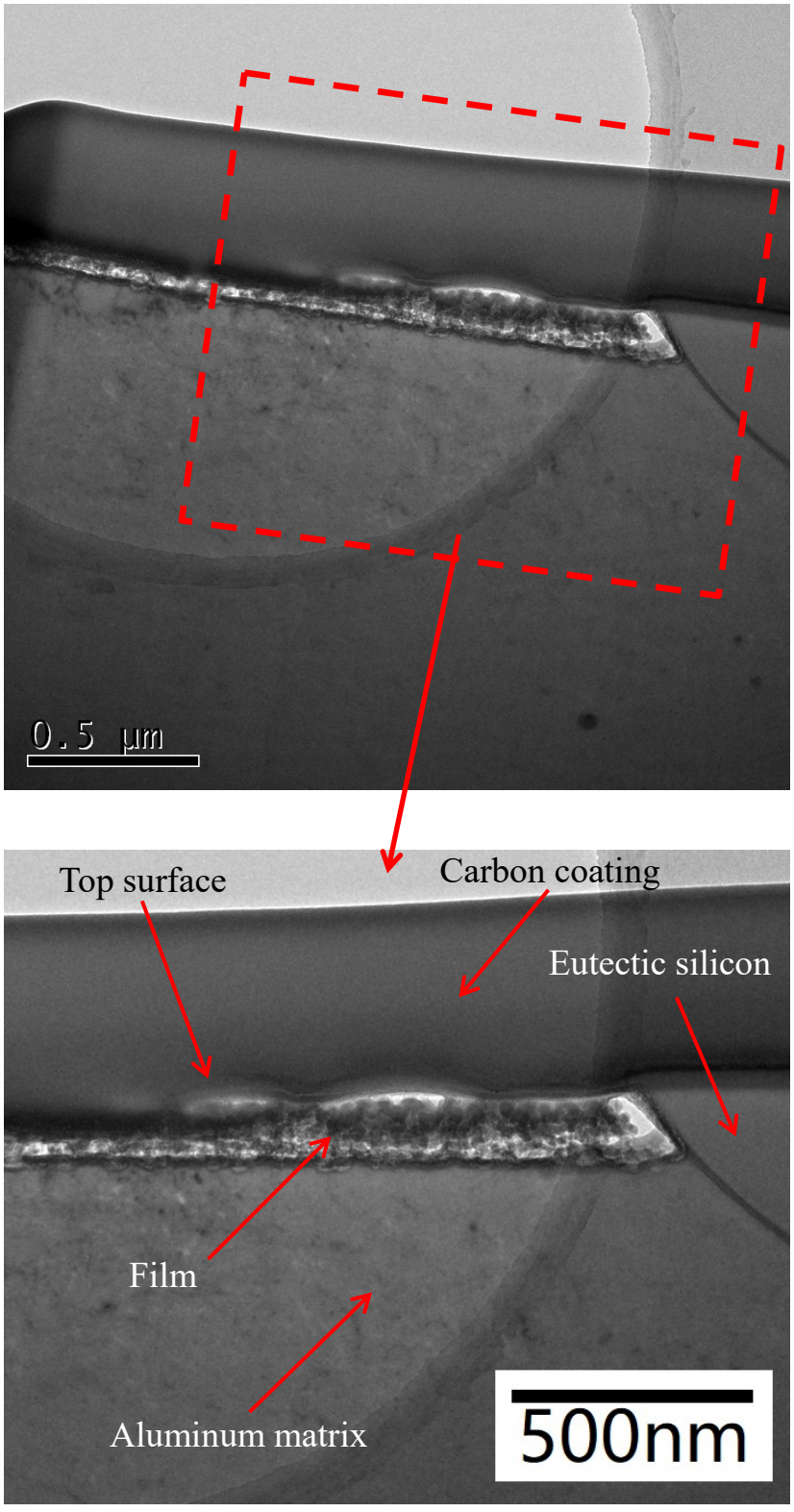
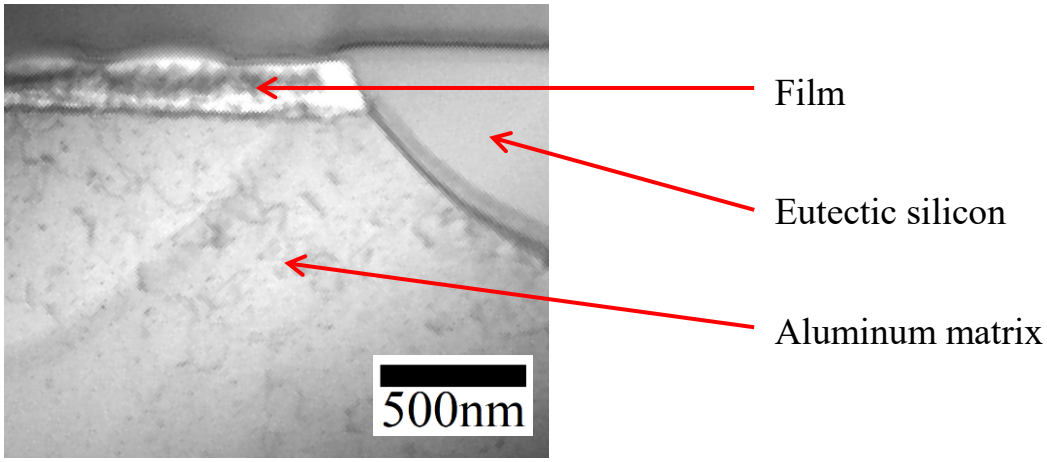
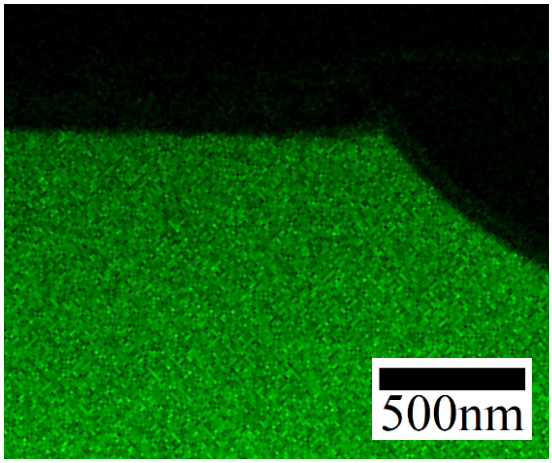


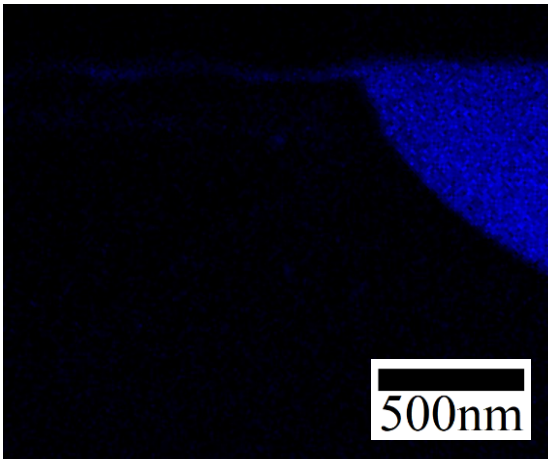
Fig. 2-15. Cross-section of the eutectic solidified region of solution-treated specimen observed by STEM.



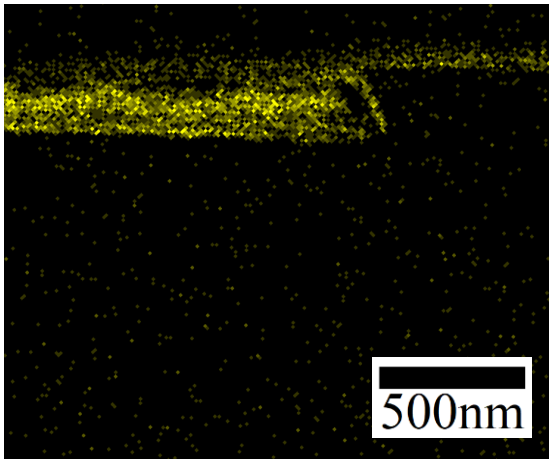
STEM



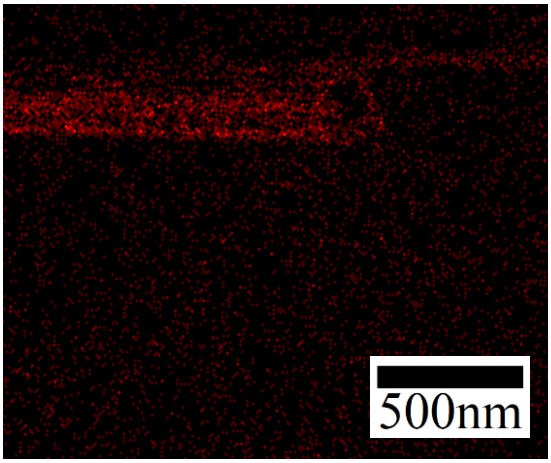
Al



Si



Mn



O

Fig. 2-16. Composition analysis of solution-treated specimen by STEM equipped with EDS.

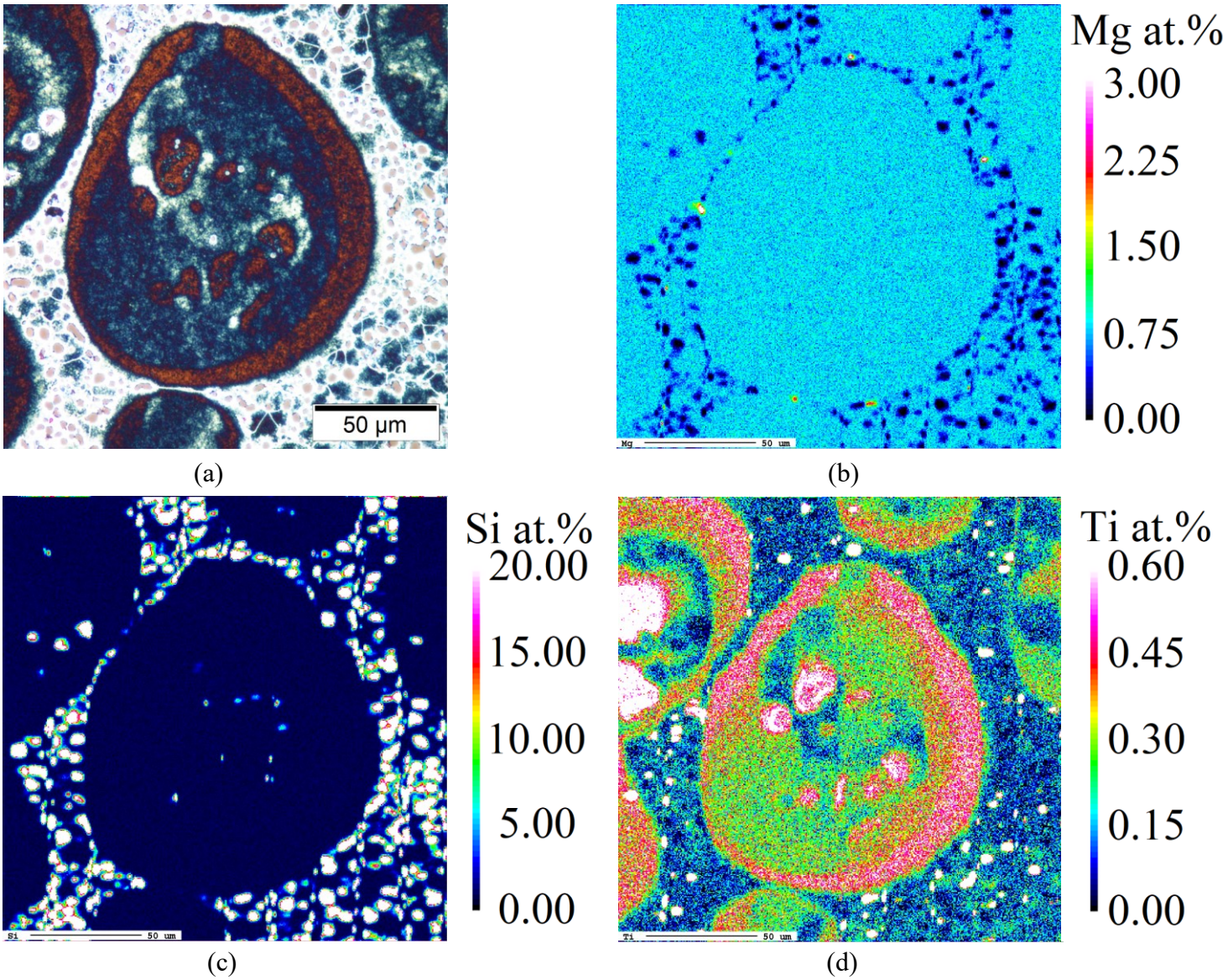


Fig. 2-17. Optical micrograph of the large primary α-Al grain etched by Weck's reagent (a) and results of EPMA analysis, (b) Mg, (c) Si, (d) Ti.

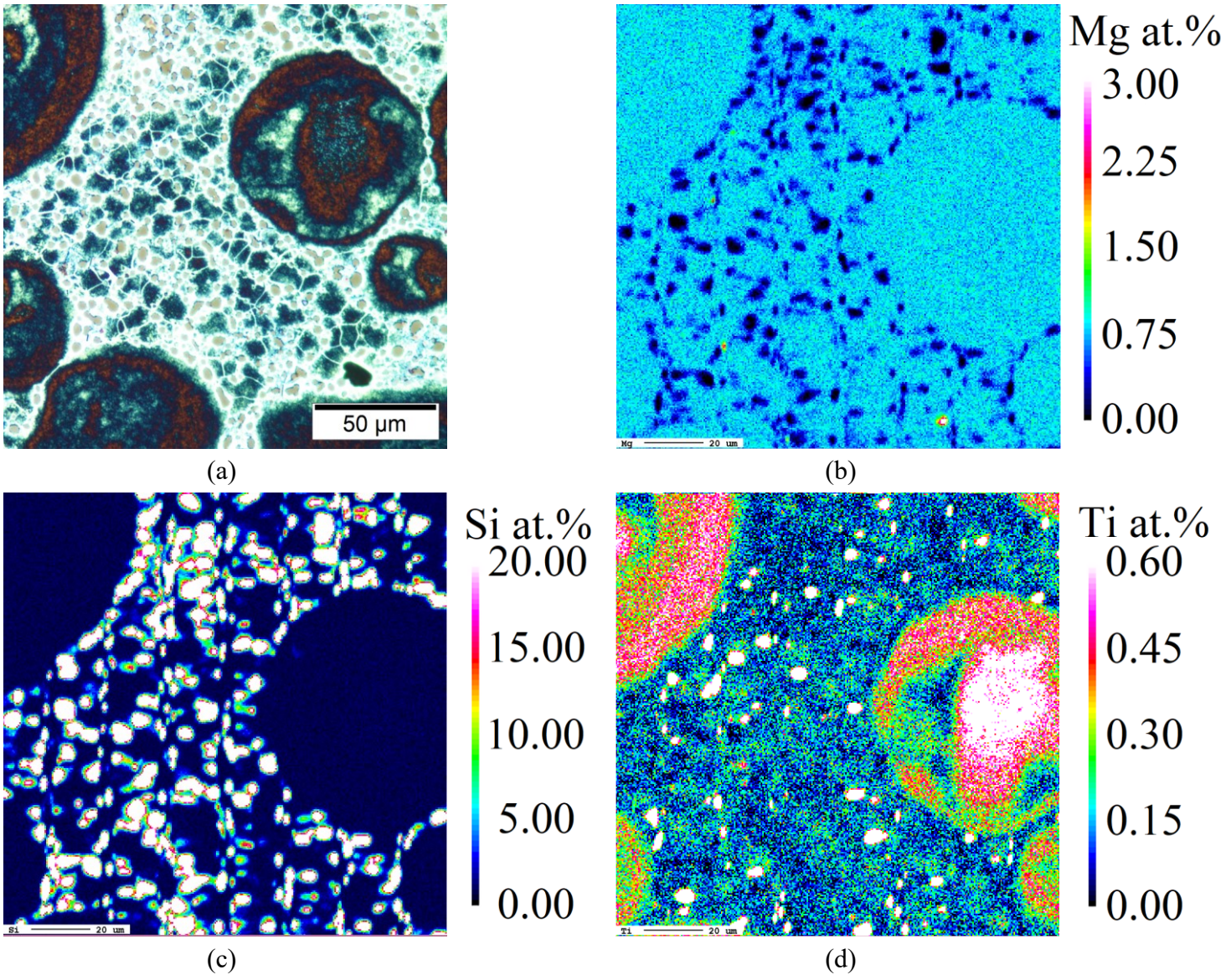
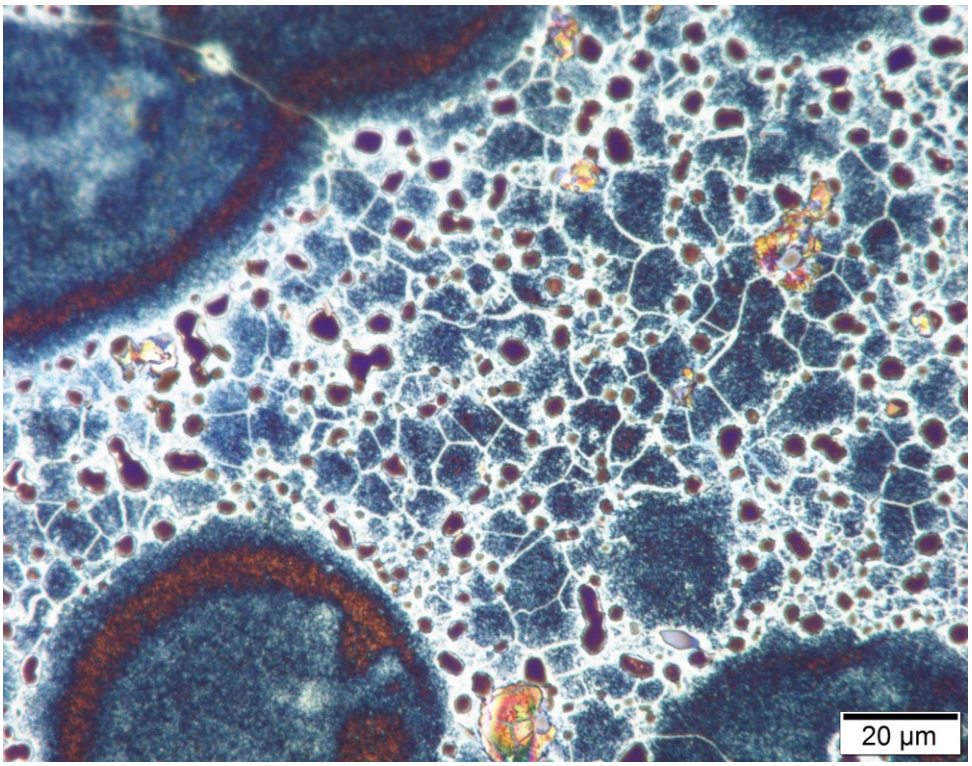
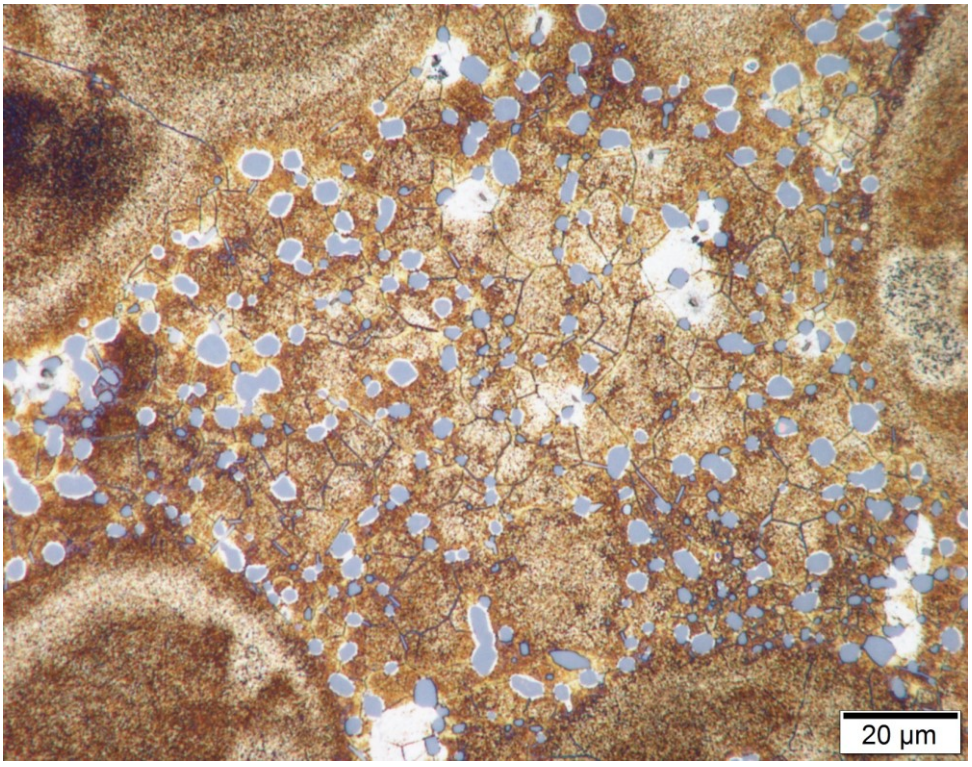


Fig. 2-18. Optical micrograph of the eutectic region etched by Weck's reagent (a) and results of EPMA analysis, (b) Mg, (c) Si, (d) Ti.

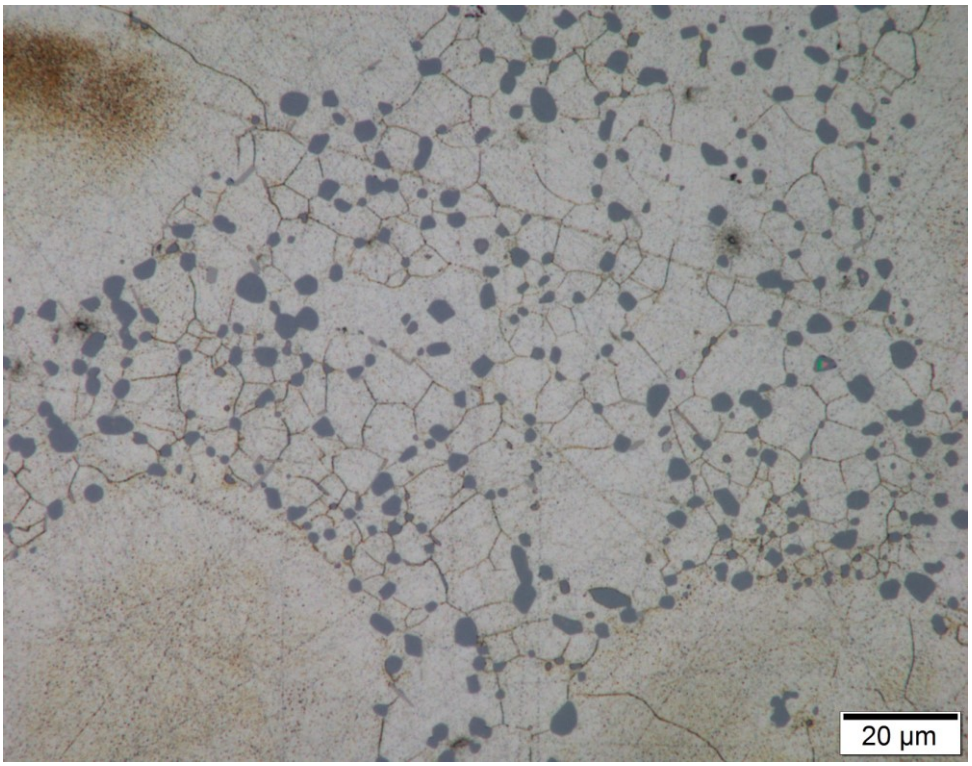


(a)

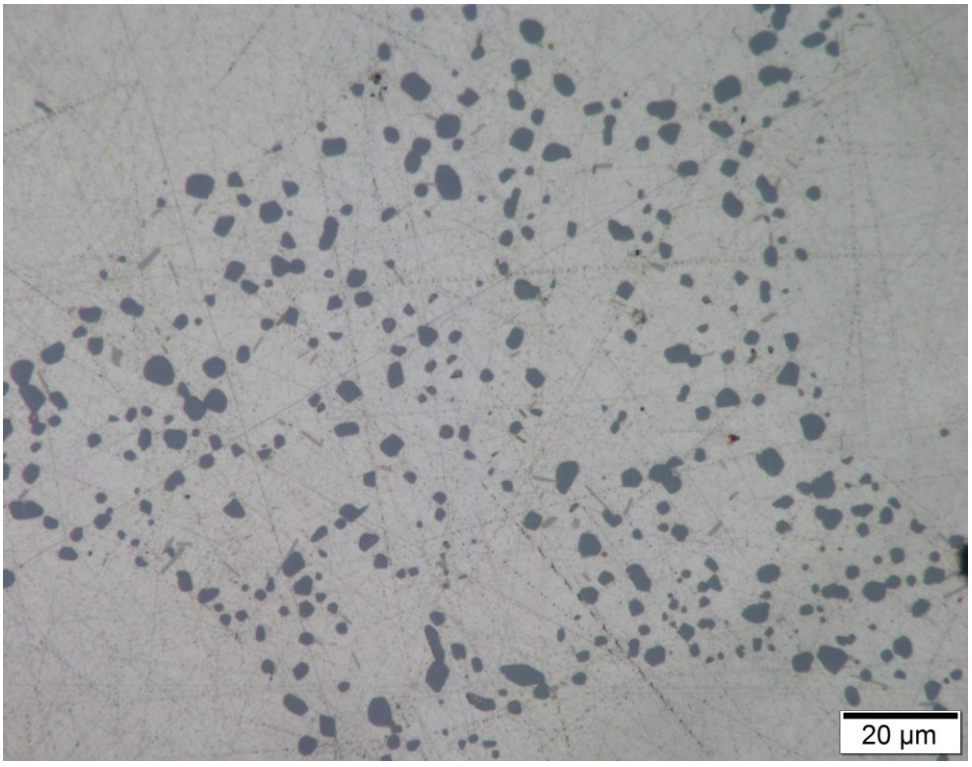


(b)

Fig. 2-19. Microstructure of the solution-treated specimen etched by Weck's reagent (a) as-etched, (b) polished for 60 s, (c) polished for 180 s and (d) polished for 300 s.



(c)



(d)

Continued

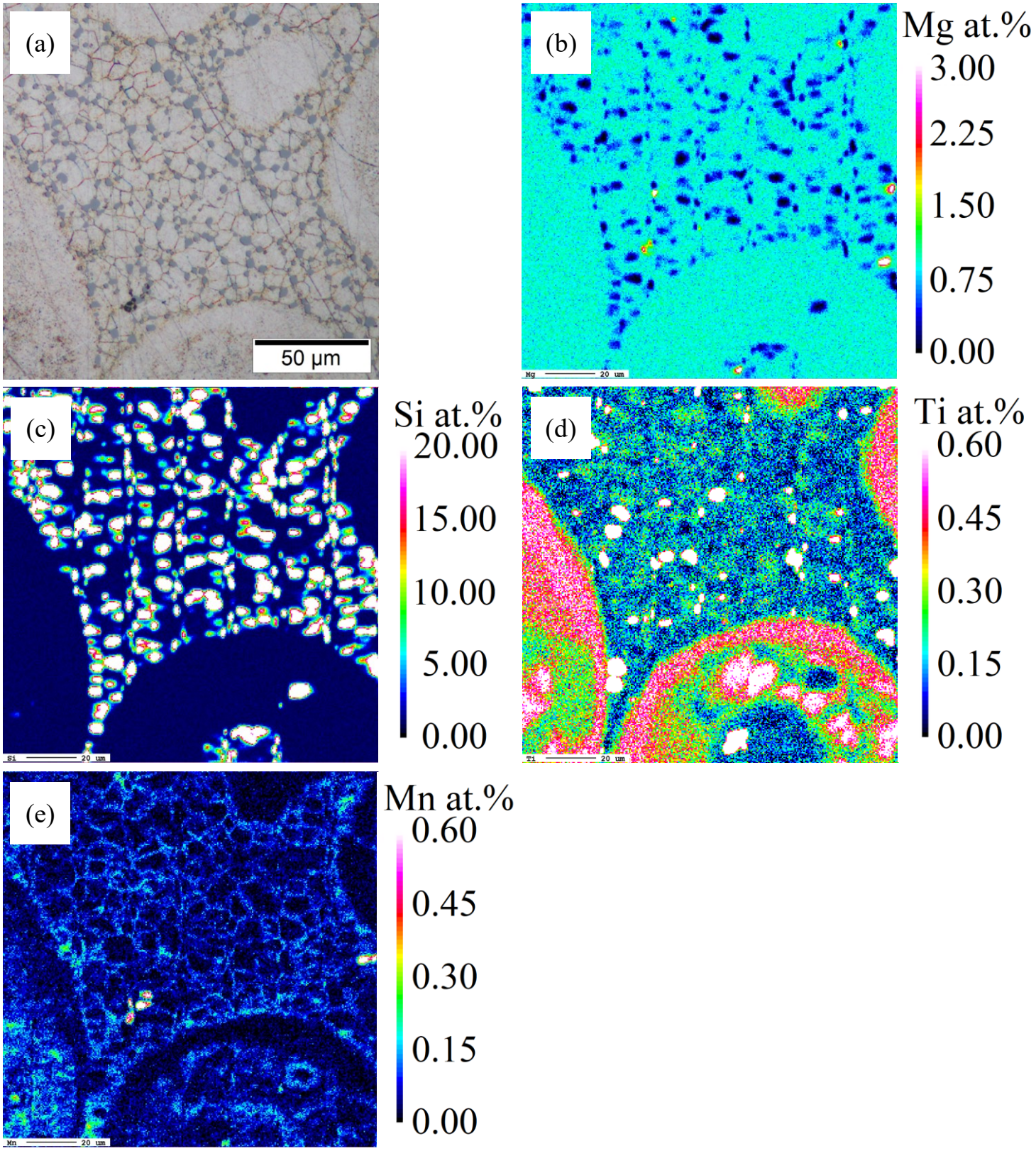
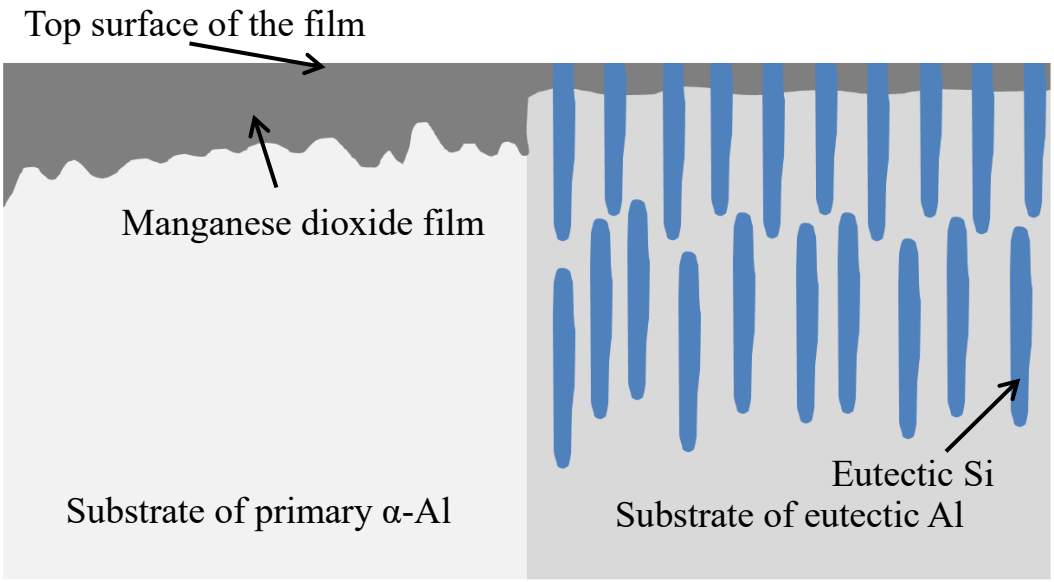
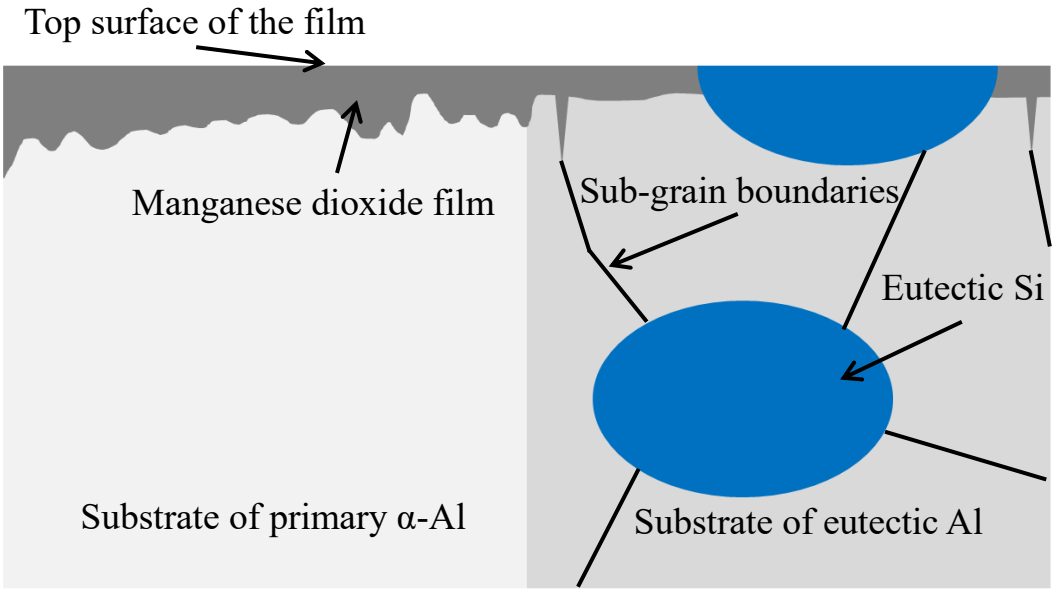


Fig. 2-20. Optical micrograph of the eutectic region etched by Weck's reagent (a) and results of EPMA analysis, (b) Mg, (c) Si, (d) Ti and (e) Mn.



(a)



(b)

Fig. 2-21. Schematic illustration showing the cross-section of the specimen (a) before and (b) after solution treatment etched by Weck's reagent

Chapter 3

Effect of etching time and temperature on coloration by Weck's reagent

3.1. Introduction

Understanding of the coloring mechanism by Weck's reagent is important for us to utilize the Weck's reagent effectively for the microstructure analysis of cast aluminum alloys.

In order to obtain the distinctive color contrast, Gao et al. [1, 2] examined the influence of etching time on the color contrast. At first the reproducibility of the color revealed by Weck's reagent was examined by repeating the same etching for four times by the same etching condition, as shown in Fig 3-1. The results confirmed that Weck's reagent has good reproducibility to revealed characteristic color for aluminum alloy, and the stable color contrast was obtained every time. Then the specimens were etched for 4 s, 8 s, 12 s, 20 s and 28 s at room temperature, and it was revealed that 12 s was the best condition to obtain the most distinctive color contrast, as shown in Fig 3-2.

However, the etchant temperature was not controlled precisely in their study. According to Suárez-Peña et al.'s research [3] and others researches concerning the chemical activity of aluminum [4, 5] and the

permanganate conversion coating on aluminum alloy [6], when aluminum alloy is etched by Weck's reagent, a manganese dioxide film is formed via the following reaction:

$$Al + MnO_4^- + 2\ H_2O \rightarrow Al(OH)_4^- + MnO_2$$

The temperature of the etchant must be one of the important factors controlling the color contrast. Therefore, in this chapter, the influence of the etching conditions (not only etching time but also etchant temperature) was investigated.

3.2. Experimental

3.2.1. Material and preparation of semi-solid slurry

The material used in this research is the same A356 aluminum alloy used in chapter 2. Chemical composition is given again in Table 3-1. In order to induce plastic deformation, the billet was compressed at the room temperature. Then the compressed billet was heated to the semi-solid state. When the temperature reaches 595 °C, the billet was die-cast. A number of small cubic specimens with 8×8×5 mm^3 were collected from the die-cast product. Some of them were solution-treated at 535 °C for 8 h and aged at 155 °C for 6 h.

3.2.2. Microstructure observation

The cubic specimens were ground using 120, 600, 1000, 2000 and 4000 grit paper, polished using 3, 1 μm diamond paste and OPS colloidal silica. The as-cast specimens were etched many times at the etchant temperature of 15, 20, 25 and 30 °C for various etching time from 8 to 16 s. The color revealed by Weck's reagent is very sensitive to the local composition difference. Therefore, the influence of the etching conditions should be investigated for the exactly the same microstructure. In order to keep the same microstructure, the specimen surface was polished very very slightly by using a 1 μm diamond paste for 180 to 300 s to remove only the etching layer produced by the prior etching. After etching, a micrograph of exactly the same location was taken by an optical microscope. The solution-treated specimen was also etched several times at 10, 15, 20 and 25 °C for 12 s in the same way.

3.2.3. Characterization of the surface morphology by scanning electron microscopy

Based on the coloring mechanism proposed by Gao et al. [1, 2], the top surface of the manganese dioxide film formed by Weck's reagent is flat in atomic scale, but the thickness and the roughness of the bottom surface change location to location. This means that the color difference mainly results from the height difference of the aluminum substrate and

the roughness of the aluminum substrate surface. SEI images taken by scanning electron microscope were used to characterize the etched substrate surface condition (height difference and roughness). The accelerating voltage was set at 5 kV. Different locations in a single spheroidal aluminum grain and the eutectic region were chosen for evaluating the substrate surface topography.

3.3. Results

3.3.1. Influence of the etchant temperature on the coloration of as-cast specimen etched for 8 s

As shown in Fig. 3-3, the difference in etchant temperature causes a big change in color. No color change was observed in the primary α-Al grains at 15 °C. Primary α-Al grains were dyed a little at 20 °C. At 25 °C, the colors in the primary α-Al grains became a little bit darker but the contrast was not so strong. The etching result at 30 °C was approximately the same with 25 °C.

Fig. 3-4 shows that SEI images exhibiting the surface topography of the specimens etched at different etchant temperature for 8 s. The surface topography in the large primary α-Al grains was generally flat regardless of the difference in etchant temperature.

3.3.2. Influence of the etchant temperature on the coloration of as-cast specimen etched for 12 s

Fig.3-5 shows the results obtained at the etchant temperature of 15, 20, 25 and 30 °C for 12 s. In this case, difference in etchant temperature caused a big change in color. There is still no obvious color in the primary α-Al grains at 15 °C. The primary α-Al grains were dyed with darker color at 20 °C. Characteristic color differences were visible in the primary α-Al grains at 25 °C. It was as in the primary α-Al grains at 30 °C too. However, the color contrast at 30 °C was weaker than that of 25 °C. These results suggest that the 25 °C and 12 s are the best for the etching temperature and etching time, respectively, to obtain the clearest color contrast.

Fig. 3-6 shows the SEI images exhibiting the surface topography of the specimens etched at different etchant temperature for 12 s. The surface topography in the large primary α-Al grains was approximately flat at 15 °C. At 20 °C, same differences were observed, but the difference in topography was not so obvious. The difference in topography increases at 25 °C. And it is in accordance with the best color contrast in the optical micrographs' as shown in Fig. 3-5 (c). The topography difference decreased at 30 °C.

3.3.3. Influence of the etchant temperature on the coloration of as-cast specimen etched for 16 s

As shown in Fig. 3-7, the difference in etchant temperature caused a big change in color for the etching time of 16 s. There were a few light colors in the primary α-Al grains at 15 °C. The colors in the primary α-Al grains became darker at 20 °C. However, the contrast was not so strong. The colors in the primary α-Al grains did not change, but the color in the eutectic solidified region became dark at 25 °C. The color contrast in the primary α-Al grains further decreased and the ring-shaped region became dark at 30 °C.

Fig. 3-8 shows the SEI images exhibiting the surface topography corresponding to the as-cast specimens etched at different temperature for 16 s. At 15 °C, a few differences were observed in topography in the large primary α-Al grains. The difference in topography in the large primary α-Al grains increased a little but still not obvious at 20 °C. At 25 °C, a local change in topography was observed clearly. The difference in topography at 30 °C was approximately the same as at 25 °C.

3.3.4. Influence of the etchant temperature on the coloration of the solution-treated specimen

The solution-treated specimens were etched at 10, 15, 20 and 25 °C for 12 s. As shown in Fig. 3-9, the difference in etchant temperature

caused a big change in color in this case, too. At 10 °C, the etching result was similar to the as-cast specimen etched at 15 °C for 8 s. There was almost no color in the large primary α-Al grains. Characteristic color differences were visible in the large primary α-Al grains at 15 °C. The peculiar network structure in the eutectic solidified region was also observed. At 20 and 25 °C, the characteristic color differences were also detected in the primary α-Al grains. However, basic colors of the microstructure turned green and brown and the clear color contrast disappeared. Consequently, it was found that 15 °C was the best etching temperature for the solution-treated specimens.

Fig. 3-10 shows the SEI images exhibiting the surface topography at various etchant temperatures. The surface topography in the large primary α-Al grains was approximately flat at 10 °C. The peculiar network structure was not observed in the eutectic solidified regions. The difference in the topography in the large primary α-Al grains increases and provided the best contrast in height in the micrograph at 15 °C. The eutectic solidified region also exhibited the peculiar network structure. This is in good accordance with the best color contrast in the optical micrographs' as shown in Fig. 3-9 (c) and (d). The difference in topography in the large primary α-Al grains decreased at 20 and 25 °C. The peculiar network structure in the eutectic solidified region was not observed.

3.3.5. Comparison of the coloration of the as-cast and solution-treated specimen etched with different etching conditions

The temperature-time chart of color contrast of the as-cast specimen etched with different etching conditions was shown in Fig. 3-11. The results showed that the color contrast revealed by Weck's reagent was controlled by both etching time and etchant temperature. The etching time couldn't be too short or too long even the etchant temperature was adjusted. The best etching condition to obtain the best color contrast in the as-cast semi-solid die-cast A356 aluminum alloy is the etching time of 12 s and the etchant temperature of 25 °C.

The temperature-time chart of color contrast of the solution-treated specimen etched with different etching conditions at different locations was shown in Fig. 3-12. The best coloring condition changes with the micro-segregation in the aluminum substrate. The best etching condition to obtain the best color contrast in the solution-treated semi-solid die-cast A356 aluminum alloy is the etching time of 12 s and the etchant temperature of 15 °C.

3.4. Discussion

3.4.1. Chemical reactions during etching process and its relationship with the etching conditions

As mentioned in the chapter 1, by the etching with Weck's reagent, the substrate (Al) reacts with MnO_4^- ions, and produces a manganese dioxide film on the etched surface. This mechanism is called "conversion coating". Gao et al. [1, 2] confirmed the existence of the manganese dioxide film by the composition analysis of STEM and EDS. The optical micrographs and SEI images of the specimen surface etched by Weck's reagent, as shown in Fig. 3-5 (c) and 3-6 (c), suggest that the coloration of the etched surface by Weck's reagent has a strong correlation with the surface topography. According to Gao et al.'s research [1, 2], the top surface of the manganese dioxide film is flat in atomic scale. In contrast, the interface between the bottom surface of the manganese dioxide film and the top surface of aluminum substrate is rough. The color of manganese dioxide film is basically light brown and the roughness of the interface between the bottom surface of the film and the aluminum substrate is influenced the brightness of the brown color.

3.4.2. Origin of different color contrast in the as-cast specimen and the effect of etching condition

The roughness of the aluminum substrate, namely the "interface" between the bottom surface of manganese dioxide film and aluminum substrate is closely related to the coloring behavior. The height difference and the roughness of aluminum substrate surface observed by SEI are

important information to estimate the film morphology, since the top surface of the film is flat in atomic scale.

For the as-cast specimen etched for 8 s, no obvious color appeared in the large primary α-Al grains at low temperature of 15 °C (Fig. 3-3 (a)), probably due to the insufficient progress in chemical reaction between the aluminum substrate and Weck's reagent. The large primary α-Al grains were dyed with a little, but the contrast was still weak at 20 °C (Fig. 3-3 (b)). This suggests that the aluminum substrate reacted with Weck's reagent and produced the manganese dioxide film, but the interface between the bottom surface of the manganese dioxide film and the top surface of aluminum substrate was also approximately flat. The result is in agreement with the observed surface topography by SEI (Fig. 3-4 (b)). At the increased temperatures of 25 and 30 °C, the colors in the large primary α-Al grains changed. However, the contrast was still weak (Fig. 3-3 (c) and (d)). This may be due to the fact that the thickness of the manganese dioxide films increased, but the bottom surface of the manganese dioxide film was kept still flat. The result is also in agreement with the topography of the aluminum substrate observed by SEI (Fig. 3-4 (c) and (d)). The schematic illustration showing the effect of etchant temperature on the morphological change in film for 8 s is shown in Fig. 3-13.

For the as-cast specimen etched for 12 s, there is still no obvious

color appeared in the large primary α-Al grains at low temperature of 15 °C (Fig. 3-5 (a)). As discussed before, the longer etching time cannot produce the sound film due to the insufficient progress in chemical reaction between the aluminum substrate and Weck's reagent. At the etchant temperature of 20 °C, the chemical reaction of the substrate with Weck's reagent went well, the color in the large primary α-Al grains became obvious (Fig. 3-5 (b)). This is due to the increase in interface roughness as shown in Fig. 3-6 (b). The color in the eutectic solidified region was also different from that at 15 °C. This may result from the progress in film formation in this area. Etching at 25 °C provided the best color contrast (Fig. 3-5 (c)). This is because the difference in film thickness as well as roughness of the aluminum substrate from location to location was enhanced. This corresponds to the large difference in topography, as shown in Fig. 3-6 (c). The color contrast in the large primary α-Al grains decreased at 30 °C. The color of the eutectic solidified region also became darker. This may suggest that the interface between the bottom surface of the film and the top surface of aluminum substrate became flat at an elevated temperature. The effect of etchant temperature for 12 s is shown in Fig. 3-14.

As for 16 s, a color in the large primary α-Al grains was pale at 15 °C (Fig. 3-7 (a)). The etching time was relatively long, but the temperature was low to activate the chemical reaction. In contrast, at

20 °C, the chemical reaction between the aluminum substrate and Weck's reagent went well and a good color contrast was obtained, as shown in Fig. 3-7 (b). The interface between the bottom surface of the film and the top surface of aluminum substrate, namely the morphology of the film, changed from location to location reflecting the local solute segregation. At 25 and 30 °C shown in Fig. 3-7 (c) and (d), there was no obvious change in contrast in the large primary α-Al grains. This suggests that the local difference in morphology of the film reduced due to the long reaction time. SEI images as shown in Fig. 3-8 (c) and (d), revealed that the differences in topography took place in some localized area and this resulted in the formation of sharp steps. The schematic illustration showing the change of film morphology for 16 s etching is given in Fig. 3-15.

The schematic illustrations (Fig. 3-13, Fig. 3-14 and Fig. 3-15) indicate that 8 s etching is not enough for producing the manganese dioxide films with sufficient thickness. While, the etching time for 16 s is too long for producing the manganese dioxide films with local change in morphology and thickness, since the reaction temperature is high. 12 s etching is good for producing the manganese dioxide films with a large local change in morphology and thickness.

Consequently, we can say that the etching time couldn't be too short or too long even at the most suitable etchant temperature. The etchant

temperature directly influences the chemical reaction to form the manganese dioxide film by convention coating mechanism. The color contrast is strongly influenced by the roughness of the interface morphology between the film and the aluminum substrate. The difference in etchant temperature changed the roughness of the interface morphology between the film and the aluminum substrate drastically. The growth rate of the film increased as increasing the etchant temperature. The adequate etchant temperature is useful to form the film with large local thickness difference and roughness. When the etchant temperature is too high, difference in thickness and roughness of the bottom surface of the film become small. This results in the similar coloration in the optical micrograph. The combination of etchant temperature of 25 °C and the etching time of 12 s was the best etching condition to obtain the best color contrast in the as-cast semi-solid die-cast A356 aluminum alloy.

3.4.3. Origin of different color contrast in the solution-treated specimen and the effect of etching condition

As mentioned in chapter 2, the solution-treated specimen showed the different color contrast compared to the as-cast specimen. These differences come from the change in solute distribution in the large spheroidal α-Al grains and the formation of boundaries of recrystallized grains in the eutectic solidified region by the solution treatment. Gao et al.

reported that the film's morphology affected by the local distribution of the solute elements [1, 2]. Therefore, the most suitable etching condition should be different from that of as-cast specimen. The optical micrographs (Fig. 3-9) and SEI images (Fig. 3-10) of the solution-treated specimens show that the etchant temperature affect on the etching result in this case, too. When the solution temperature is low, such as 10 °C, only a pale color was observed sporadically in the large spheroidal α-Al grains (Fig. 3-9 (a)). The growth of film is seemed to be poor considering from the flat topography as shown in SEI images of Fig. 3-10 (a). At 15 °C, the chemical reaction between the aluminum substrate and Weck's reagent was considered to go well and the best color contrast was obtained (Fig. 3-9 (b)). The peculiar network structure in the eutectic region was clearly observed in the SEI images as shown in Fig. 3-10 (b). The film thickness as well as the interface roughness is considered to be different from location to location with respect to the change of the local concentration of solute elements. But at higher etchant temperature of 20 and 25 °C (Fig. 3-10 (c) and (d)), the color contrast in the large primary α-Al grains gradually disappeared and the peculiar network structure in the eutectic region was not observed, either. This suggests that the interface between the film and the substrate became flat. The schematic illustrations, indicating the change in film morphology of the solution-treated specimen are shown in Fig. 3-16. The best contrast was

obtained at 15 °C for 12 s. The most suitable etchant temperature depends on the solute elements distribution.

The etchant temperature influences the formation of manganese dioxide film and change the roughness of the interface between film and aluminum substrate. The formation rate of the film in the solution-treated specimen seems to be faster than that of as-cast specimen. The etchant temperature of 15 °C was the best condition to produce the largest thickness difference in the film and the largest local morphological change from location to location for the solution-treated specimen.

3.5. Conclusions

In this chapter, the influence of etching conditions (etching time and etchant temperature) on the color contrast revealed by Weck's reagent was examined. As-cast and solution-treated specimens were etched by Weck's reagent with different etching conditions and the change in surface topography of the etched specimens was also characterized by SEI observation. The results showed that the color contrast revealed by Weck's reagent was very sensitive to both etching time and etchant temperature. The as-cast specimen was etched at 15 to 30 °C for 8 to 16 s. The etching time couldn't be too short or too long, and the etchant temperature couldn't be too low or too high too. The etching condition for

the best color contrast was at 25 °C for 12 s. The solution-treated specimen was etched at 10 to 25 °C for 12 s, the etchant temperature at 15 °C provided the best color contrast.

The surface topography is in strong correlation with the color difference revealed by Weck's reagent. The morphology of the manganese dioxide film formed during etching corresponds to the etching depth and roughness of the etched aluminum substrate.

The best coloring condition (etching time and etching temperature) changes depending on the micro-segregation in the aluminum substrate since the thickness and morphology of the manganese dioxide film were controlled by the local distribution of the solute elements.

References

[1] L. Gao, Y. Harada, S. Kumai, Microstructural characterization of aluminum alloys using Weck's reagent, part I: Applications, Mater Charact. 107 (2015) 426-433.

[2] L. Gao, Y. Harada, S. Kumai, Microstructural characterization of aluminum alloys using Weck's reagent, part II: Coloring mechanism, Mater Charact. 107 (2015) 434-452.

[3] B. Suárez-Peña, J. Asensio-Lozano, G.F. Vander-Voort, Colour metallography in commercial Al-Si alloys. Optimization of the microstructural characterization techniques in light optical microscopy, Rev. Metal 46(2010) 469-476.

[4] H.P. Godard, W.P. Jepson, M.R. Bothwell, R.L. Kane, The corrosion of light metals, John Wiley and Sons, New York, 1967.

[5] M. Pourbaix, Aluminium atlas of electrochemical equilibrium in aqueous solutions, Pergamon, Oxford, 1966.

[6] S.A. Kulinich, A.S Akhtar, P.C. Wong, K.C. Wong, K.A.R. Mitchell, Growth Of Permanganate Conversion Coating On 2024-Al Alloy, Thin Solid Films 515 (2007) 8386-8392.

Table 3-1 Chemical compositions of A356 alloy used in this chapter (mass%).

Si	Mg	Fe	Ti	Sr	Mn	Al
6.90	0.39	0.10	0.14	0.025	<0.10	Bal.

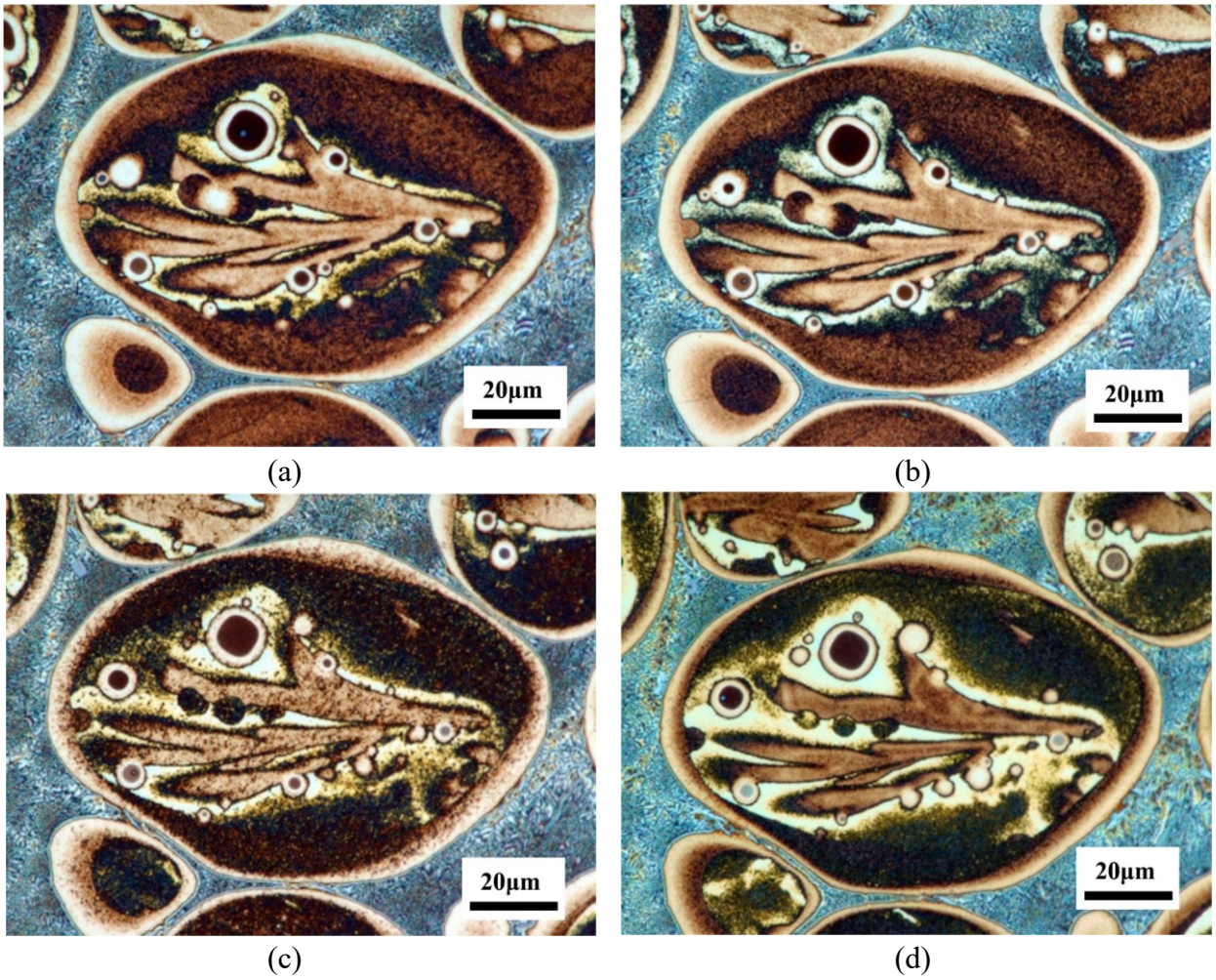


Fig. 3-1. Repeating etching using Weck's reagent for four times with the same etching time of 12 s [1].

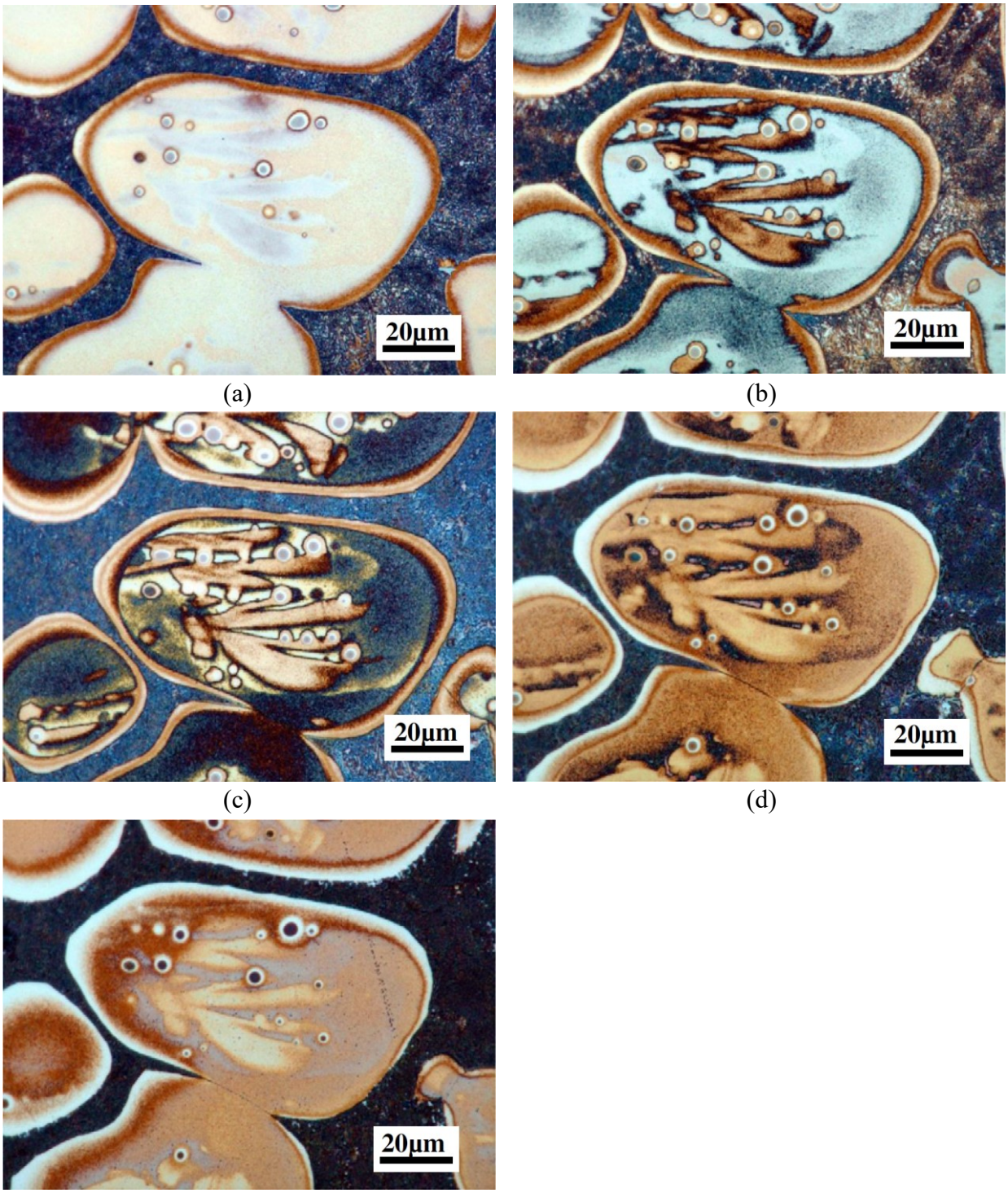
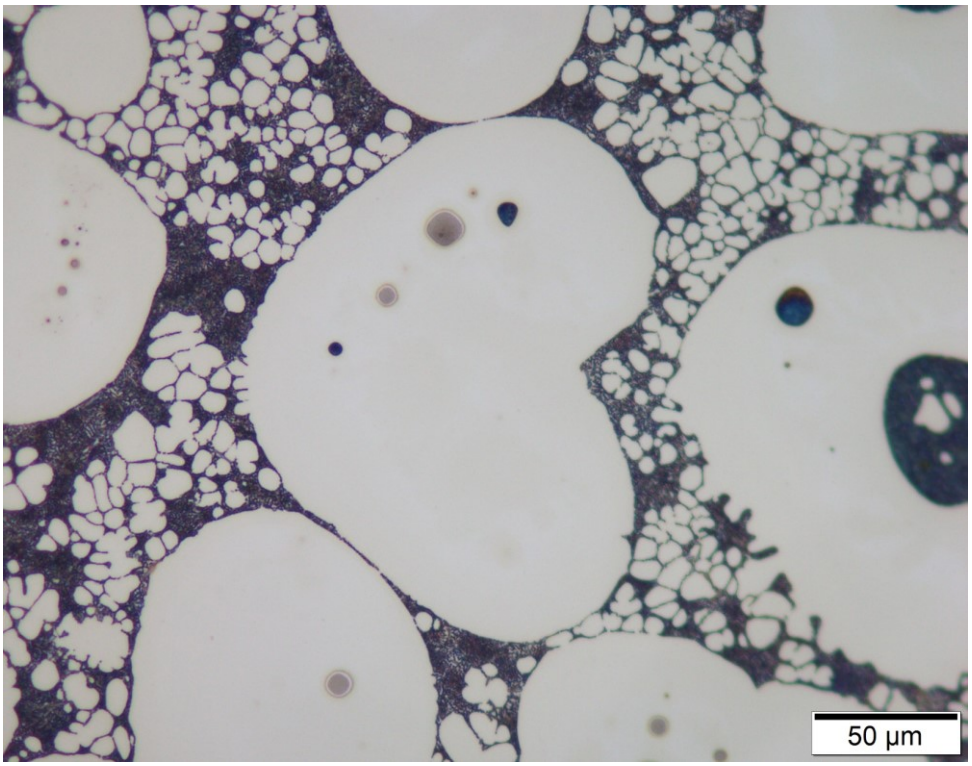
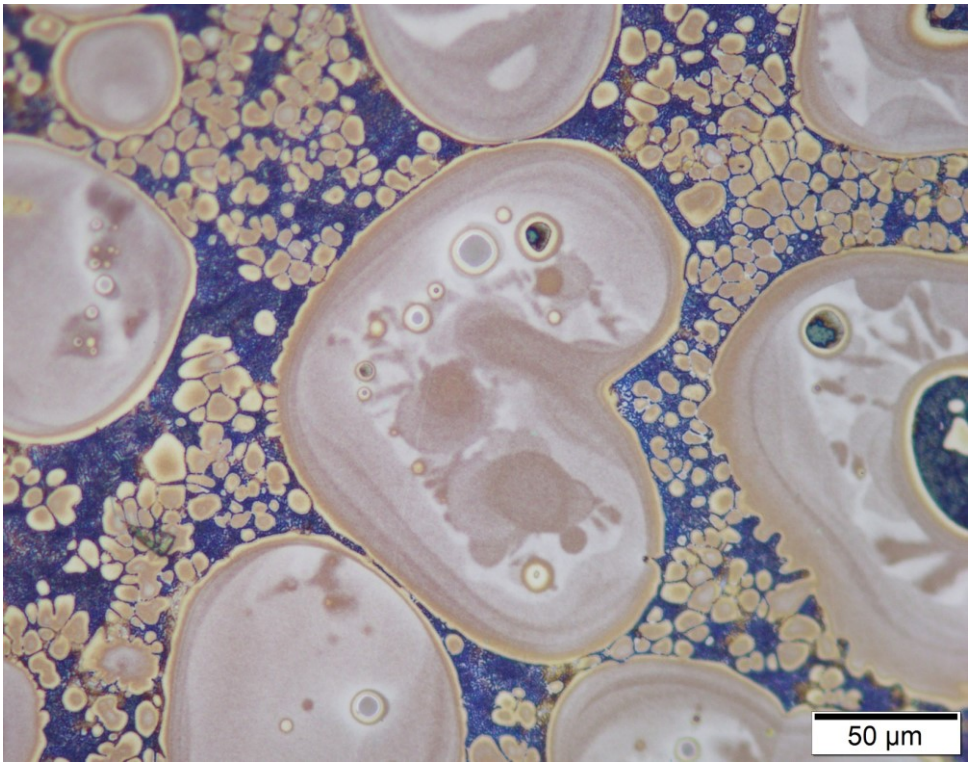


Fig. 3-2. Microstructures of A356 aluminum alloy specimen etched for (a) 4 s, (b) 8 s, (c) 12 s, (d) 20 s and (e) 28 s at room temperature [2].

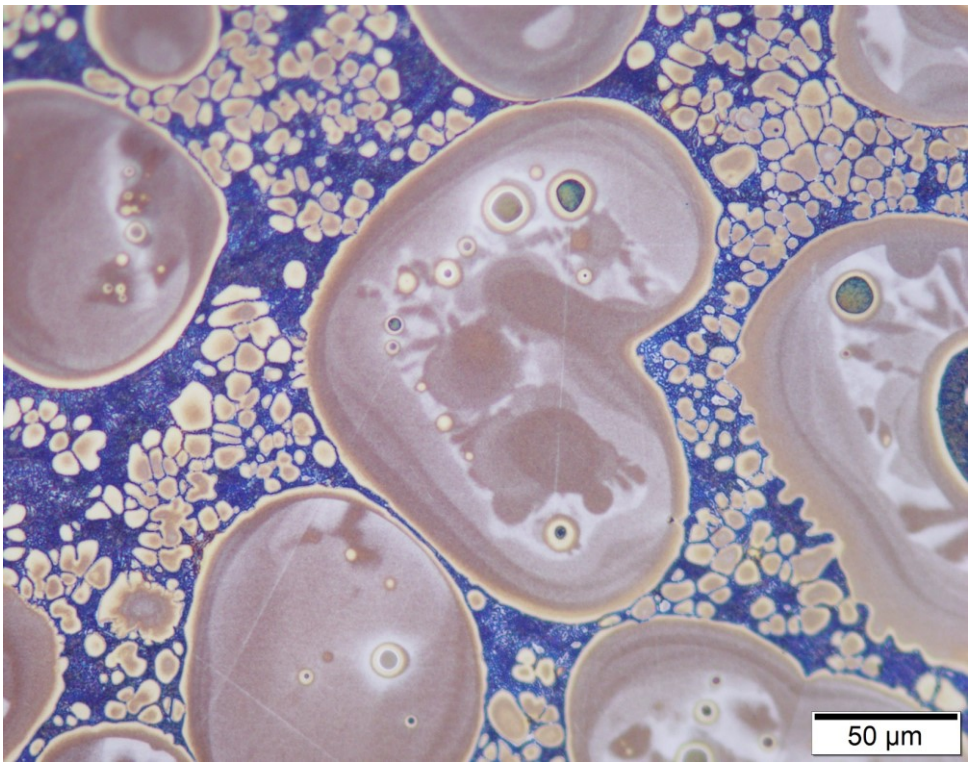


(a)

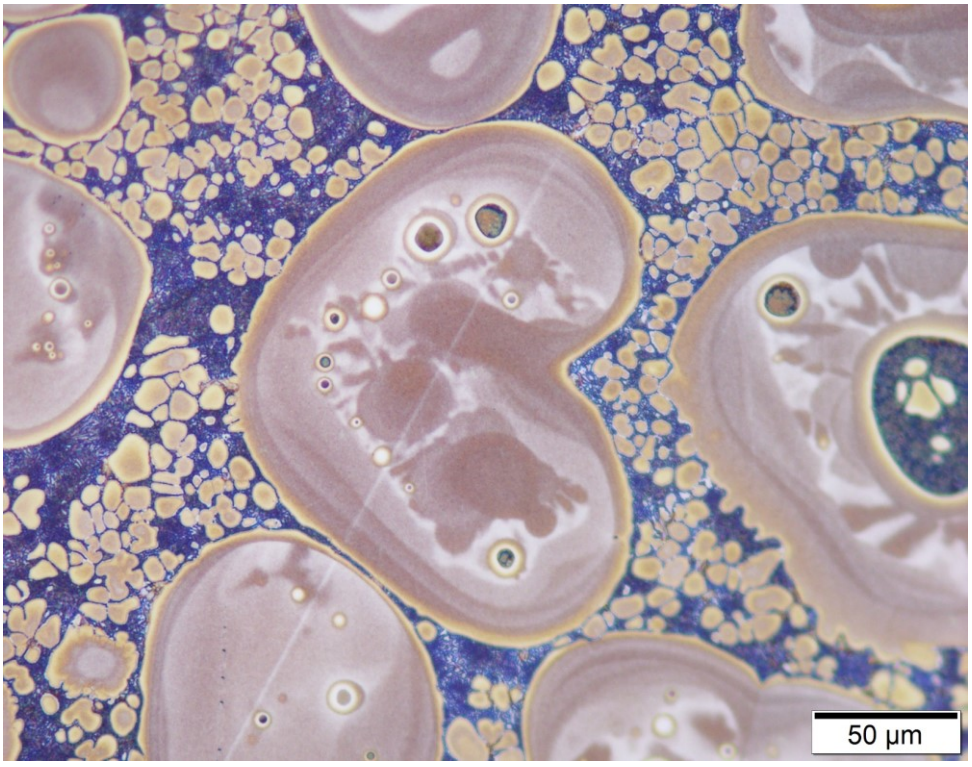


(b)

Fig. 3-3. Optical micrograph of the as-cast specimen etched by Weck's reagent with the etchant temperature of (a) 15 °C, (b) 20 °C, (c) 25 °C and (d) 30 °C for 8s.

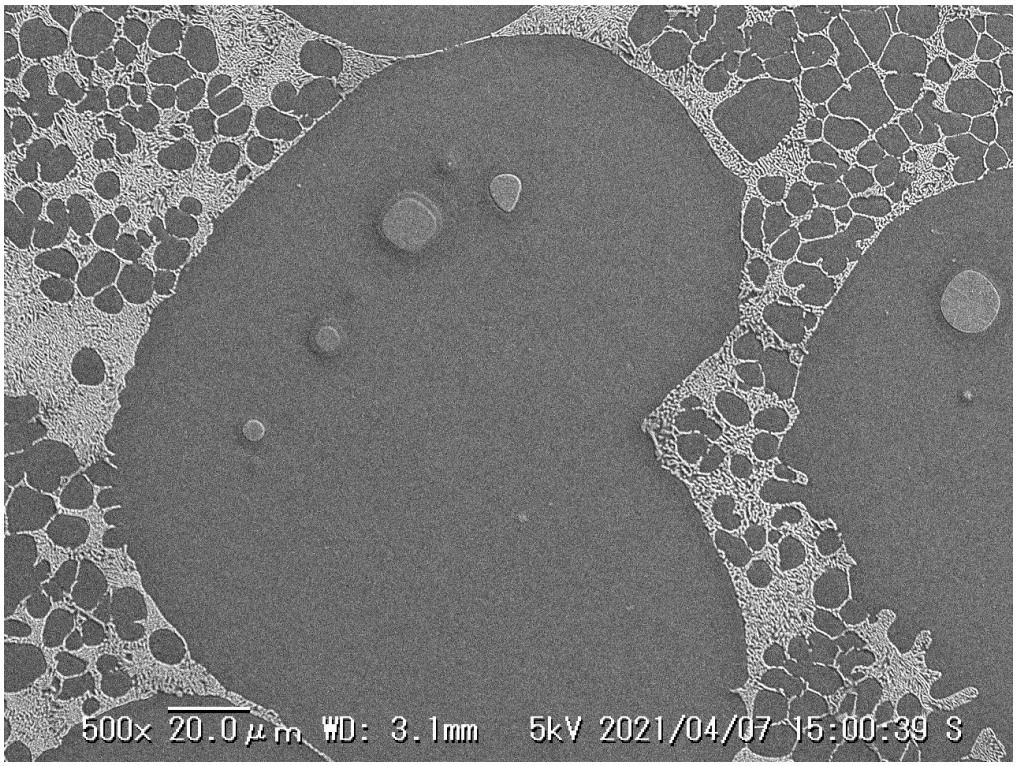


(c)

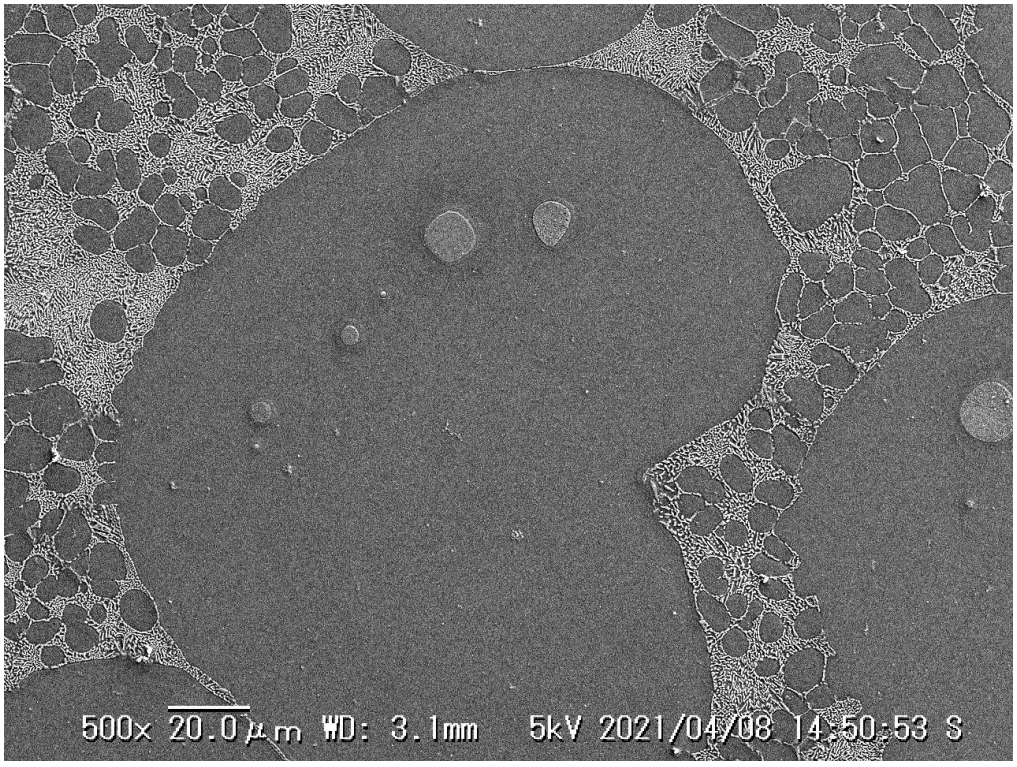


(d)

Continued

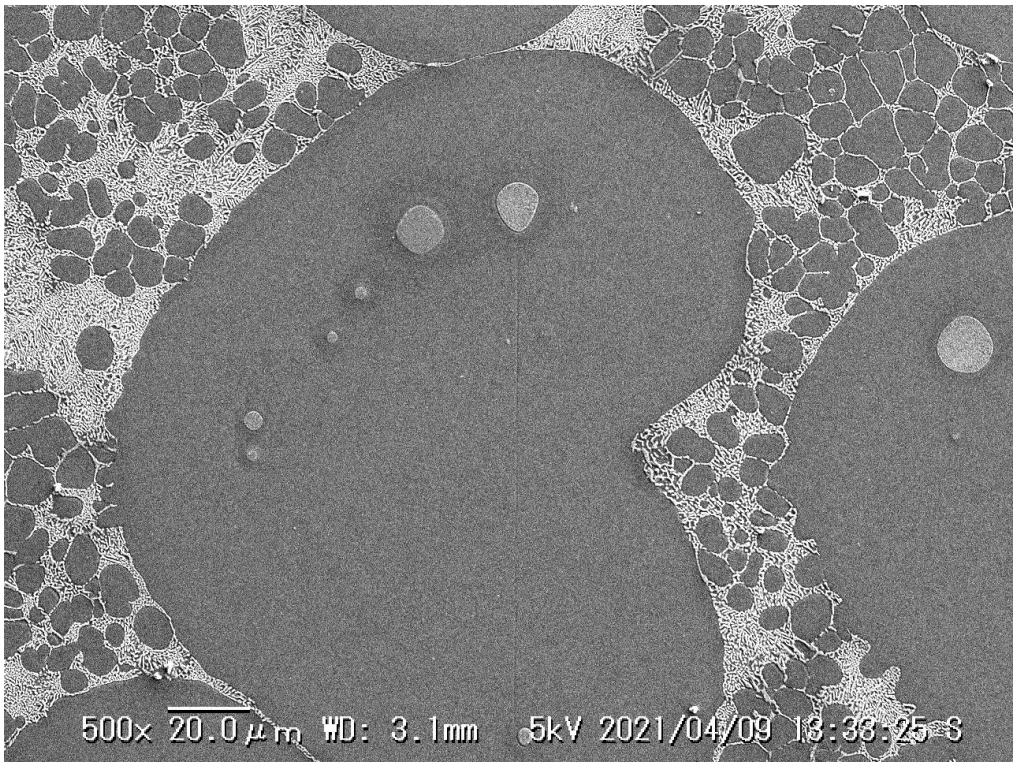


(a)

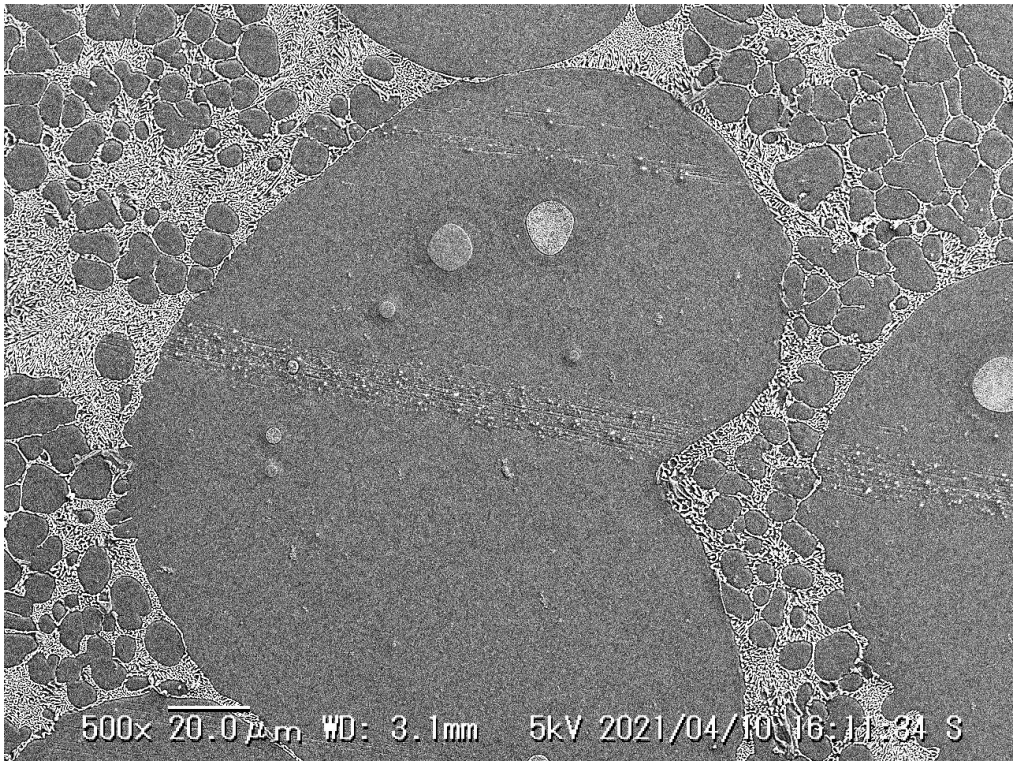


(b)

Fig. 3-4. SEI image of the as-cast specimen etched by Weck's reagent with the etchant temperature of (a) 15 °C, (b) 20 °C, (c) 25 °C and (d) 30 °C for 8s.

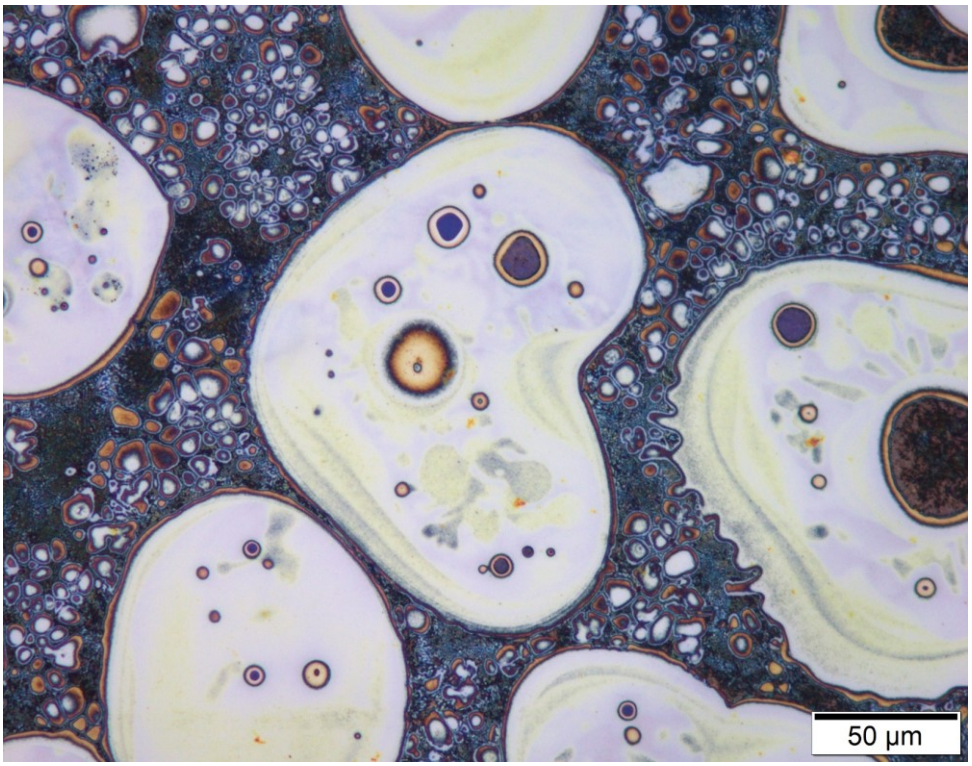


(c)

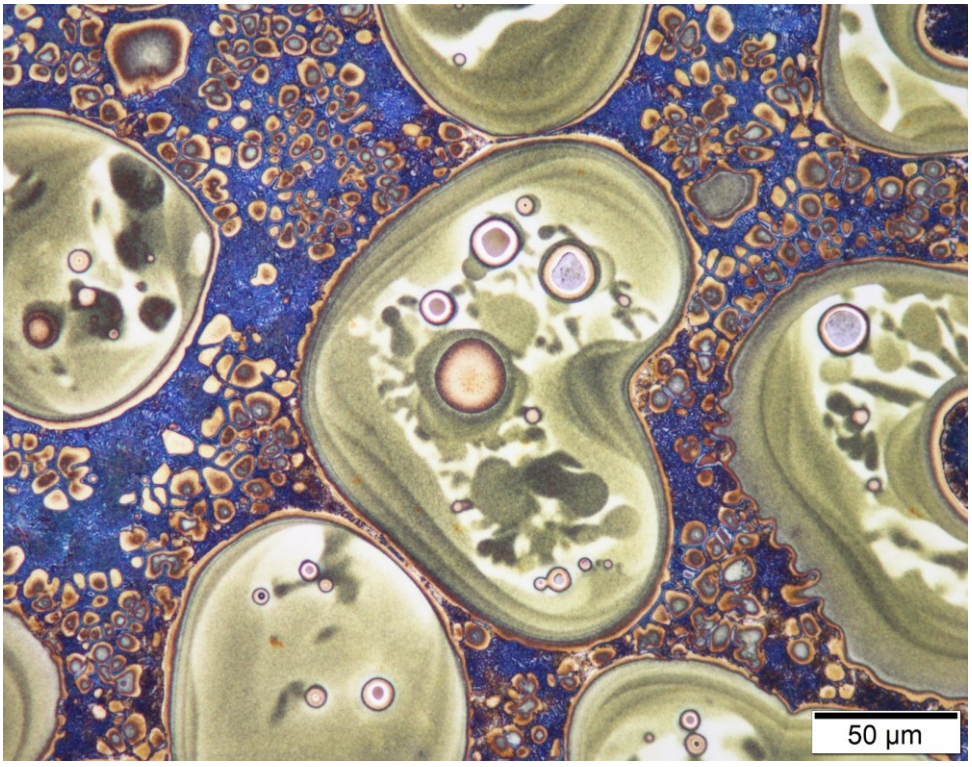


(d)

Continued

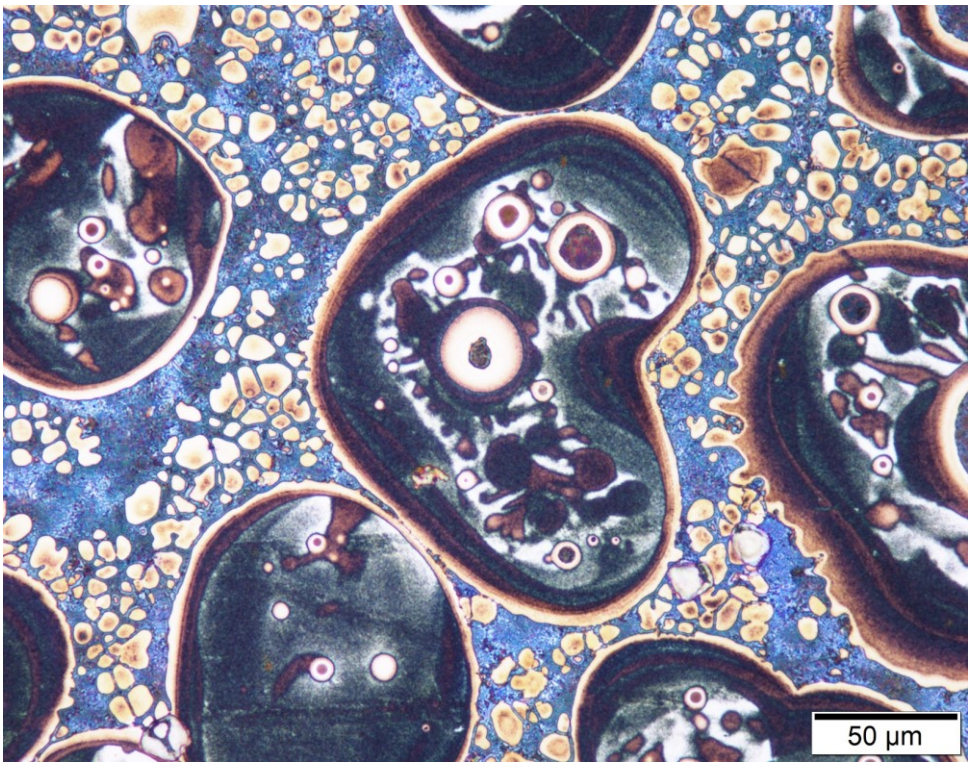


(a)

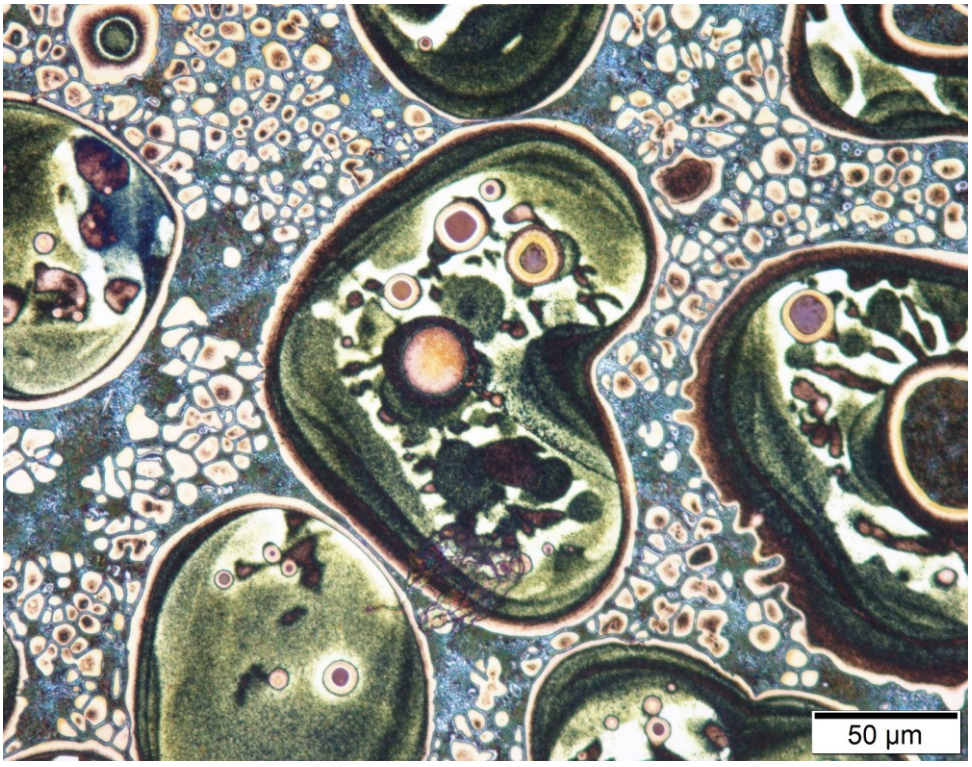


(b)

Fig. 3-5. Optical micrograph of the as-cast specimen etched by Weck's reagent with the etchant temperature of (a) 15 °C, (b) 20 °C, (c) 25 °C and (d) 30 °C for 12s.

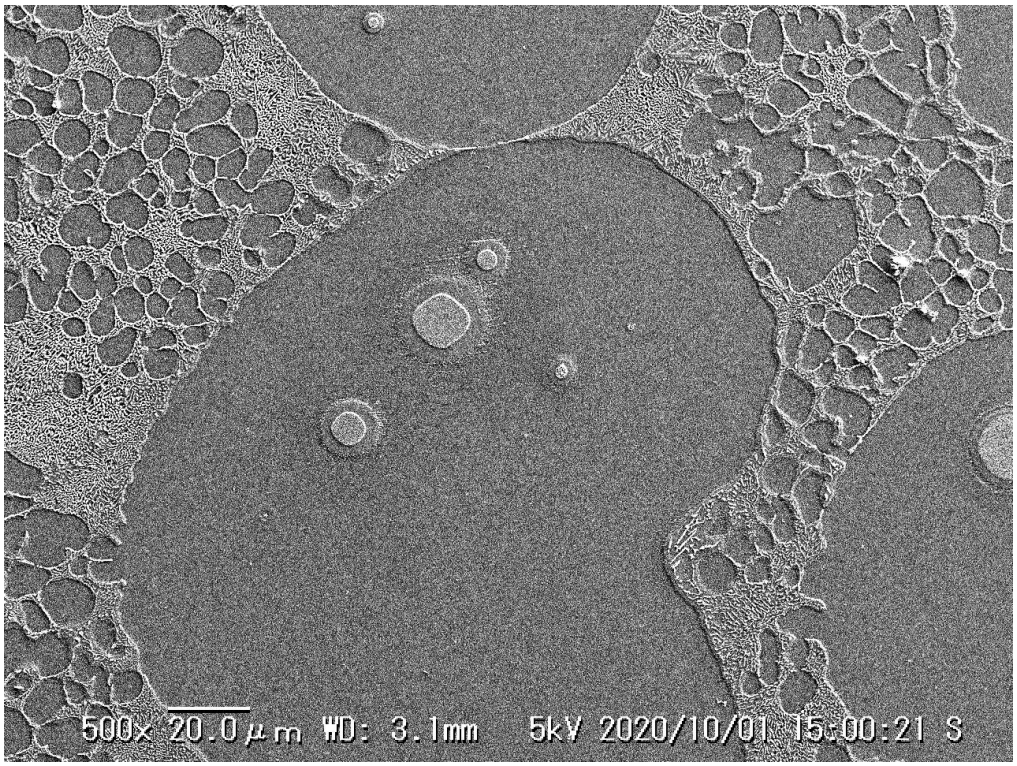


(c)

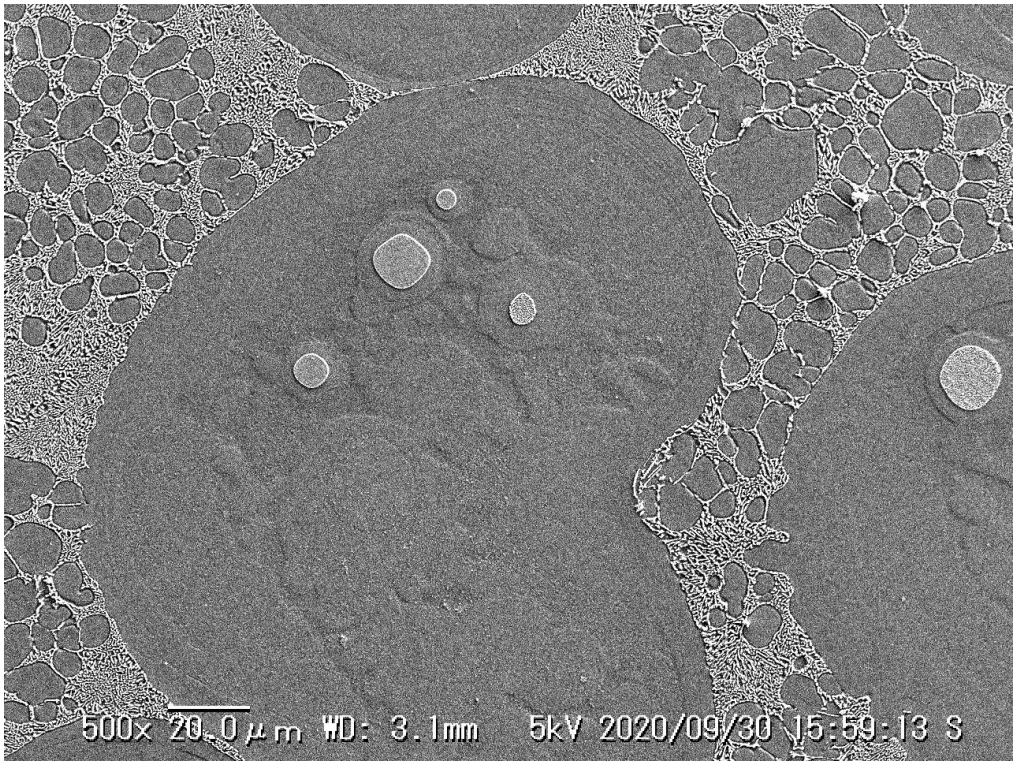


(d)

Continued

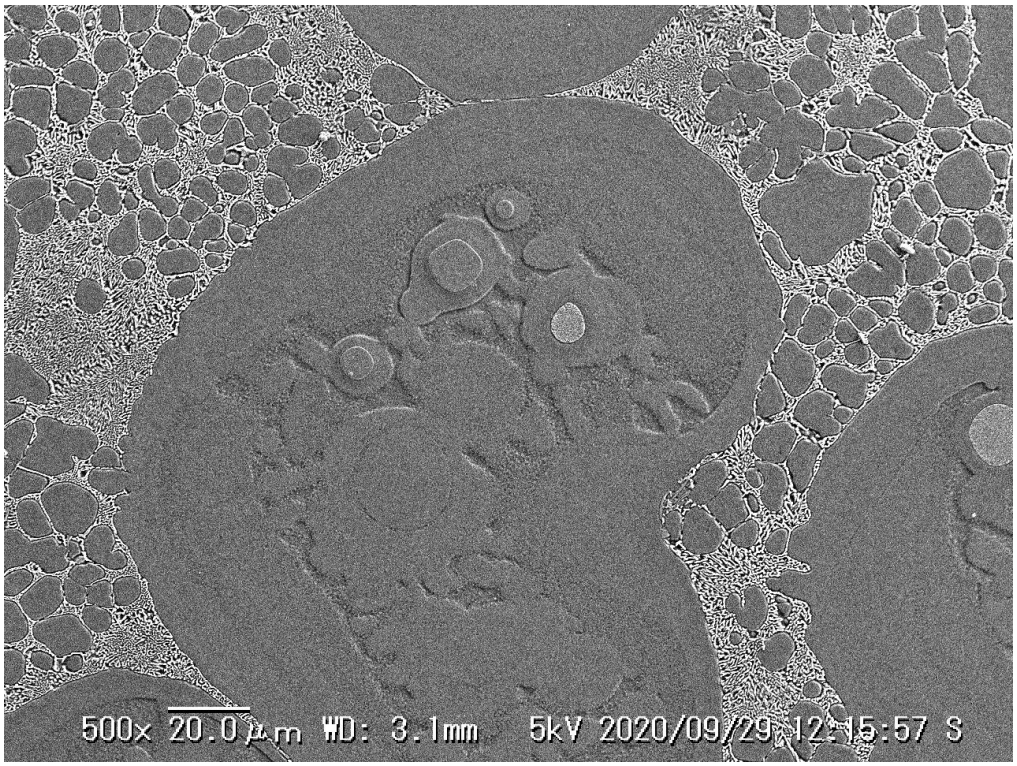


(a)

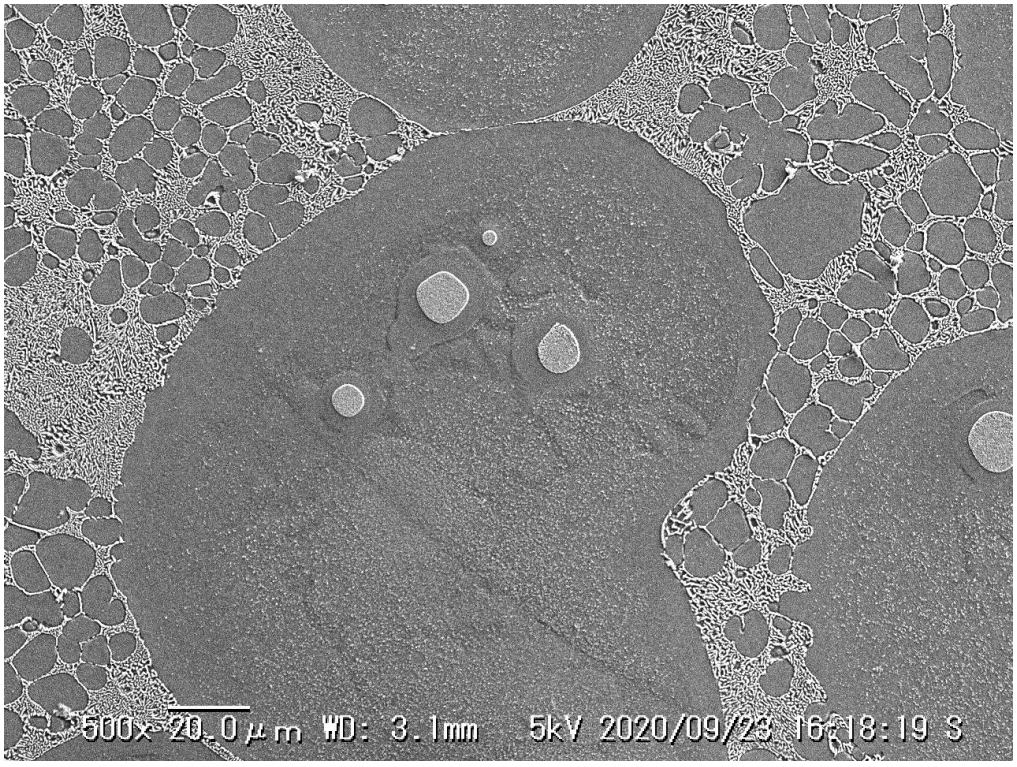


(b)

Fig. 3-6. SEI image of the as-cast specimen etched by Weck's reagent with the etchant temperature of (a) 15 °C, (b) 20 °C, (c) 25 °C and (d) 30 °C for 12s.

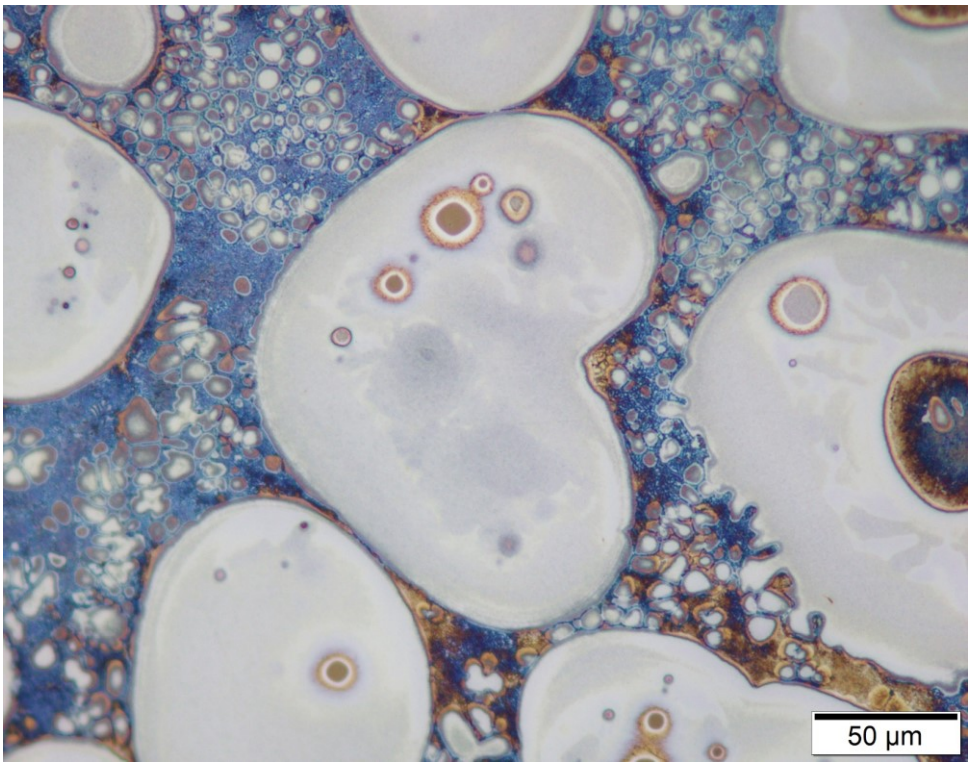


(c)

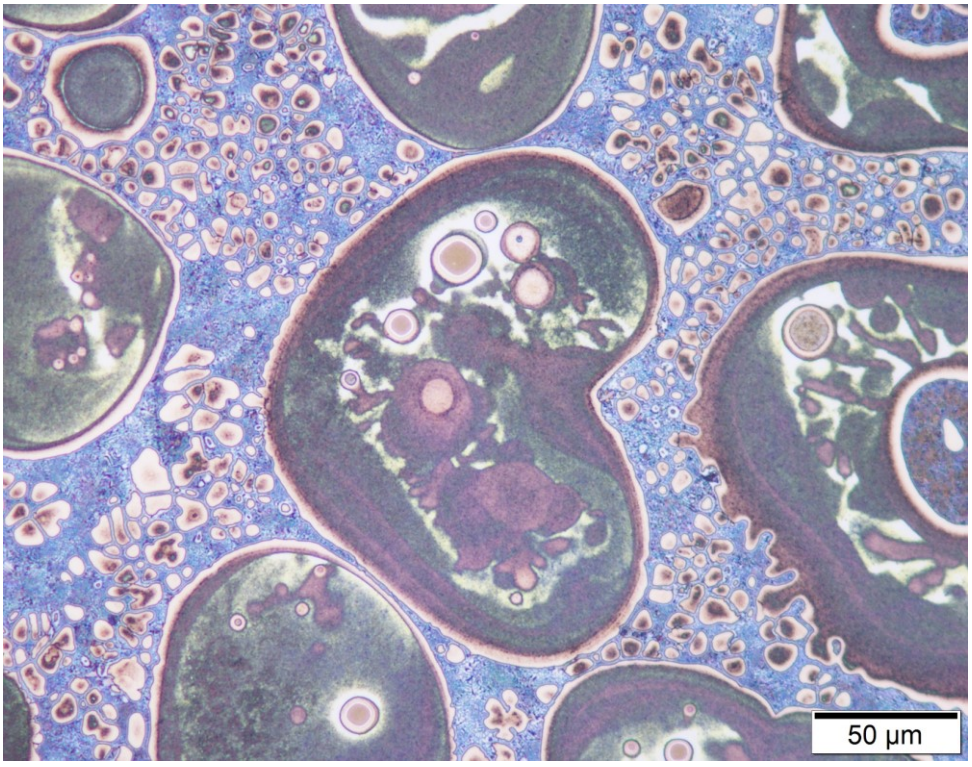


(d)

Continued

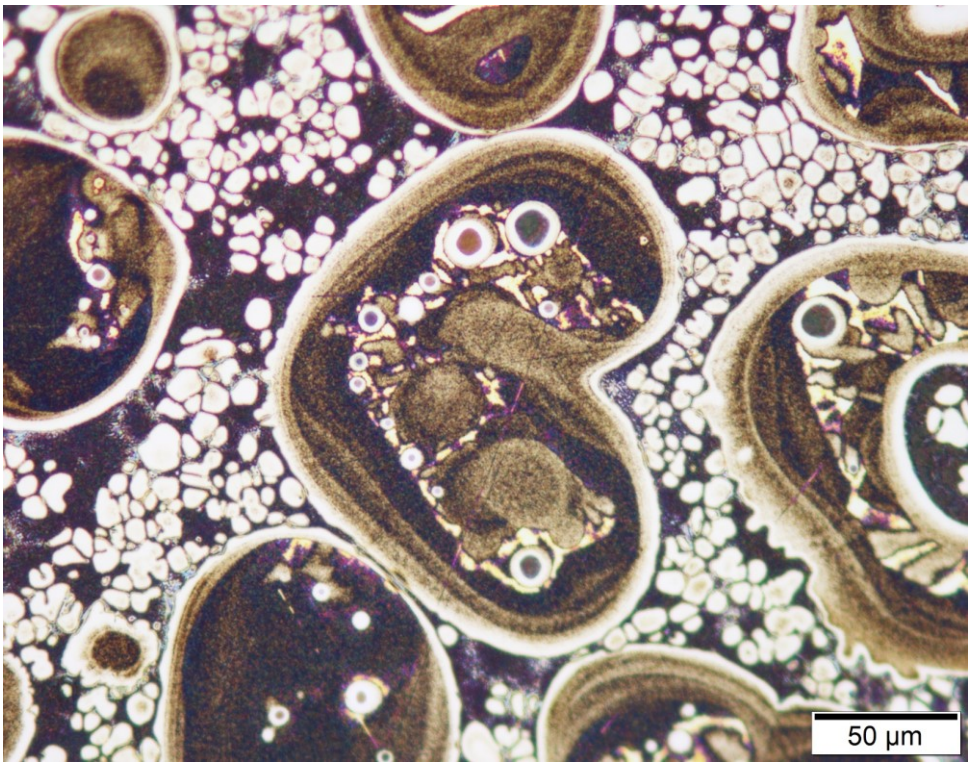


(a)

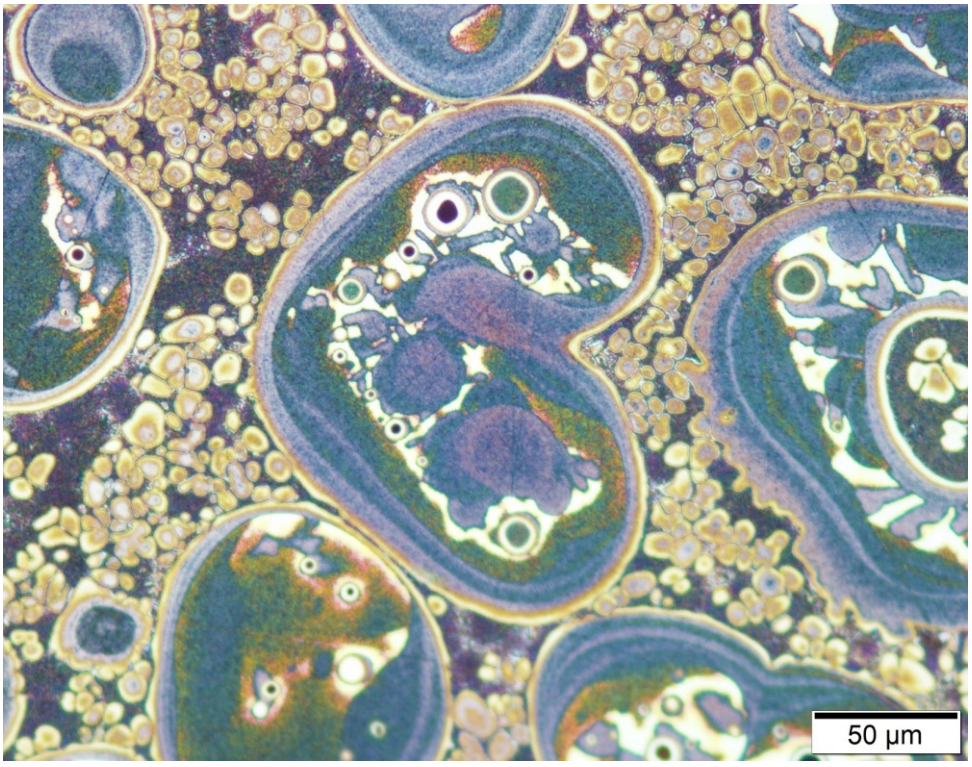


(b)

Fig. 3-7. Optical micrograph of the as-cast specimen etched by Weck's reagent with the etchant temperature of (a) 15 °C, (b) 20 °C, (c) 25 °C and (d) 30 °C for 16s.

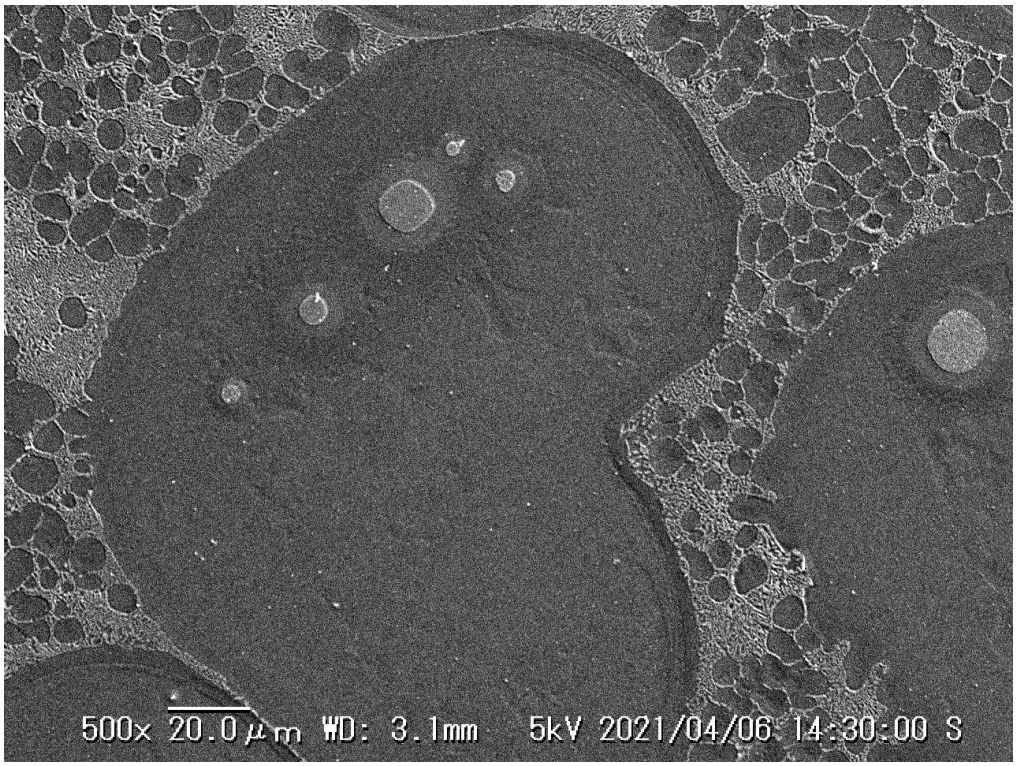


(c)

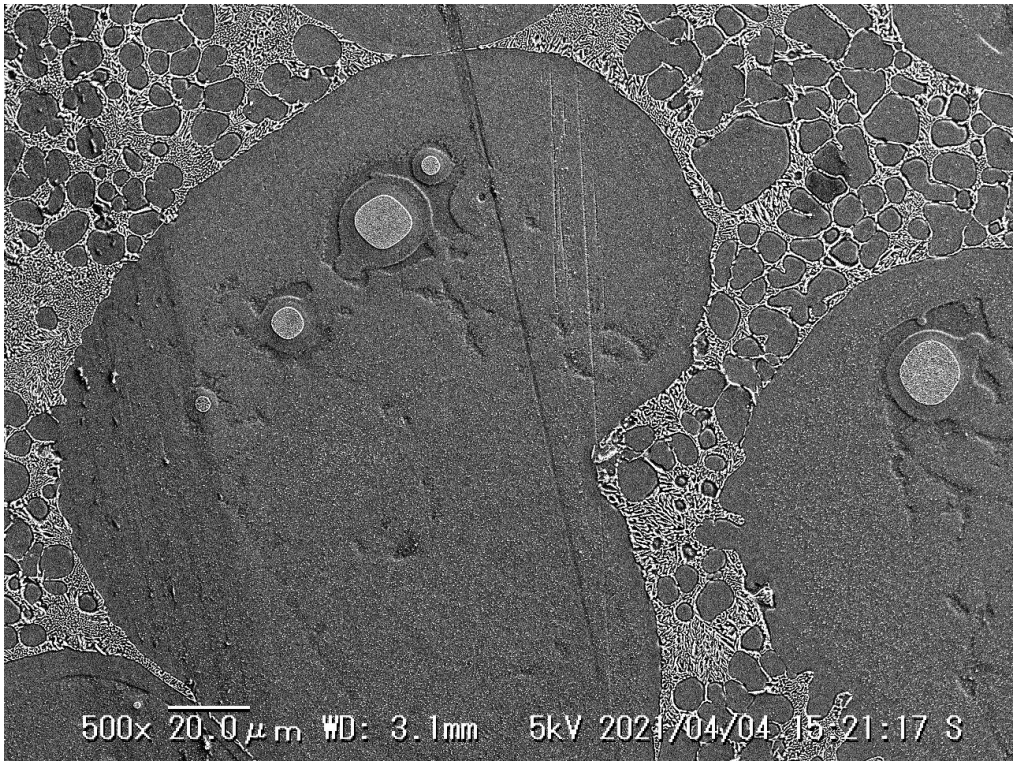


(d)

Continued

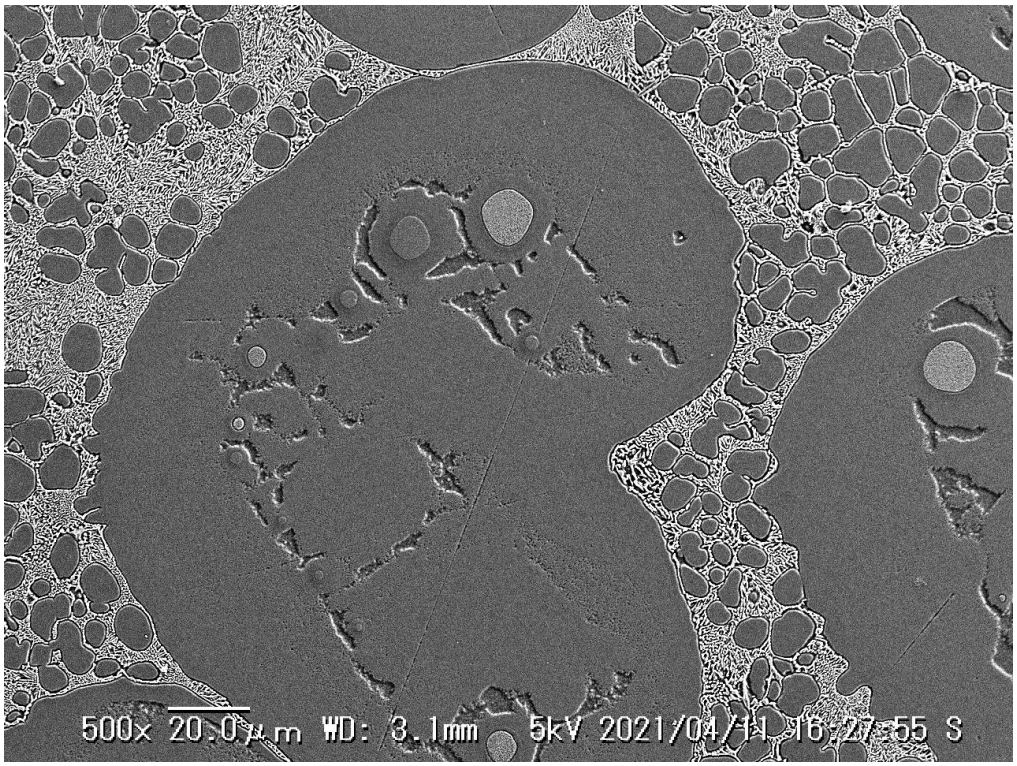


(a)

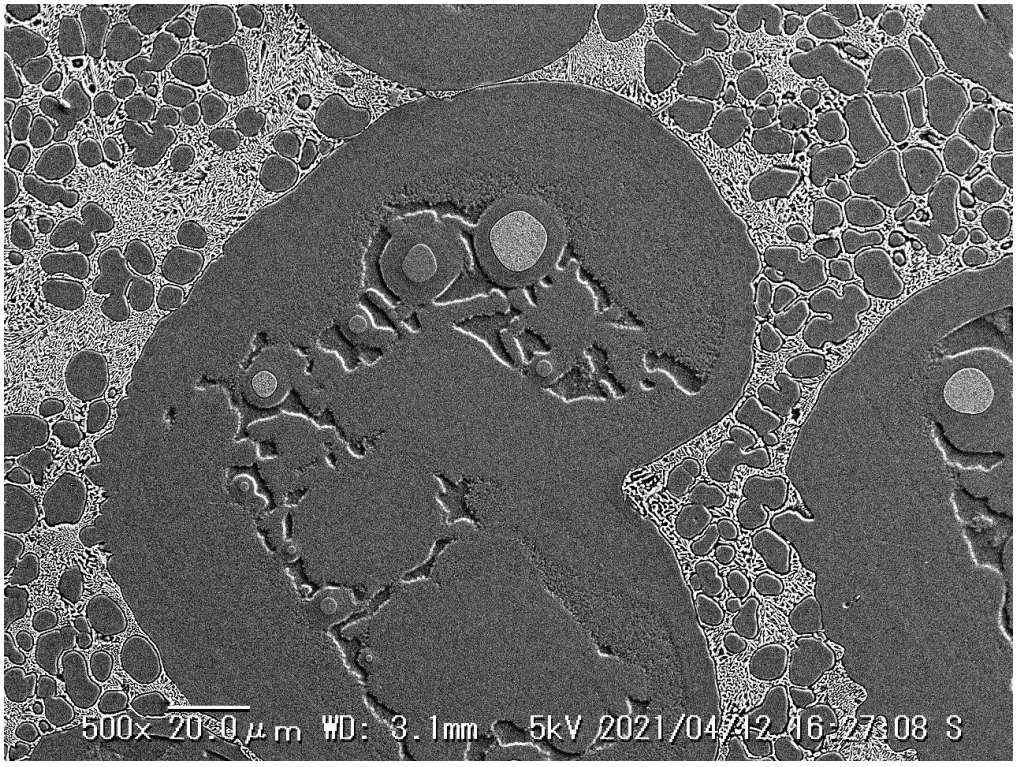


(b)

Fig. 3-8. SEI image of the as-cast specimen etched by Weck's reagent with the etchant temperature of (a) 15 °C, (b) 20 °C, (c) 25 °C and (d) 30 °C for 16s.

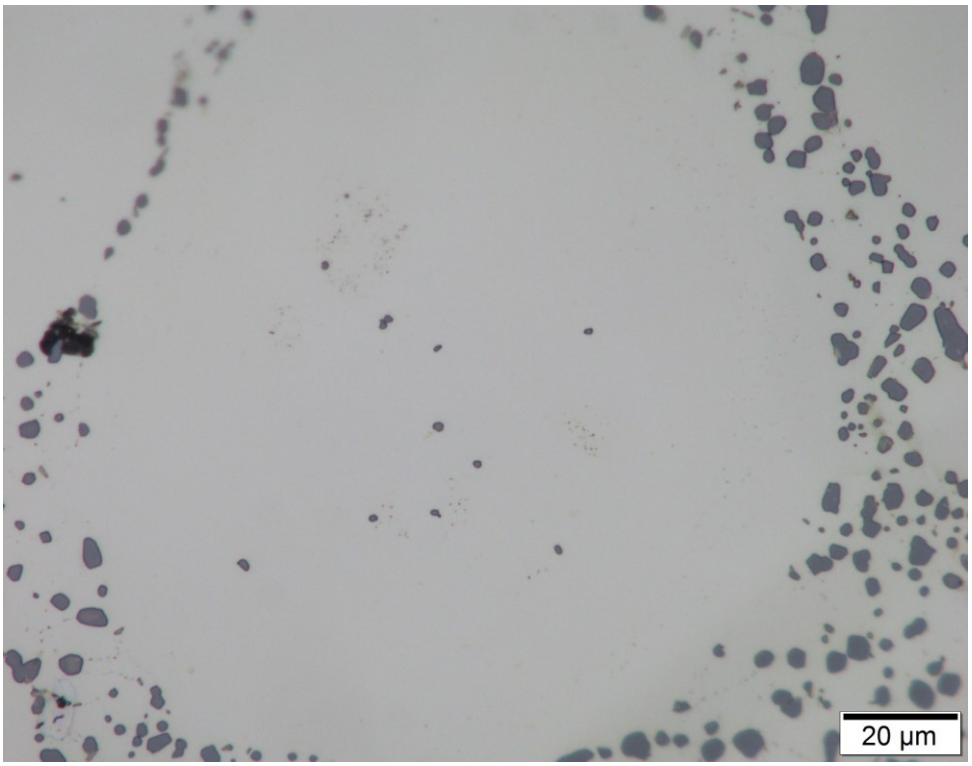


(c)

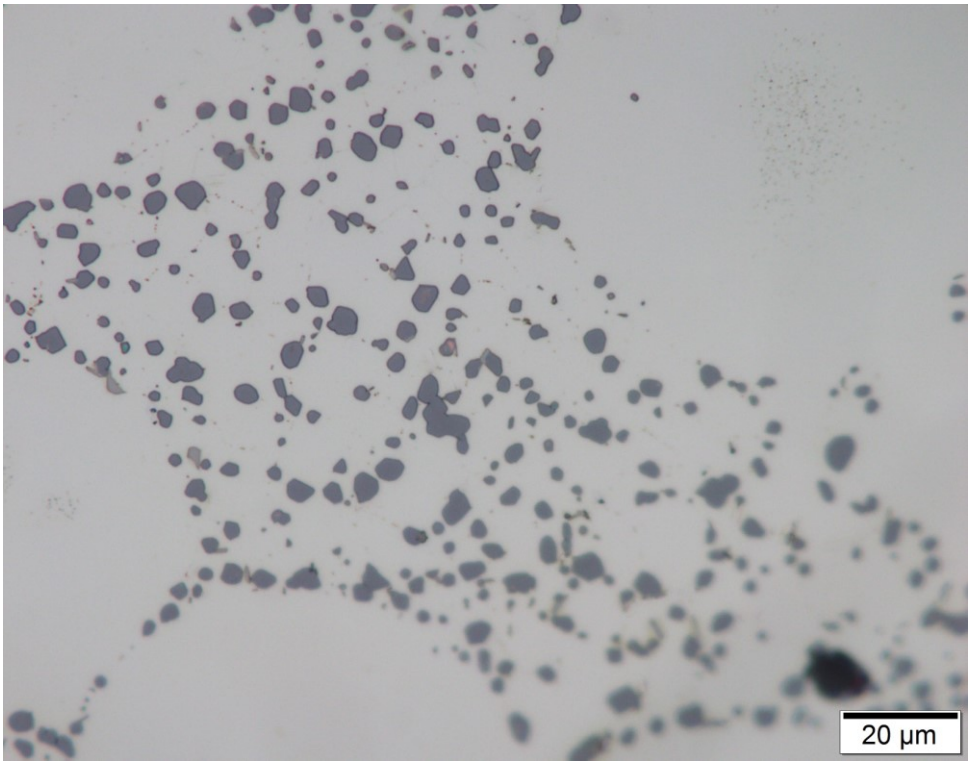


(d)

Continued

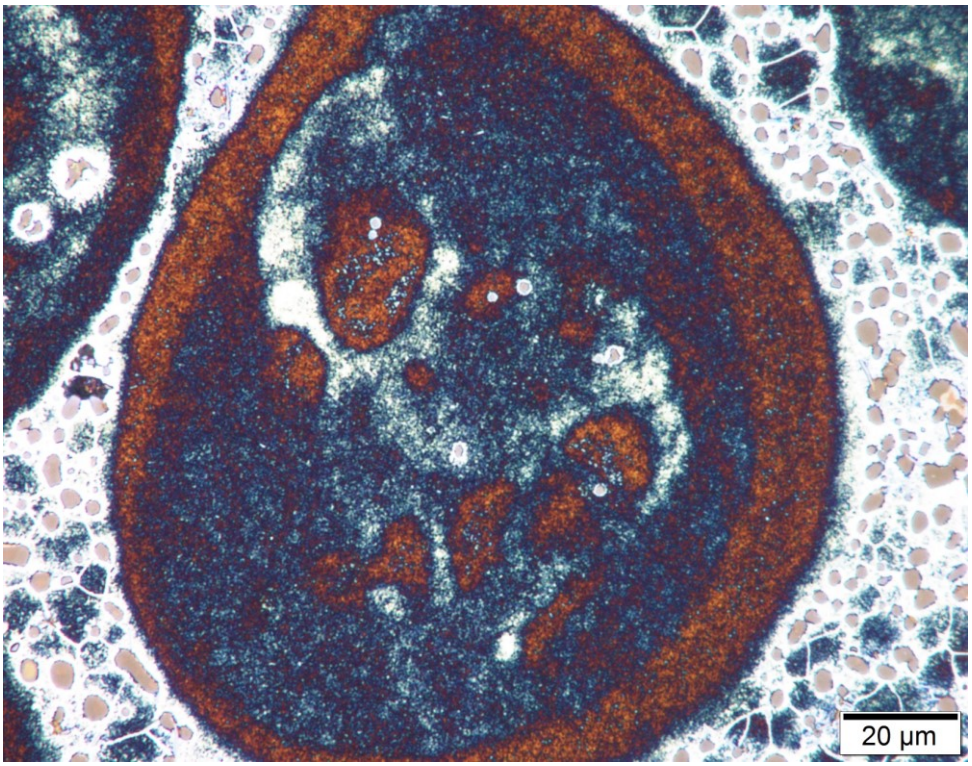


(a)



(b)

Fig. 3-9. Optical micrograph of the solution treated specimen etched by Weck's reagent with the solution temperature of (a) and (b)10 °C, (c) and (d) 15 °C, (e) and (f) 20 °C and (g) and (h) 25 °C.

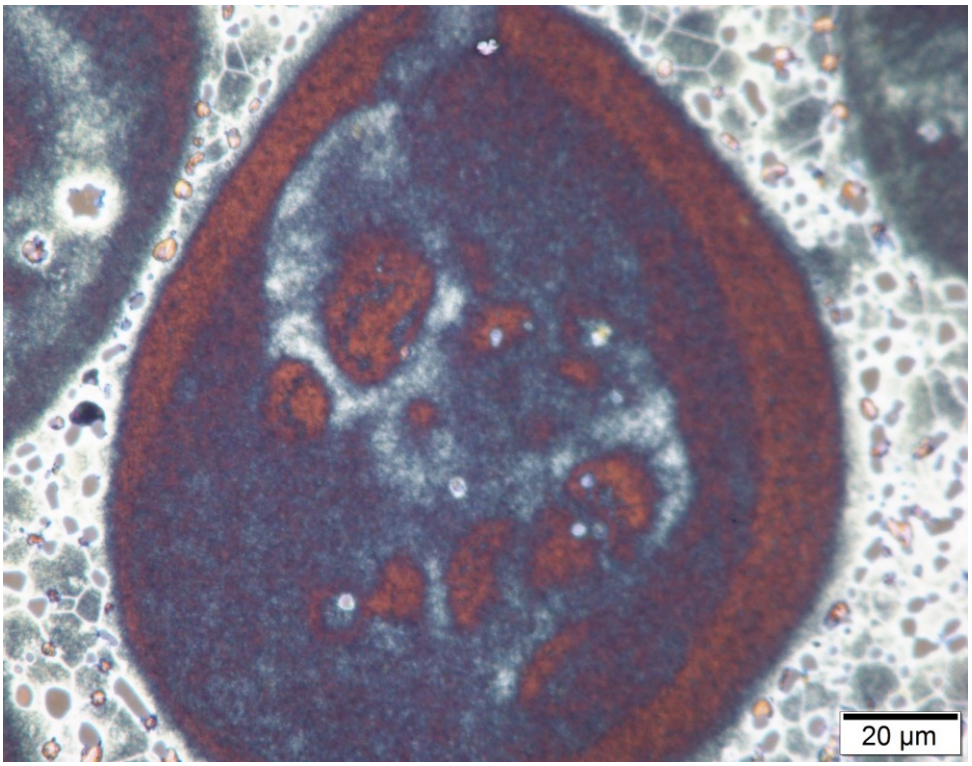


(c)

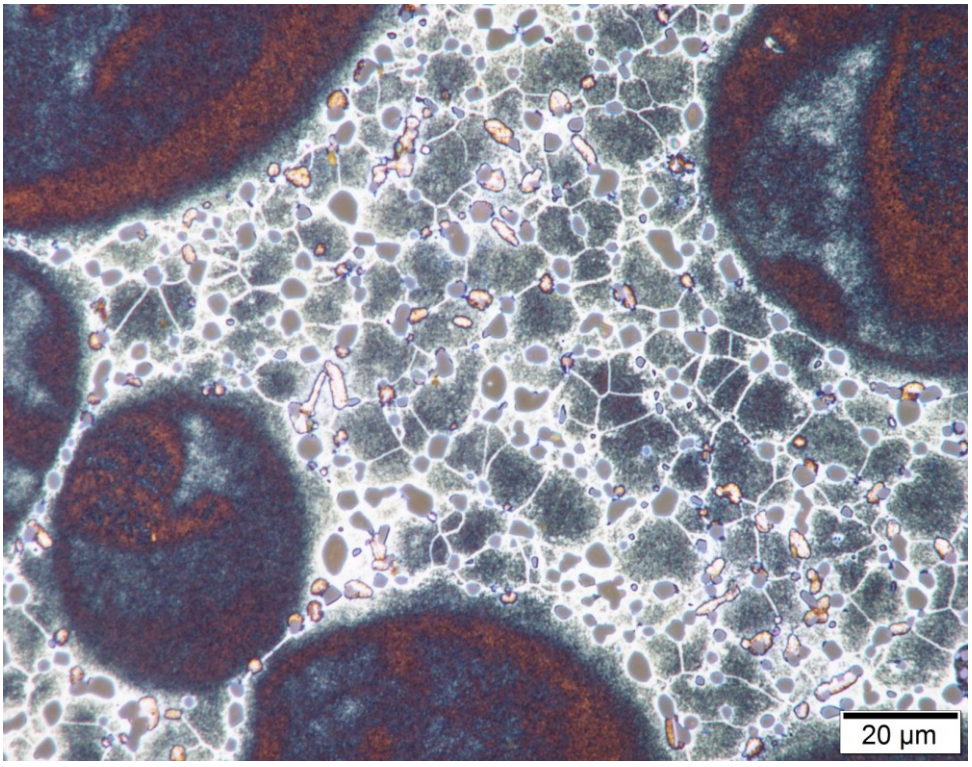


(d)

Continued

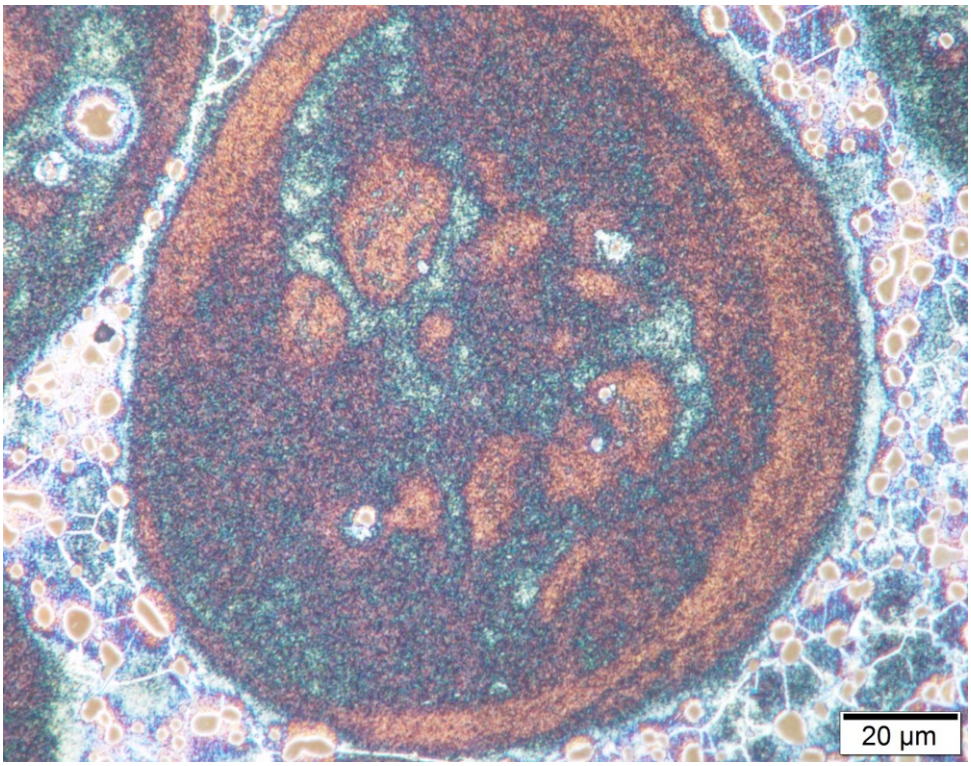


(e)

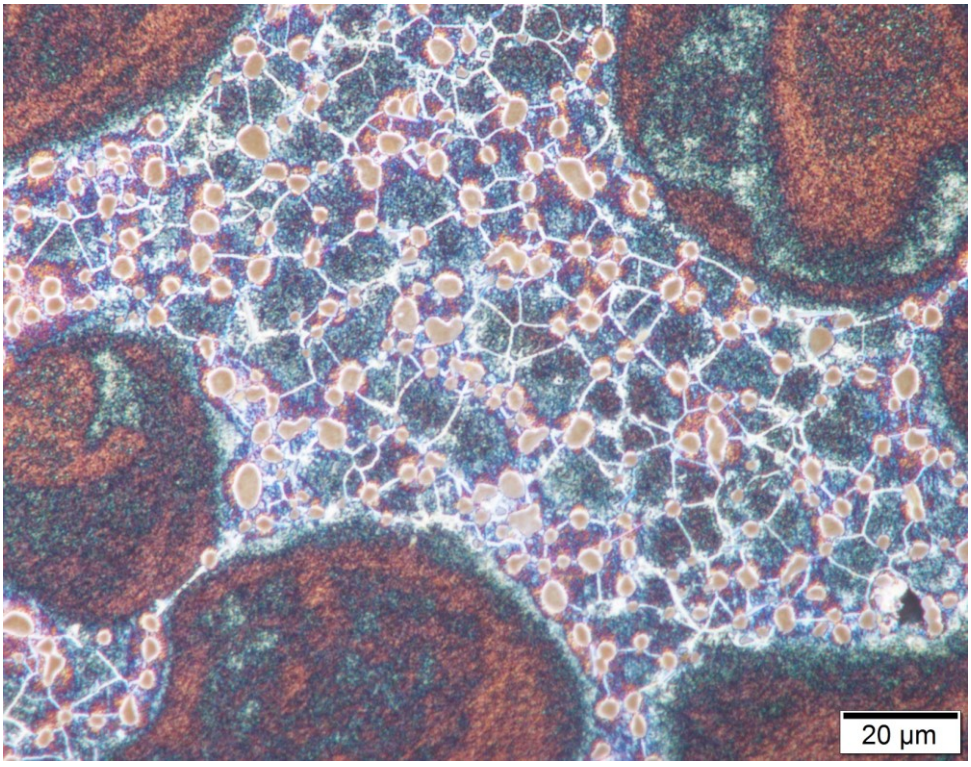


(f)

Continued

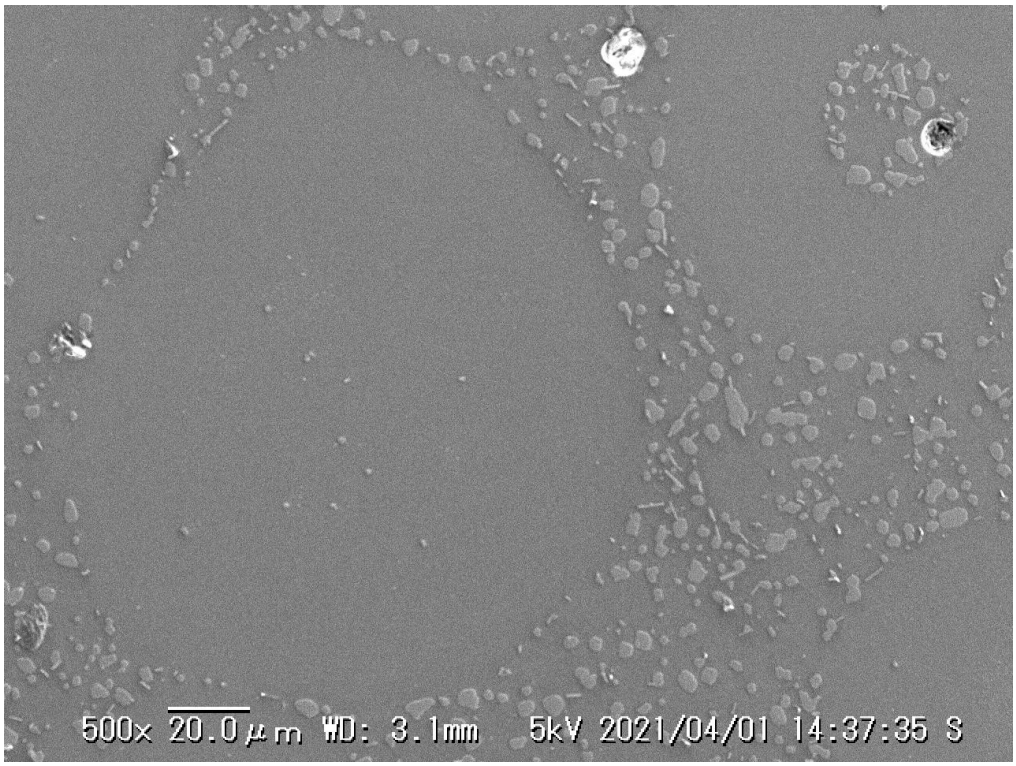


(g)

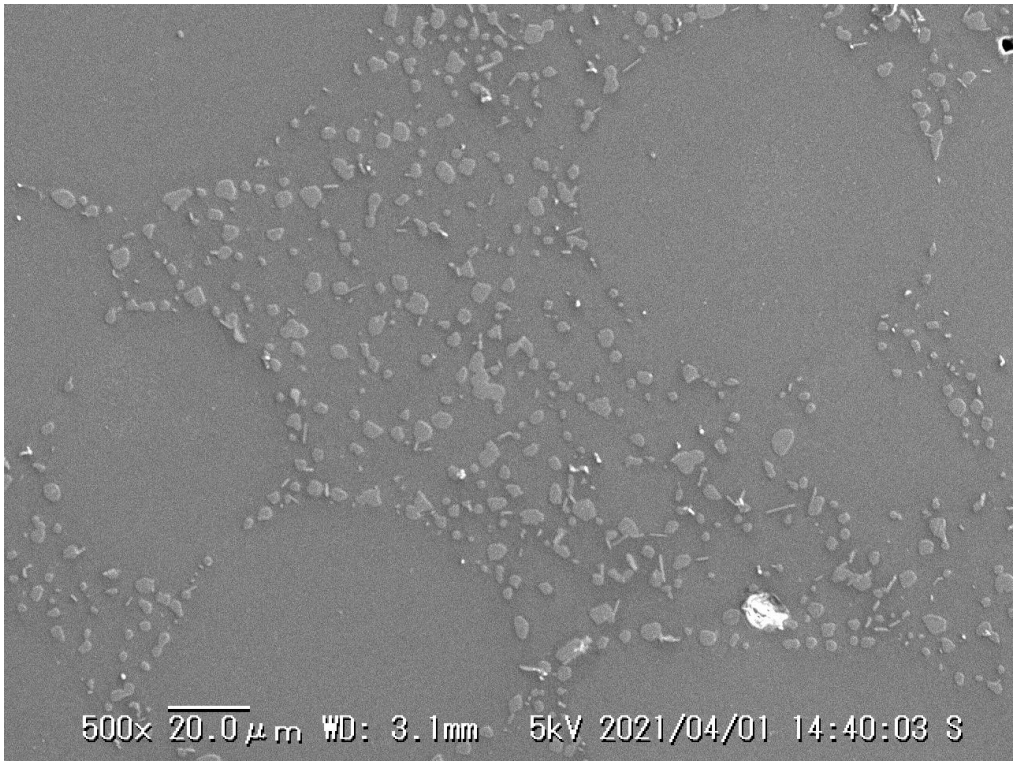


(h)

Continued

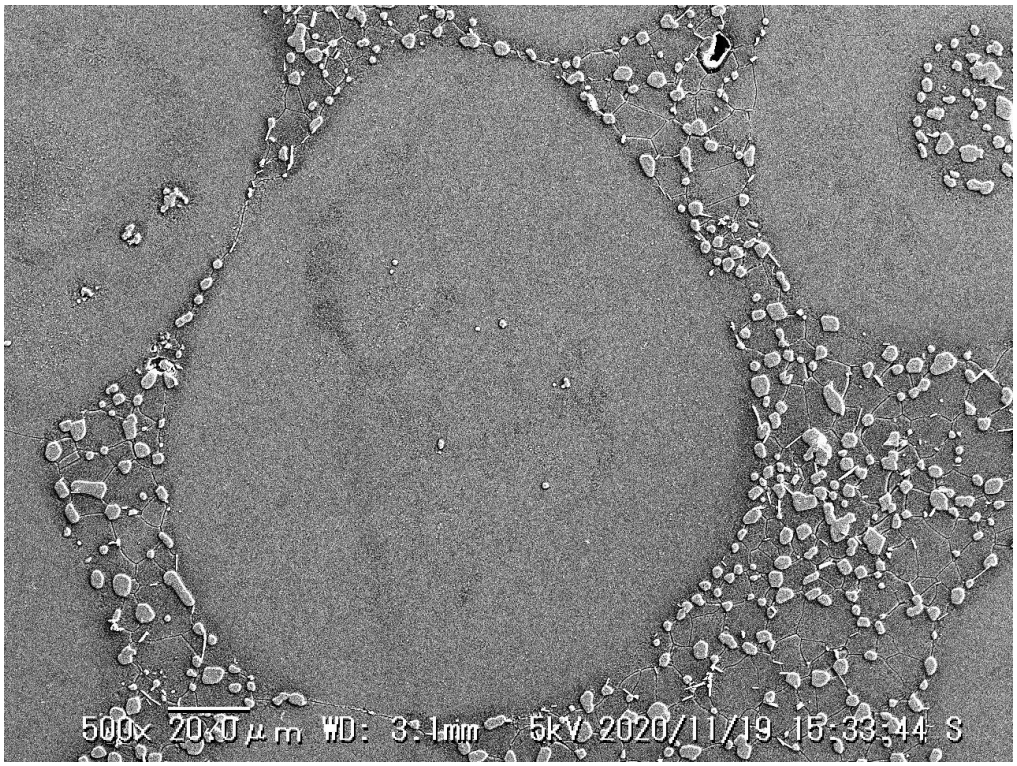


(a)

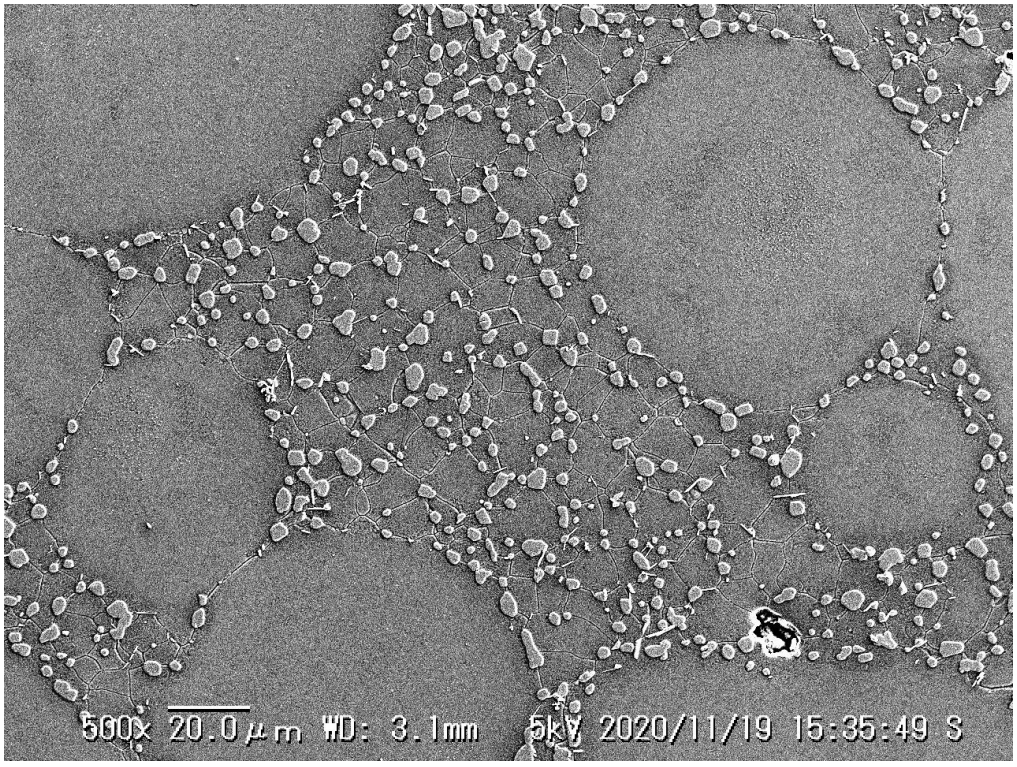


(b)

Fig. 3-10. SEI image of the solution treated specimen etched by Weck's reagent with the solution temperature of (a) and (b)10 °C, (c) and (d) 15 °C, (e) and (f) 20 °C and (g) and (h) 25 °C.

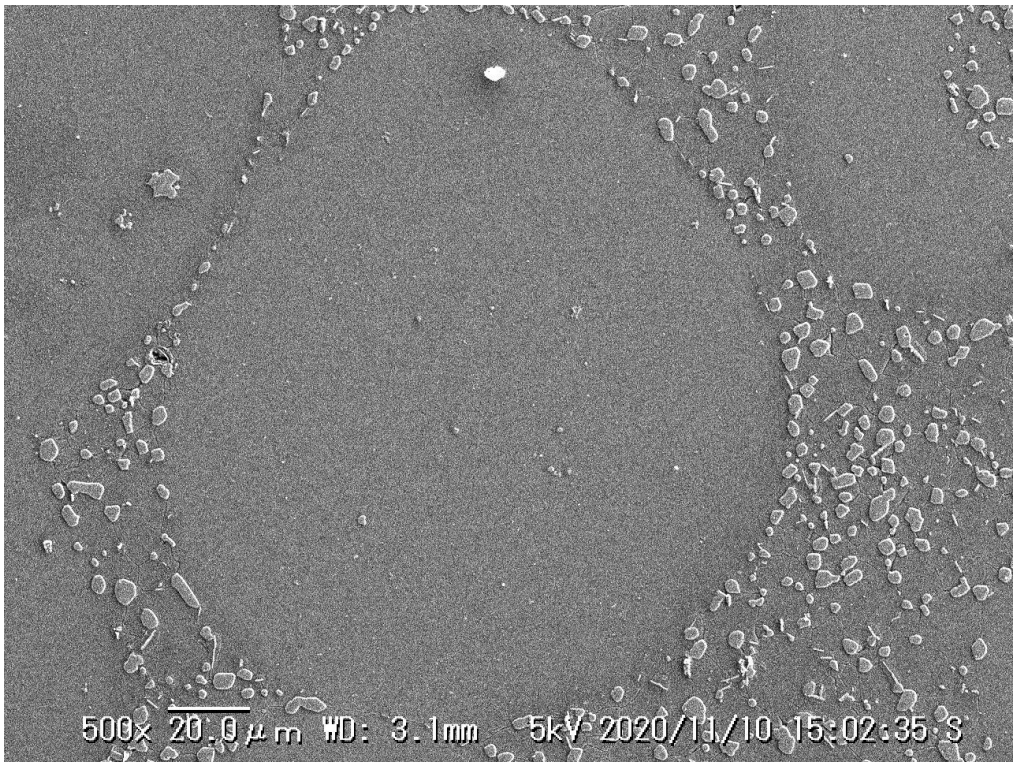


(c)

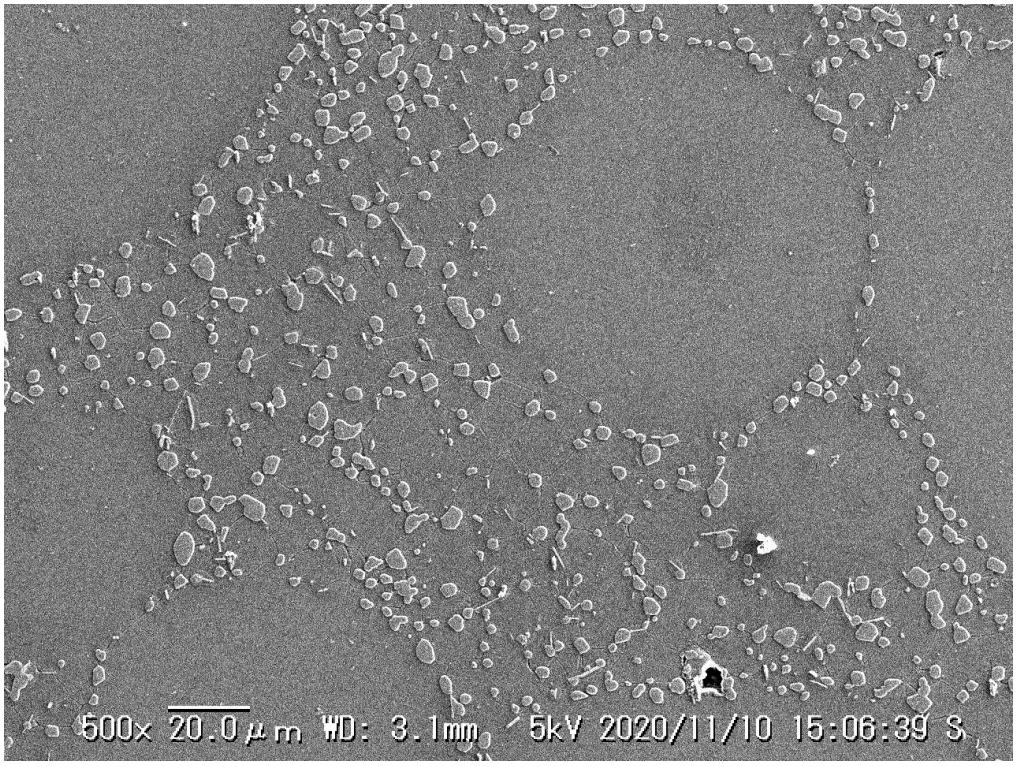


(d)

Continued

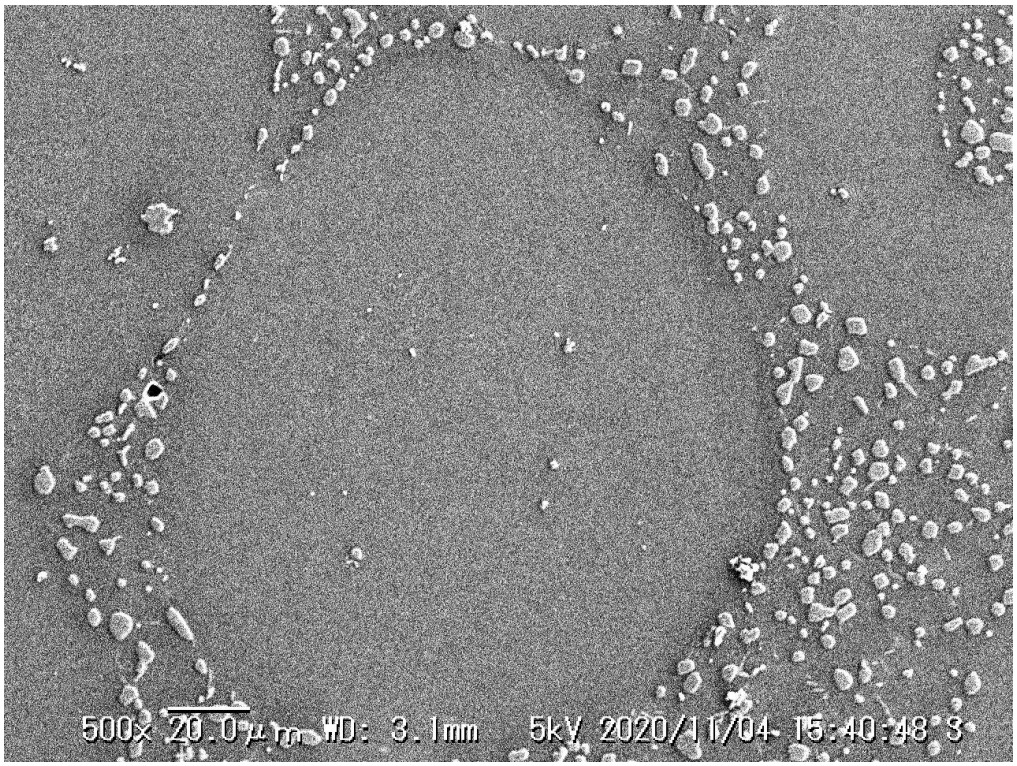


(e)

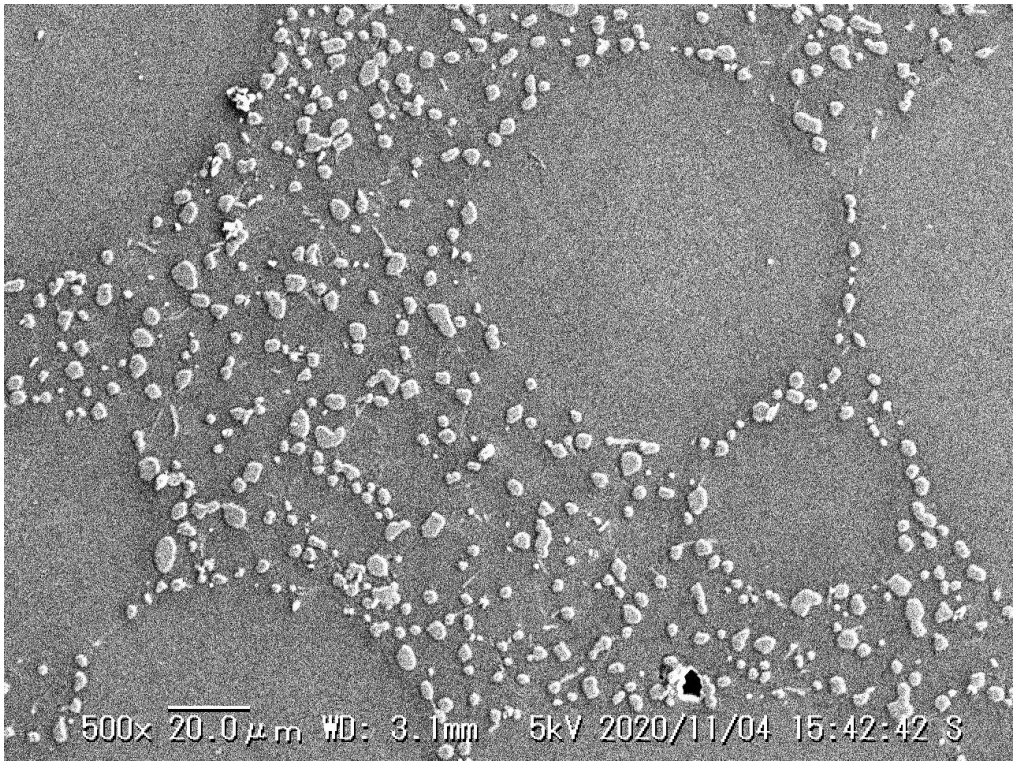


(f)

Continued



(g)



(h)

Continued

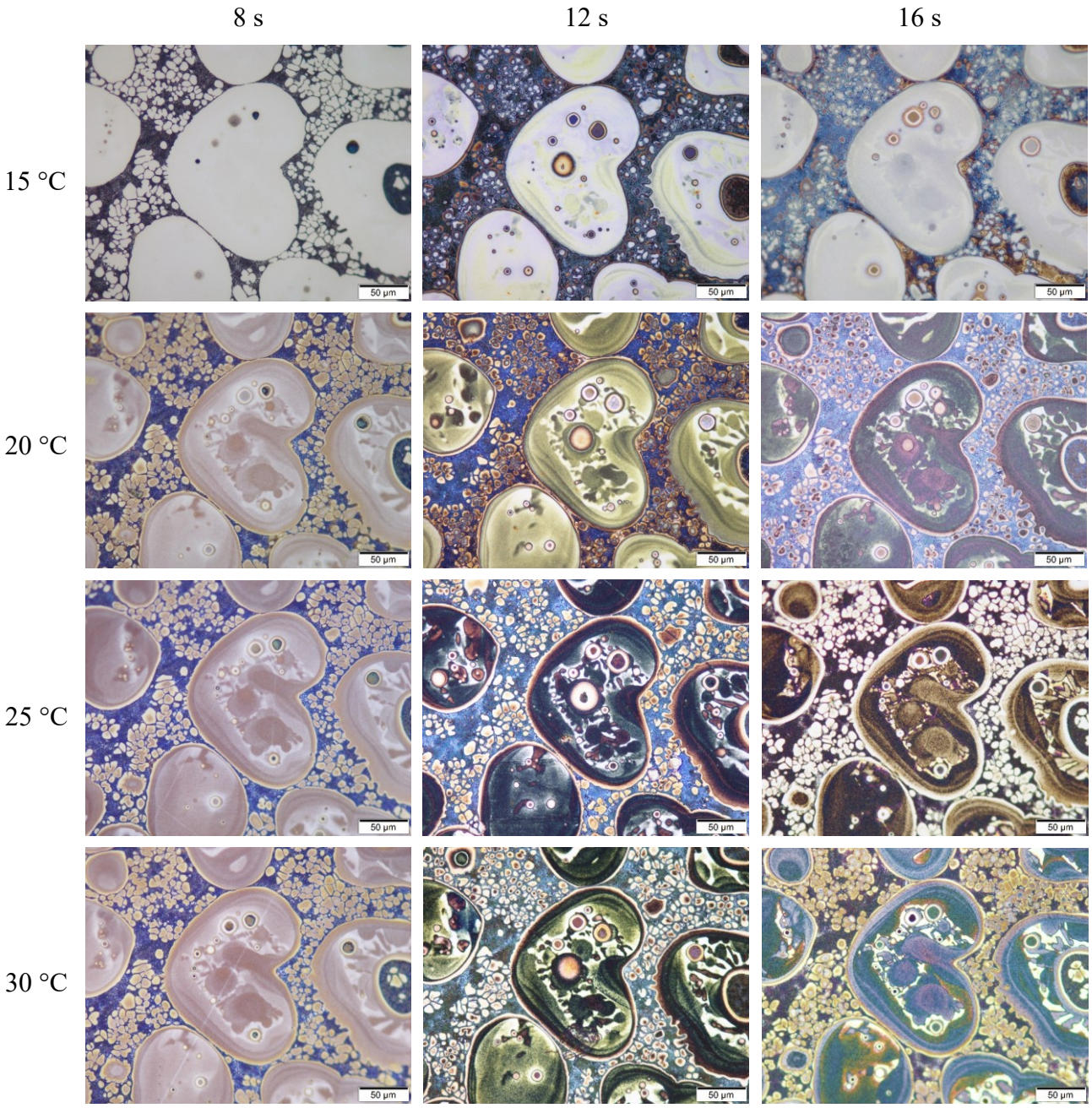


Fig. 3-11. The temperature-time chart of color contrast of the as-cast specimen etched with different etching conditions

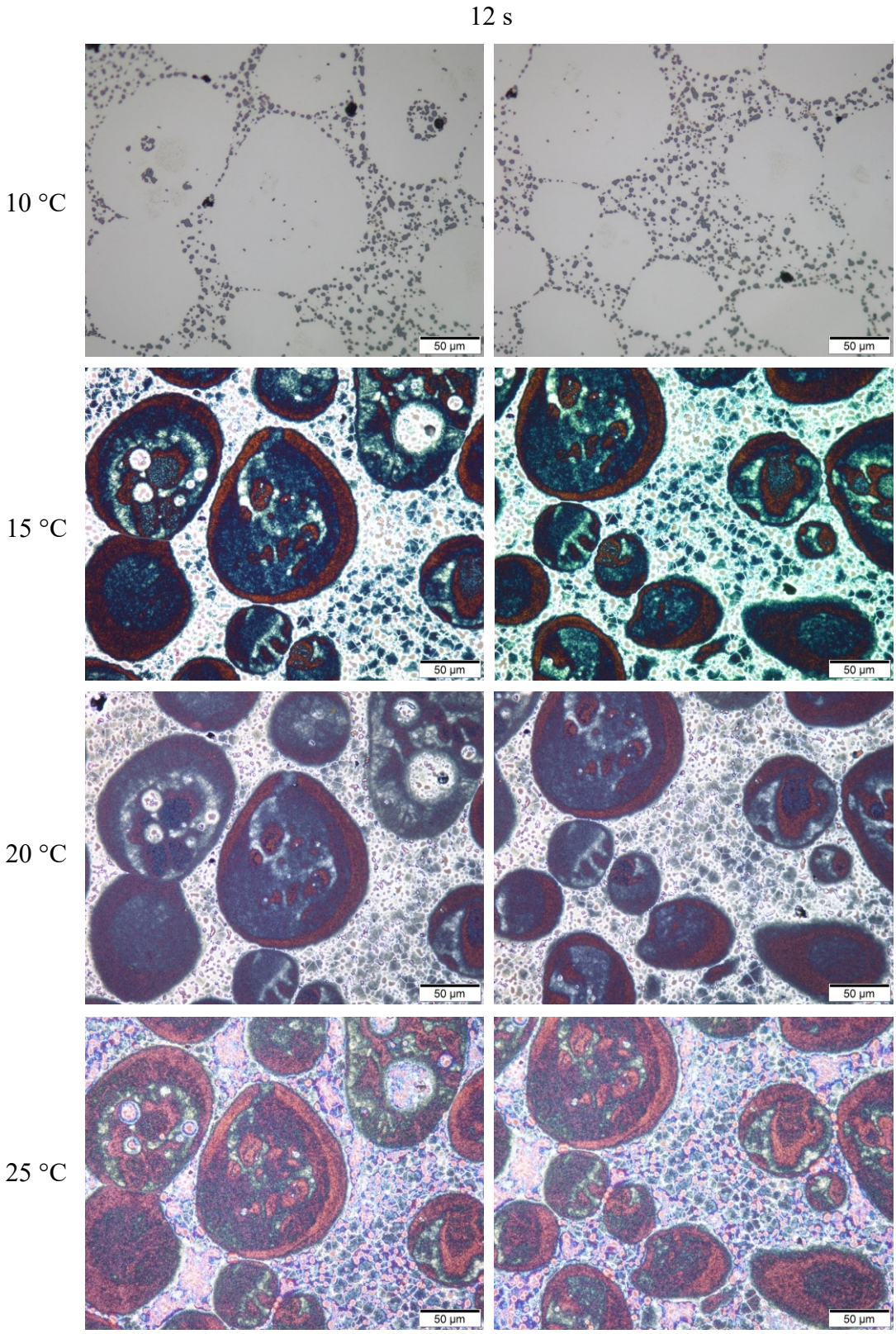
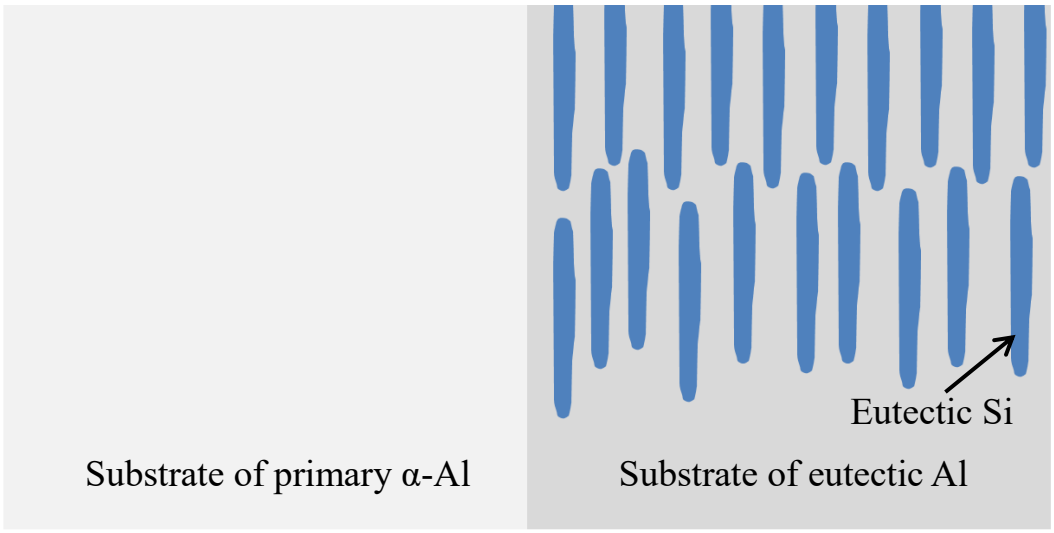
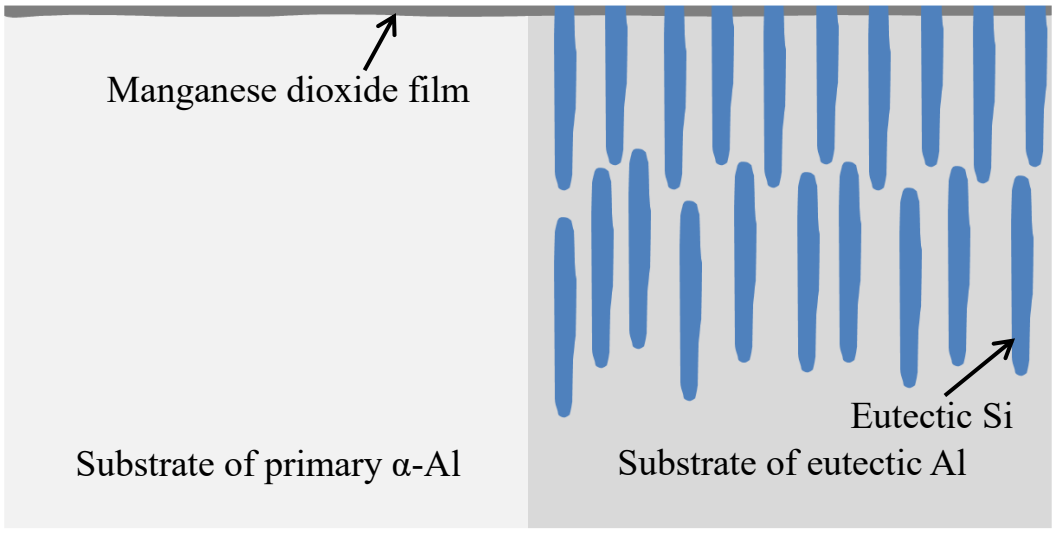


Fig. 3-12. The temperature-time chart of color contrast of the solution-treated specimen etched with different etching conditions at different locations

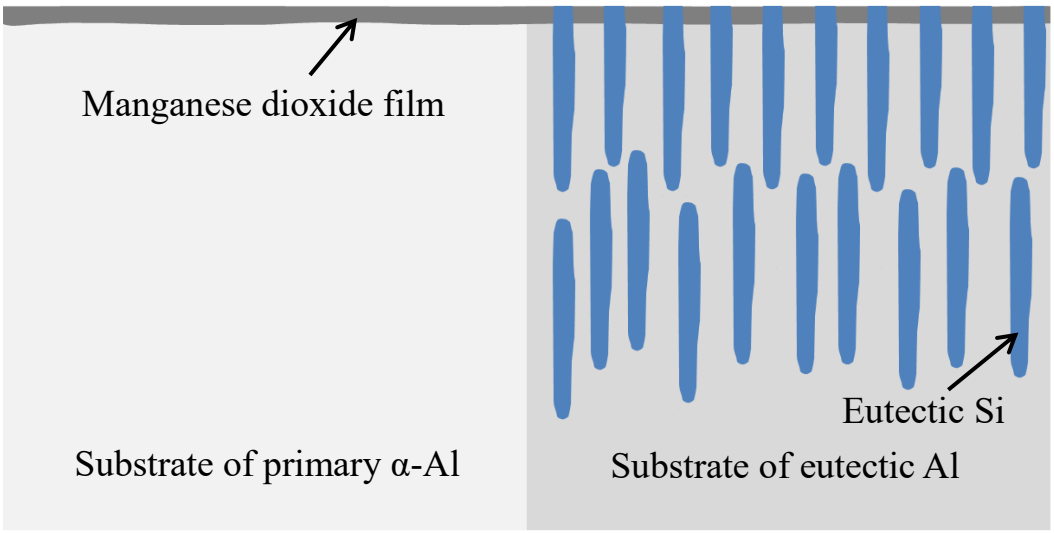


(a)

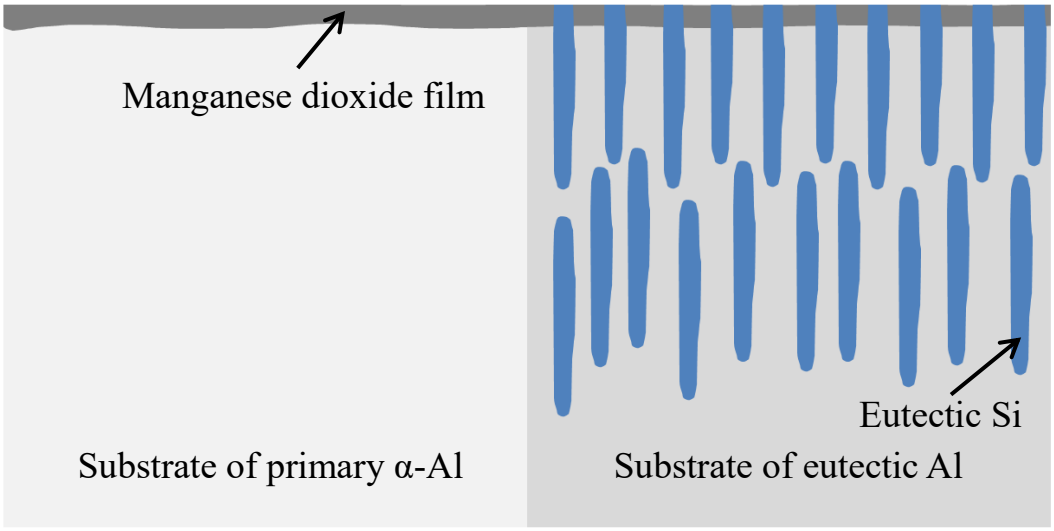


(b)

Fig. 3-13. Schematic illustration showing the cross section of the as-cast specimen etched by Weck's reagent with the solution temperature of (a) 15 °C, (b) 20 °C, (c) 25 °C and (d) 30 °C for 8 s.

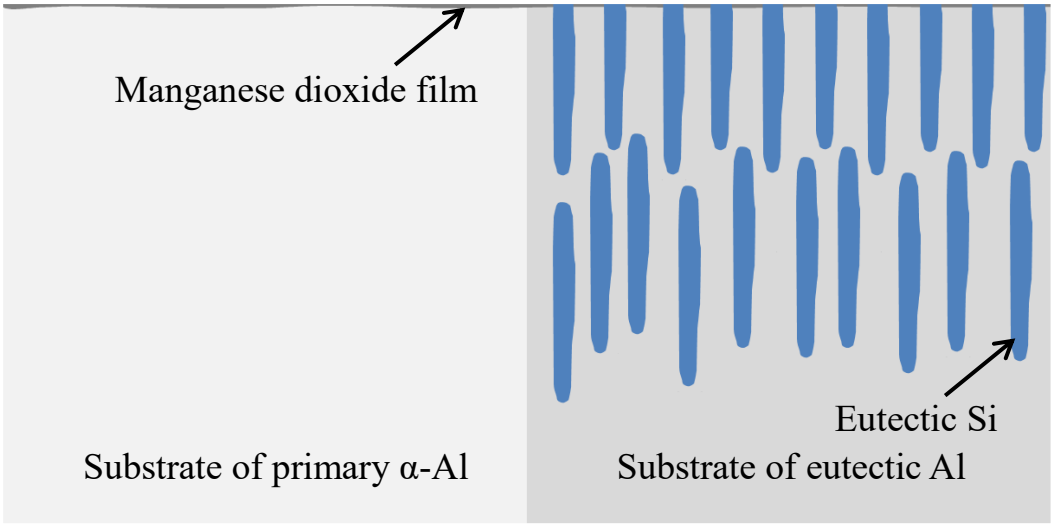


(c)

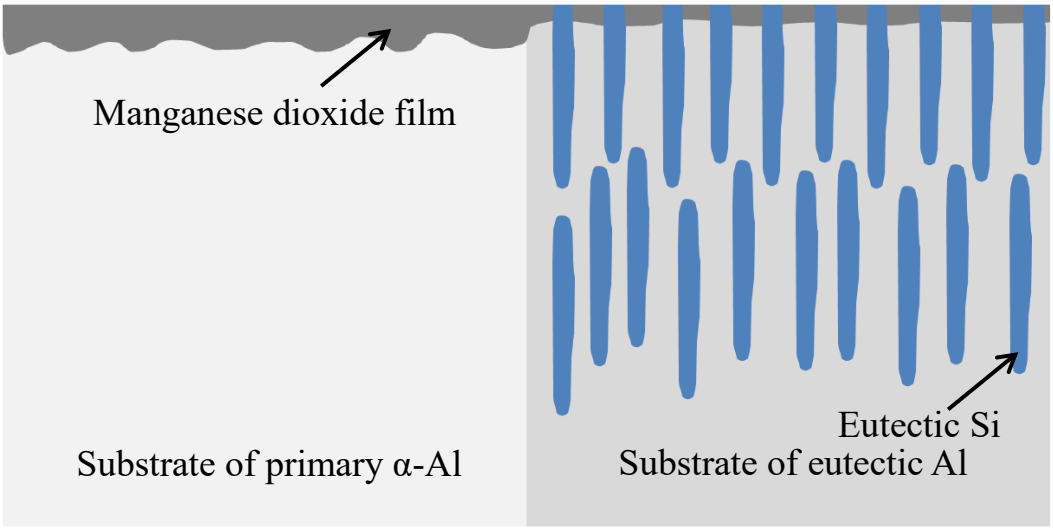


(d)

Continued

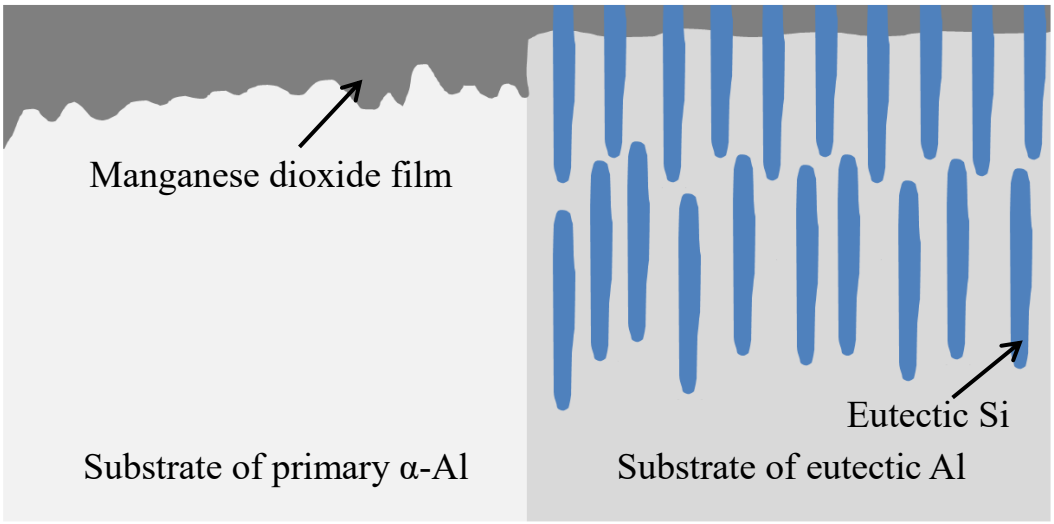


(a)

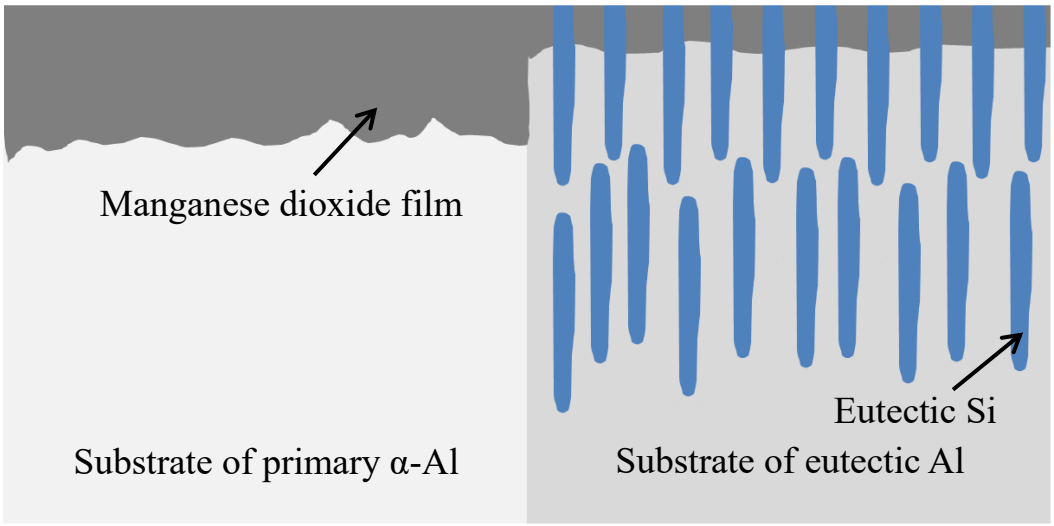


(b)

Fig. 3-14. Schematic illustration showing the cross section of the as-cast specimen etched by Weck's reagent with the solution temperature of (a) 15 °C, (b) 20 °C, (c) 25 °C and (d) 30 °C for 12 s.

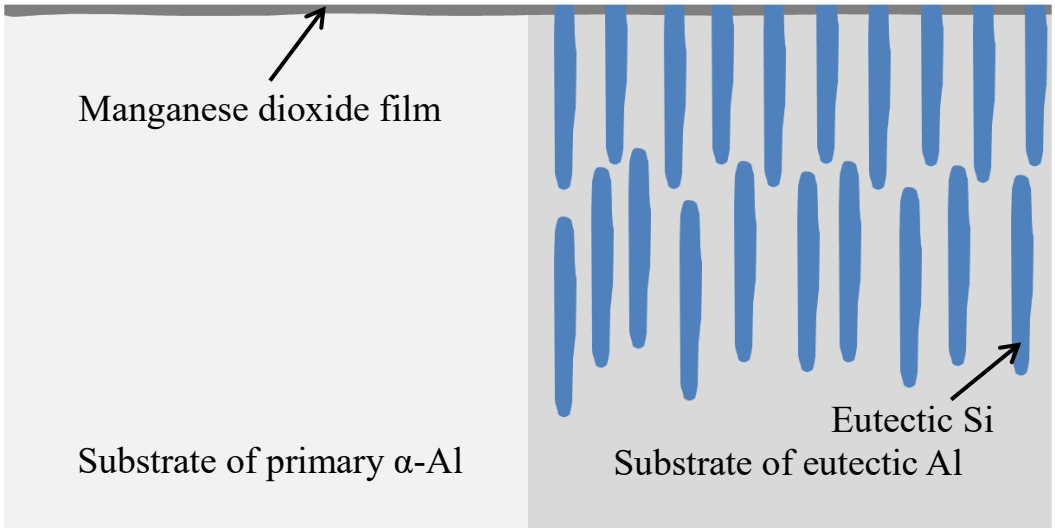


(c)

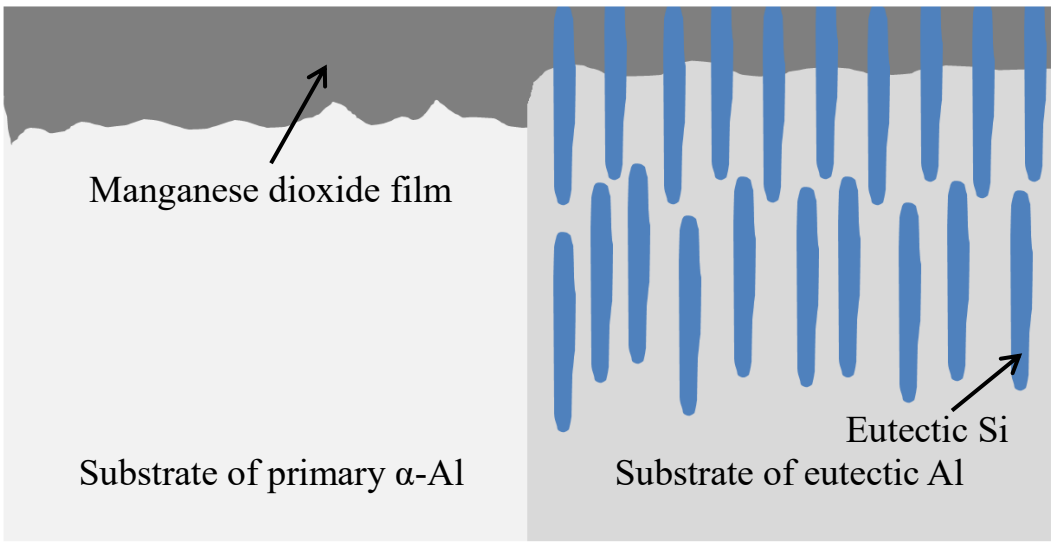


(d)

Continued

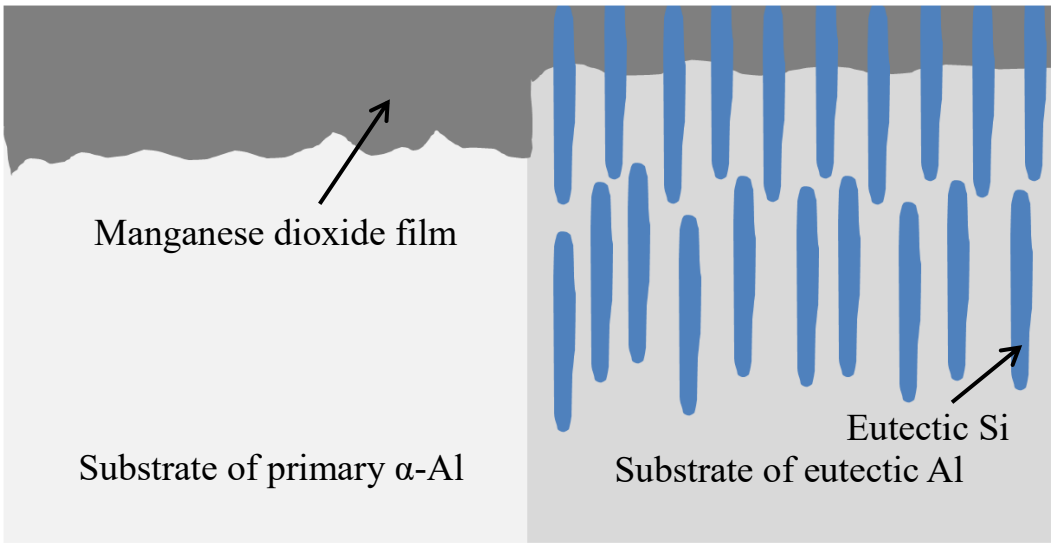


(a)

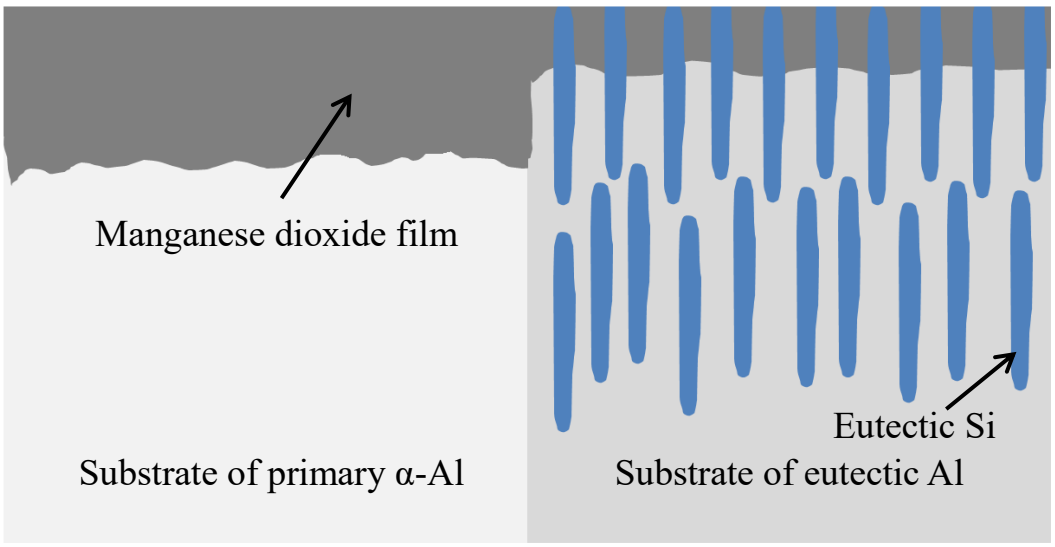


(b)

Fig. 3-15. Schematic illustration showing the cross section of the as-cast specimen etched by Weck's reagent with the solution temperature of (a) 15 °C, (b) 20 °C, (c) 25 °C and (d) 30 °C for 16 s.

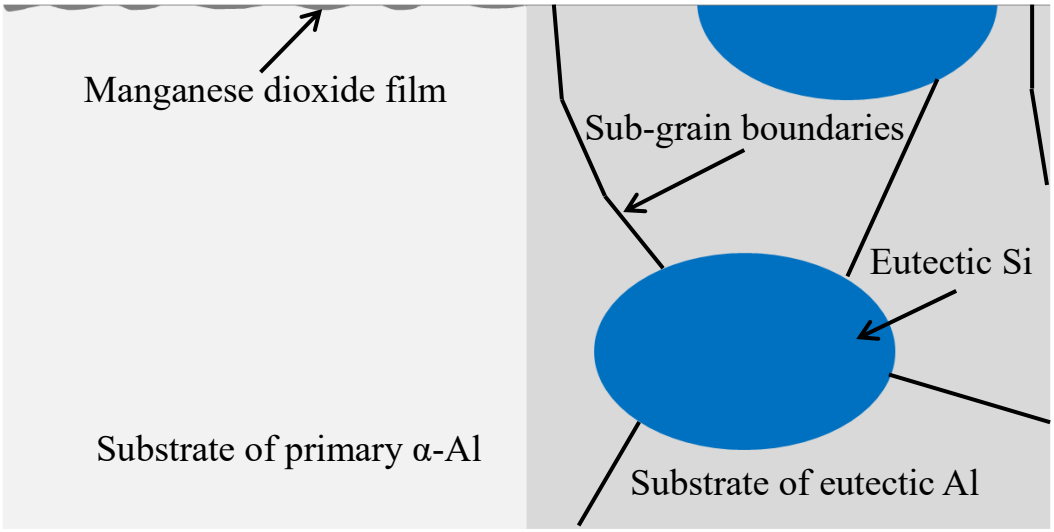


(c)

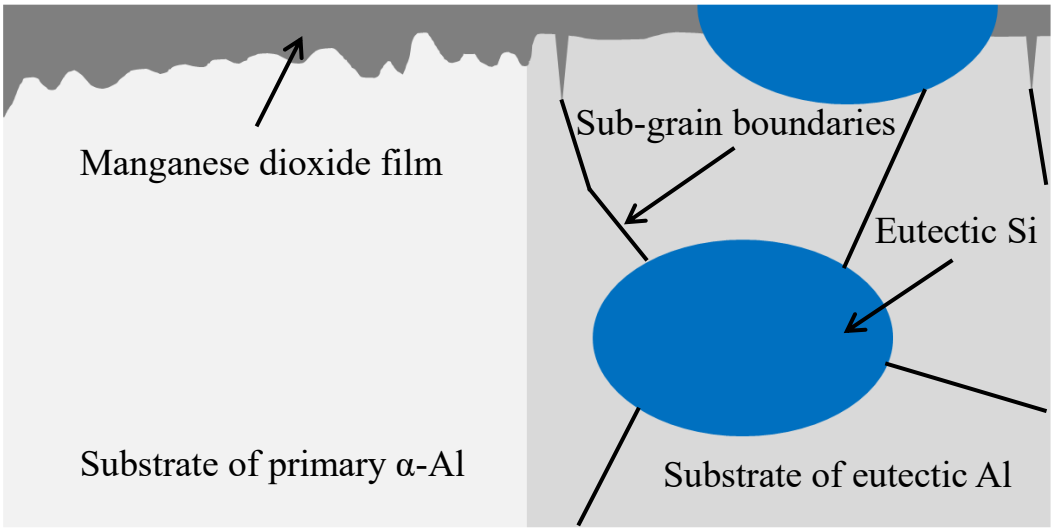


(d)

Continued

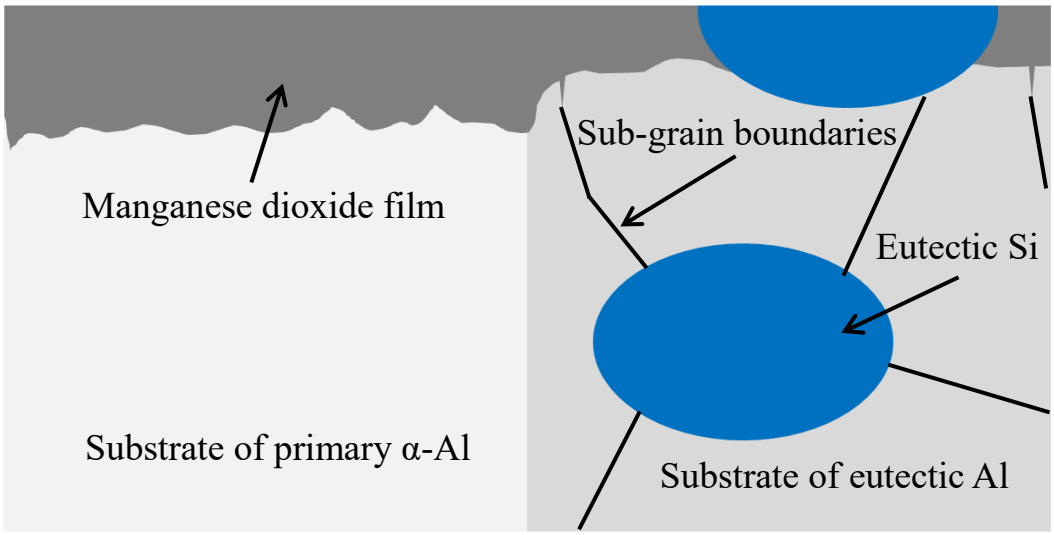


(a)

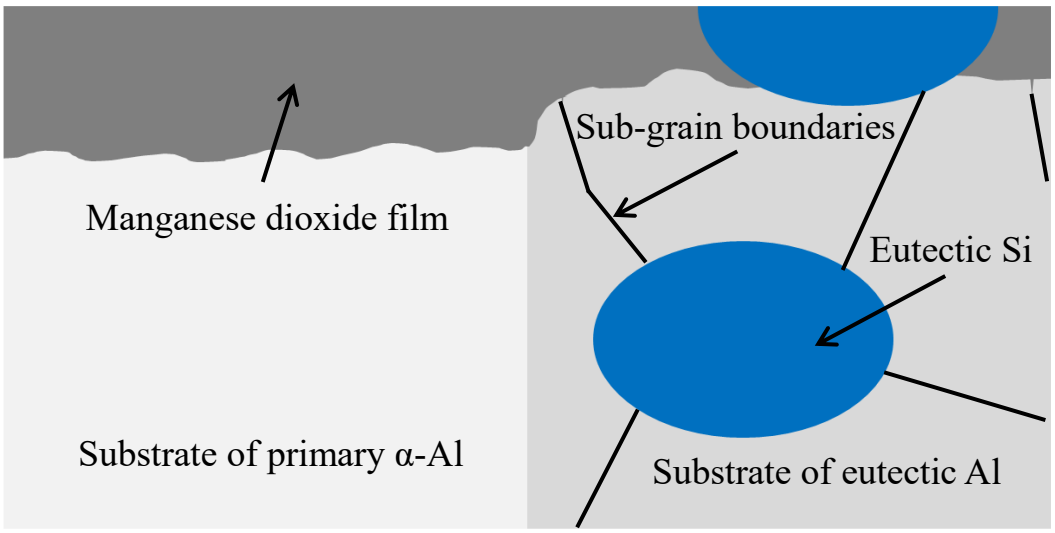


(b)

Fig. 3-16. Schematic illustration showing the cross section of the solution treated specimen etched by Weck's reagent with the solution temperature of (a) 10 °C, (b) 15 °C, (c) 20 °C and (d) 25 °C for 12 s.



(c)



(d)

Continued

Chapter 4

Applicability of Weck's reagent for accurate evaluation of solid fractions with different cooling rates

4.1. Introduction

The semi-solid process is a kind of net-shape manufacturing process, compared with the conventional casting processes using completely melted metal, the semi-solid process offers several advantages to reduce the porosity, such as better mold filling ability (solid-front fill), less air entrapment, and lower solidification shrinkage [1]. This process has two basic methods, rheocasting and thixocasting. In the rheocasting, a feedstock is completely melted and cooled down to the semi-solid temperature and stirred there to obtain the semi-solid slurry [2, 3]. As for thixocasting, the feedstock, which is prepared by rheocasting in advance, is heated up to the target temperature to obtain the semi-solid state [4-7]. It is known that the integrity and performance of components processed by thixocasting are better than those of the components fabricated through rheocasting [8].

A356 alloys with a relatively wide solidification temperature range have been widely used for the thixocasting process. To achieve a good fluidity for semi-solid casting and to control the quality of the product,

the accurate evaluation of the solid fraction is important. The solid fraction can be estimated by the lever rule using a phase diagram. The microstructure observation of the quenched specimen from the semi-solid state is often performed to check the validity of this estimation. However, during water quenching, the growth of the original solid grains, which existed at the semi-solid temperature is inevitable. Therefore, there is no doubt that this leads to an overestimation of the solid fraction. Gao et al. [9, 10] reported that Weck's reagent is applicable to solve this problem. The growth layer formed on the original spheroidal aluminum grains during water quenching was clearly visualized by etching with Weck's reagent, and the precise evaluation of the solid fraction was achieved by image analysis of the etched microstructure. For the conventional solid fraction evaluation method such as quantitative metallography, it has the problem of overestimation due to the grain growth during quenching. Using Weck's reagent to avoid the overestimation can be regard as a modified quantitative metallography. However, the microstructure analysis was performed only for the small size specimens, which were cooled at a fixed cooling rate. As mentioned in the previous chapter, in the semi-solid die-cast process, much larger size billets were used. The growth behavior of the solid layer during water quenching is considered to change depending on the cooling rate. Therefore, in order to confirm the applicability of Weck's reagent for microstructures analysis of the

semi-solid slurry, the effect of the cooling rate should be investigated. In this chapter, A356 alloy slurry specimens with different volumes were quenched from the semi-solid state, and the microstructure change due to the cooling rate difference was investigated.

4.2. Experimental

4.2.1. Material and introduction of pre-plastic strain

The material used in this research is the A356 cast aluminum alloy supplied in cylindrical shape with a diameter of 30 mm and a length of 100 mm as mentioned in the previous chapter. The chemical composition of the alloy obtained by Optical Emission Spectrometer is shown in Table 4-1. Ti and Sr were added to refine the α-Al phase and eutectic phase, respectively.

In order to obtain spheroidal grains, inducing plastic strain by cold compression before recrystallization and partial melting was adopted. The billets were compressed axially by 33% at a room temperature as shown in Fig. 4-1. The cold compression was done by a 500 ton compressing machine, and the compressing rate was 0.2mm/sec. The temperature increase of the billet during compression was about 20 °C.

4.2.2. Fabrication of semi-solid slurry with different volume

Two kinds of specimens with different volume were prepared as shown in Fig. 4-1. One is the as-compressed billet of 175g in weight. The other is a rectangular bar specimen with 20×10×6 mm^3 of 3g in weight, which was collected form the as-compressed billet. They are called “large specimens” and “small specimens”, respectively. In order to measure the temperature of the specimens, a small hole was machined at the side of each specimens and a thermocouple was inserted into the hole as shown in Fig. 4-2. They were put into the electrical furnace and heated to the several kinds of semi-solid temperature (588, 595, 602, and 608 °C), which were corresponded to the solid fraction of approximately 60%, 50%, 40% and 30%. These values were determined by the result of solid fraction evaluation in Gao et al.’s research [9]. The heating rate was about 24 °C/min. When the target temperature was reached, the specimen was isothermally held for 5 min in order to make sure that the specimen was heated homogeneously. After isothermal holding, the specimen was quickly quenched in water, as shown in Fig. 4-3.

Different cooling rates during water quenching were obtained by using different volume specimen. A set of the large (175g) and small specimens (3g) were prepared for the measurement of different cooling rates comes from the different cooling conditions. The thermocouples were set to the center and the surface of the large specimen. The

thermocouple was also set to the center of the small specimen. They were heated to 588°C and isothermally held for 5 min, then rapidly quenched in water. The cooling rates were obtained by the recorded temperature-time curves.

4.2.3. Microstructure observation

A number of small cubic specimens with 8×8×5 mm^3 were collected from the quenched large specimens for the microstructural evaluation. They were ground using 120, 600, 1000, 2000 and 4000 grit paper, polished using 3, 1 μm diamond paste and OPS colloidal silica. They were etched by Weck's reagent for 12 s at 25 °C. The etched specimens were rinsed well and observed by optical microscopy. The same treatment was made for the cross-section of small specimen.

4.2.4. Chemical composition analysis by EPMA

The micro-segregations of Mg, Si and Ti of the quenched specimens were evaluated by EPMA analysis by using X-ray Wavelength Dispersive Spectroscopy (WDS). The location for the chemical analysis was controlled to be the same as the location where the optical micrographs taken by the optical microscopy. The acceleration voltage was set to 15 kV and the electron beam current was set to 185 nA. The solute elements distribution of the quenched specimen was evaluated by the intensities of

characteristic X-rays and the distribution mappings of these solute elements were obtained. Based on the calibration standards, the intensity of each element was converted into atomic percentage and labeled in the distribution mappings.

4.3. Results

4.3.1. Microstructural features of large and small specimens revealed by Weck's reagent

Fig. 4-4 shows optical micrographs of the as-polished and the etched large specimen held at 588°C and water-quenched. The micrographs were taken from the same location. The spheroidal aluminum grains were obtained by the process of compressing, partially re-melting and rapidly cooling. The spheroidal aluminum grains were surrounded by the rapidly solidified eutectic structure, which corresponds to the liquid phase at the semi-solid state. Several round spots are observed in the spheroidal aluminum grain. They consist of very fine eutectic solidified structure, which results from the rapid cooling of the entrapped liquid droplets inside the solid grains at the semi-solid state. Fig. 4-4 (b) shows the microstructure obtained by etching with a conventional reagent of sodium hydroxide solution. The morphology of the spheroidal aluminum grains and the eutectic structure are clearly observable with the help of etching.

However, there is no large difference between Fig. 4-4 (a) and (b). In contrast, as shown in Fig. 4-4 (c), characteristic color differences are visible in the microstructure etched by Weck's reagent. In addition to the complicated color difference inside the spheroidal aluminum grain, a ring-shaped pale color contrast is observed around the spheroidal aluminum grain. It is considered to be the ring-shaped region indicating the grain growth during water quenching. The original liquid region by the water quenching turned to the fine eutectic solidified structure. The eutectic solidified region exhibited a blue color in the picture.

Fig. 4-5 (a) and (b) show the microstructures of the large specimen and the small specimen etched by Weck's reagent, respectively. The ring-shaped layers formed during water quenching can be clearly seen in both specimens. Fig. 4-5 (c) and (d) show highly magnified SEM images of the eutectic solidified region formed by quenching of the remaining liquid. The eutectic structure in the large specimen is much coarser than that of the small specimen. This is due to the lower cooling rate in the large specimen during quenching. It is clear that the thickness of the ring-shaped region surrounding the spheroidal aluminum grain is thicker in the large specimen (Fig. 4-5 (a)) than that of the small specimen (Fig. 4-5 (b)). This fact supports the hypothesis that the ring-shaped area is formed during quenching and the amount of solid growth increases as decreasing the cooling rate.

4.3.2. Chemical analysis of large specimen by EPMA

The origin of the color difference was examined by the EPMA analysis. Fig. 4-6 (a) shows the optical micrograph of the etched specimen. Fig. 4-6 (b) to (d) show the solute distribution in the structure for Mg, Si and Ti, respectively. The attached color bars show the level of composition for each element. High concentration of Mg and Si was observed in the eutectic solidification region, which is located around the spheroidal grains and inside the each spheroidal grain (Fig. 4-6 (b) and (c)).

Segregation of Si and Mg could not be observed inside the spheroidal aluminum grain, except for the entrapped region. The characteristic solute distribution patterns were observed for Ti, as shown in Fig. 4-6 (d). The first is the heavy segregation at the center of the spheroidal aluminum grain. The second is the ring-shaped segregation pattern surrounding the spheroidal aluminum grain.

4.4. Discussion

4.4.1. Micro-segregation and grain growth in large specimen during water quenching

From the result of microstructure observation by optical microscope and the chemical analysis by EPMA, the characteristics of the

micro-segregation in large specimen could be summarized as follow.

The first pattern of the characteristic solute distribution results from the original segregation of Ti in the dendrite structure of the cast billet. As reported in Gao et al.'s research [9, 10], the heavy segregation of Ti in the dendrite branches remain even after the holding at the semi-solid temperature. This is due to the low diffusion rate of Ti in Al at this temperature compared to those of Si and Mg [11-15]. Therefore, even though Si and Mg are homogenized enough in the spheroidal aluminum grain, the core structure of Ti can be preserved like this.

The second pattern is probably due to the normal segregation of Ti corresponding to the phase diagram of Al-Ti system. The partition coefficient of Ti in Al is larger than 1. This means that the concentration of Ti should be high at the start of solidification and then gradually decreases as in the solidification progresses. Comparing Fig. 4-6 (a) and (d), the solute distribution of Ti from the inside to the outside of the ring-shaped region is consistent with this segregation pattern. This fact also supports the hypothesis that the ring-shaped region results from the solid growth during water quenching from the original spheroidal aluminum grain surface.

4.4.2. Correct evaluation of solid fraction at semi-solid state

The correct evaluation of solid fraction is important because it controls the fluidity of semi-solid slurry and affects to the mold-filling ability. In Gao et al.'s research [9], the solid fraction measurement for the quenched small specimens was performed with the help of Weck's reagent. As mentioned in the previous paragraphs, etched by using Weck's reagent can visualize the spheroidal grain growth during water quenching. This ability helps us to evaluate the solid fraction by using the optical micrography. The grain growth area of large specimen was confirmed in this research. The evaluation of solid fraction at semi-solid state of both large and small specimen was carried out.

Fig. 4-7 (a) shows an example of the microstructure of the quenched semi-solid slurry. The specimen was etched with sodium hydroxide solution. The spheroidal grains were distinguishable from the matrix, which were the quenched of residual liquid at the semi-solid state. In this case, the solid fraction evaluated by conventional metallography etching method $f_{s(NaOH)}$ can be evaluated by the following equation:

$$f_{s(NaOH)} = \frac{\sum A}{S}$$

where, $(NaOH)$ of the $f_{s(NaOH)}$ means the value obtained by the conventional metallography etching method by using sodium hydroxide solution as the etching reagent. A represents the area of each spheroidal aluminum grain, $\sum A$ is the total sum, and S represents the total area of

the image for analysis. Note that A should include the solid growth around the original spheroidal grain during quenching. In contrast, in the picture of microstructure etched with Weck's reagent, a ring-shaped area was clearly visualized around each spheroidal aluminum grain, as shown in Fig. 4-7 (b). As mentioned in the previous session, the ring-shaped area results from the solid growth during water quenching from the original spheroidal aluminum grain surface (A_q). Therefore, the original solid phase before the solid growth during water quenching (A_0), can be represented as $A_0 = A - A_q$. These areas are shown in yellow in Fig. 4-7 (c). The solid fraction evaluated by using color metallography etching method $f_{s(Weck)}$ can be expressed by the following equation:

$$f_{s(Weck)} = \frac{\sum A_0}{S}$$

where, $(Weck)$ of the $f_{s(Weck)}$ means the value obtained by the color metallography etching method by using Weck's reagent as the etching reagent. In some cases, α-Al dendrites also formed with eutectic Al-Si phase during quenching. However, they are much smaller compared to the spheroidal aluminum grains, and so they are easily distinguishable.

In this research, the solid fraction of both quenched small specimens and large specimens were evaluated with the help of Weck's reagent. For the small specimen, 6 micrographs with 100x magnification (with an area of about 2 mm^2) were taken from the cross-section of the quenched specimen. For the large specimen, 5 cubic specimens (8×8×5 mm^3) were

collected from the quenched large specimen. 4 micrographs with 100x magnification (with an area of about 2 mm^2) were taken from each of them, and provided for evaluation. The solid fraction $f_{s(NaOH)}$ and $f_{s(Weck)}$ were evaluated by using the NaOH-etched and Weck's reagent-etched specimen, respectively.

Fig. 4-8 (a) shows the relationship between $f_{s(NaOH)}$ and holding temperature for the small and large specimen. The results obtained by the previous study are also included. A solid curve is shown in the figure. This is the estimated change of solid fraction of Al-7%Si alloy obtained by using the Al-Si binary phase diagram. The chemical composition of A356 alloy is comparable to that of Al-7%Si binary alloy. Both $f_{s(NaOH)}$ curves for the small and large specimens show a large deviation from the estimated values. It is also found that $f_{s(NaOH)}$ of the large specimen is higher than that of the small specimen.

Fig. 4-8 (b) shows the relationship between $f_{s(Weck)}$ and holding temperature for the small and large specimen. In this case, $f_{s(Weck)}$ of the small specimen and that of large specimen are almost the same. In addition, these curves are close to the solid fraction estimated from the phase diagram. These results suggest that $f_{s(Weck)}$ represents the solid fraction at the semi-solid state of each holding temperature. Therefore, it is confirmed that the removal of A_q, resulting from the solid growth during quenching, is reasonable to evaluate the solid fraction correctly,

and the color metallography by using Weck's reagent is effective.

4.4.3. Effect of cooling rates on the amount of solid growth during quenching

The cooling rate during quenching of the large specimen was about 520 °C/s at the central part, and about 730 °C/s at the top surface. It was about 1400 °C/s for the small specimen.

The precise microstructure analysis was performed for the specimens collected from the different parts of the large specimen, and the amount of solid growth during water quenching was compared. The amount of solid growth during water quenching was evaluated by using the following parameter:

$$\Delta q = \frac{A_q}{A_0} = \frac{A - A_0}{A_0}$$

This parameter refers to the relative contribution of solid growth during quenching to the original spheroidal grain. A slight difference in solid fraction was observed from location to location. In addition, the amount of solid growth during water quenching (Δq) was also different from location to location as shown in Fig. 4-9. The local solid fraction $f_{s(local)}$ is the solid fraction only in a small visual field (one 200x magnification micrographs with an area of about 0.5 mm^2). The evaluations of the solid fraction of small specimen (average of 6 micrographs with 100x magnification micrographs) and large specimen (average of 20

micrographs with 100x magnification micrographs) were considered about 1800 grains and 6000 grains, respectively, the evaluation of local solid fraction only considered about 75 grains. It was evaluated by color metallography etching method by using Weck's reagent as the etching reagent.

Fig. 4-10 shows the relationship between Δq and the local solid fraction for three different cooling rate conditions. Δq decreases for an increasing local solid fraction for all the cooling rate conditions. This result also shows that the amount of solid growth is controlled by the local cooling rate, which corresponds to the amount of residual liquid before quenching. The thermal conductivity of solid is higher than that of liquid, which means the local cooling rate decreases for an increasing amount of residual liquid. With decreasing the amount of residual liquid, the amount of solid growth around the spheroidal aluminum grain during water quenching was considered to be reduced. In addition, the larger amount of residual liquid also results in a larger mutual distance between the spheroidal aluminum grains and provided more space for solid growth during water quenching. Therefore, the amount of solid growth is probably controlled by the amount of residual liquid before quenching.

4.5. Conclusions

In this chapter, the applicability of Weck's reagent for accurate evaluation of solid fractions with different cooling rates was focused. Semi-solid processed specimens with different cooling rates were etched by Weck's reagent to visualize the grain growth during water quenching.

The semi-solid slurry of A356 alloy with different volume of various solid fractions were fabricated and water quenched to freeze the morphology of the aluminum grain in the semi-solid state. Optical microstructure observation was carried out by using Weck's reagent to visualize the inner microstructure of spheroidal aluminum grains, with a focus on the solid growth during water quenching of each spheroidal aluminum grain. A ring-shaped pale color contrast region was observed around the spheroidal aluminum grain, and this region corresponded to the solid growth during water quenching from the original spheroidal aluminum grain surface. The amount of solid growth during quenching Δq, increased as decreasing the cooling rate. It was found that Δq of each spheroidal aluminum grain also increased when the local solid fraction decreased.

These results suggest that the present color metallography is effective for the correct evaluation of solid fraction of the A356 alloy slurry. Comparing with in-situ observation technique, the present color

metallography method is time saving and economical. Furthermore, this color etching method can be applied to both equilibrium and unequilibrium state without influence of the experiment conditions.

References

[1] M.C. Flemings, Behavior of metal alloys in the semisolid state, Metall Trans A. 22A (1991) 957-981

[2] S. Lü, S. Wu, C. Lin, Z. Hu and P. An, Preparation and rheocasting of semisolid slurry of 5083 Al alloy with indirect ultrasonic vibration process, Mater Sci Eng A. 528 (2011) 8635-8640.

[3] I.G. Chung, A. Bolouri and C.G. Kang, A study on semisolid processing of A356 aluminum alloy through vacuum-assisted electromagnetic stirring, Int J Adv Manuf Tech. 58 (2012) 237-245.

[4] A. Bolouri, M. Shahmiri and C.G. Kang, Coarsening of equiaxed microstructure in the semisolid state of aluminum 7075 alloy through SIMA processing, J Mater Sci. 47 (2012) 3544-3553.

[5] Y. Birol, Thixoforming of EN AW-2014 alloy at high solid fraction, J Mater Proc Technol. 211 (2011) 1749-1756.

[6] G. Yan, S. Zhao, S. Ma and H. Shou, Microstructural evolution of A356. 2 alloy prepared by the SIMA process, Mater Charact. 69 (2012) 45-51.

[7] H.V. Atkinson, K. Burke and G. Vaneetveld, Recrystallisation in the semi-solid state in 7075 aluminium alloy, Mater Sci Eng A. 490 (2008) 266-276.

[8] Z. Fan, X. Fang and S. Ji, Microstructure and mechanical properties

of rheo-diecast (RDC) aluminium alloys, Mater Sci Eng A. 412 (2005) 298–306.

[9] L. Gao, Y. Harada, S. Kumai, Microstructural characterization of aluminum alloys using Weck's reagent, part I: Applications, Mater Charact. 107 (2015) 426-433.

[10] L. Gao, Y. Harada, S. Kumai, Microstructural characterization of aluminum alloys using Weck's reagent, part II: Coloring mechanism, Mater Charact. 107 (2015) 434-452.

[11] D.H. Kirkwood, C.M. Sellars and L.G. Elias-Boyed: European Patent 0305375, B1 (1992).

[12] S. Fujikawa and K. Hirano, Diffusion of /sup 28/Mg in aluminium, Mater Sci Eng. 27 (1977) 25-33.

[13] W.B. Alexander and L.M. Slifkin, Diffusion of solutes in aluminium and dilute aluminium alloys, Phys Rev B. 1 (1970) 3274-3282.

[14] D. Bergner, Diffusion von fremdelementen in aluminium, Neue Hütte. 29 (1984) 207-210.

[15] D.H. St John and L.M. Hogan, Thermal stability in the Al-Al 3 Ti system, J Mater Sci. 15 (1980) 2369-2375.

Table 4-1 Chemical compositions of A356 alloy used in this chapter (mass%).

Si	Mg	Fe	Ti	Sr	Mn	Al
6.90	0.39	0.10	0.14	0.025	<0.10	Bal.

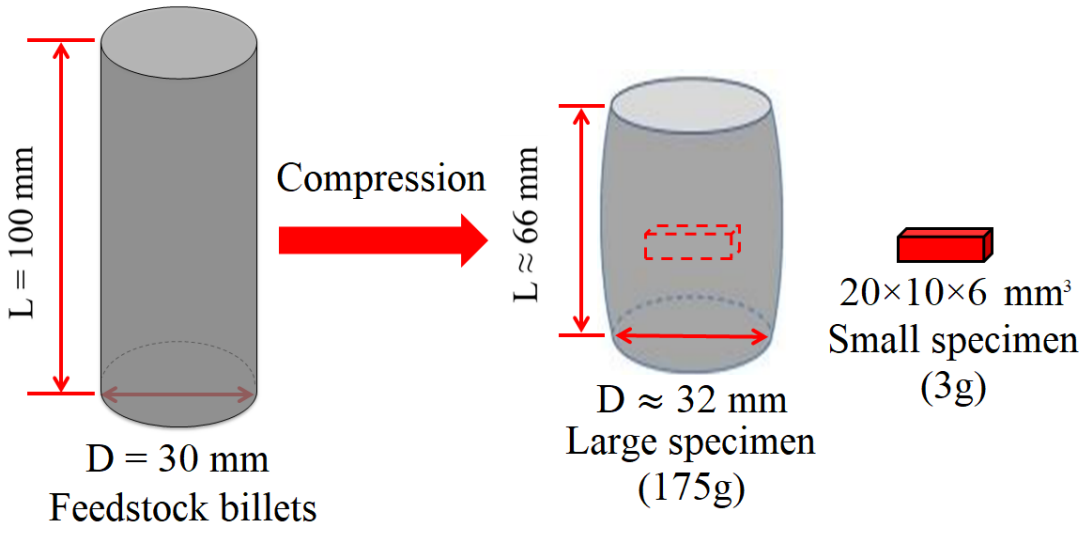


Fig. 4-1. Definition of large specimen and small specimen used in this chapter.

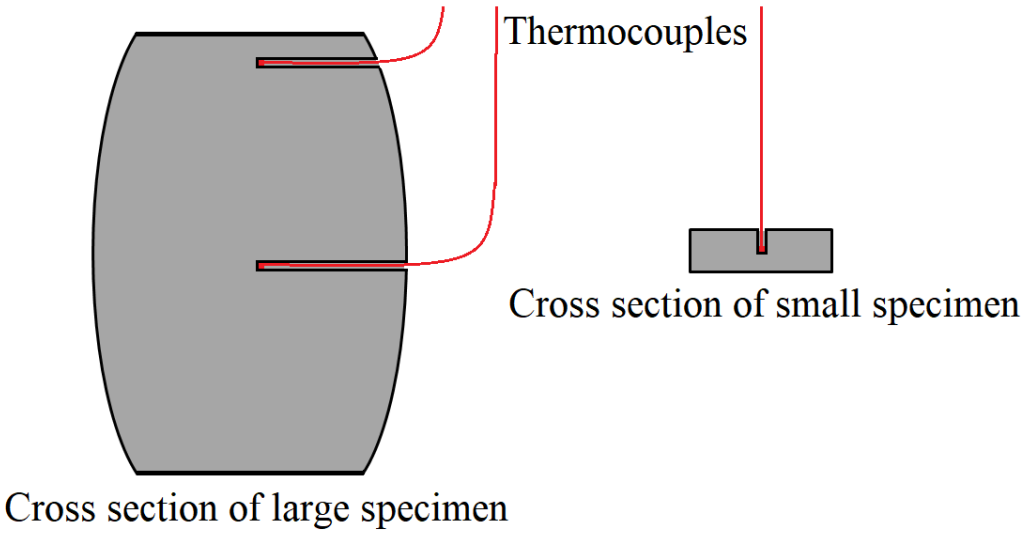


Fig. 4-2. Schematic of thermocouples insert in the specimens in in this chapter.

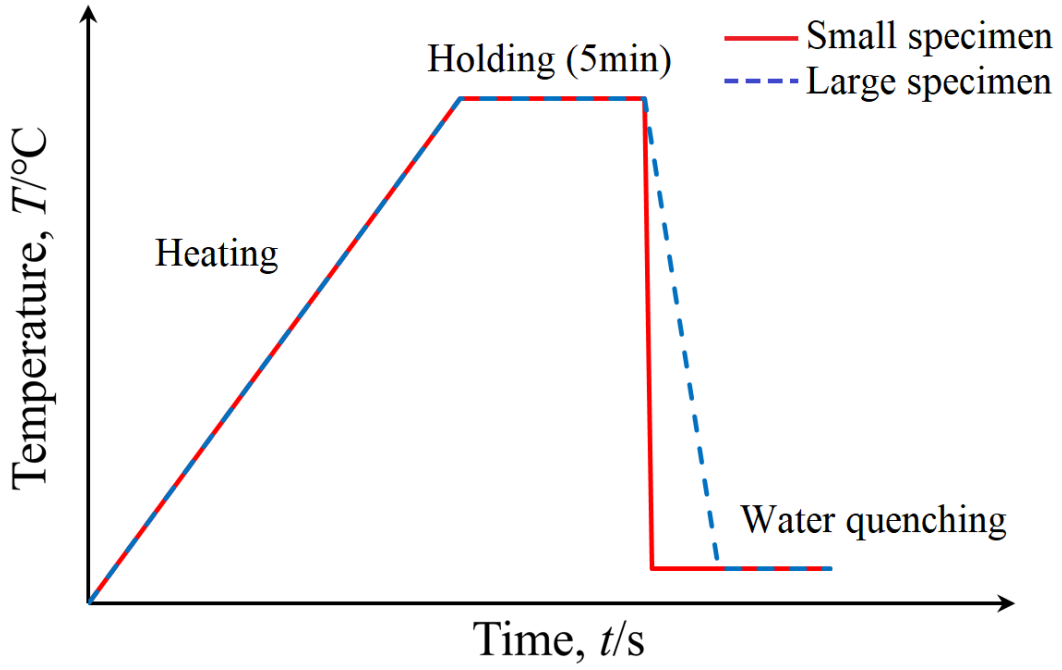
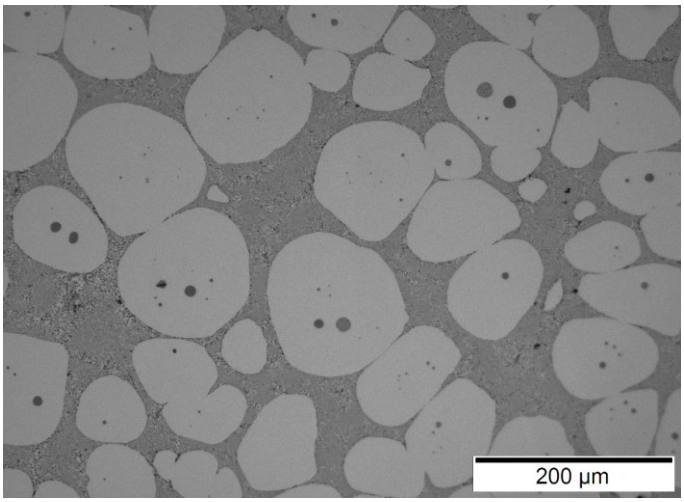
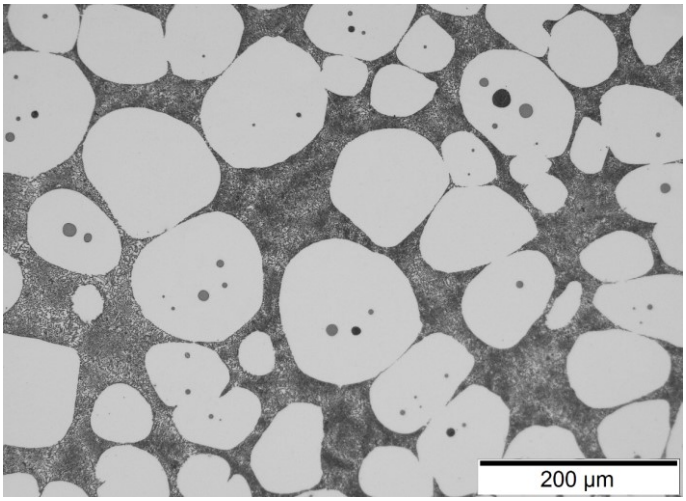


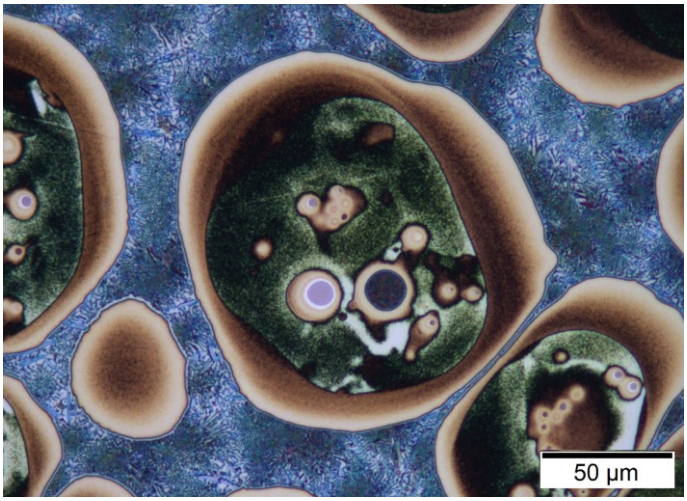
Fig. 4-3. Schematic temperature-time curve for heating, holding and cooling process in this chapter.



(a)



(b)



(c)

Fig. 4-4. Microstructure of the quenched large specimen from 588°C (a) as-cast (b) etched by NaOH and (c) etched by Weck's reagent.

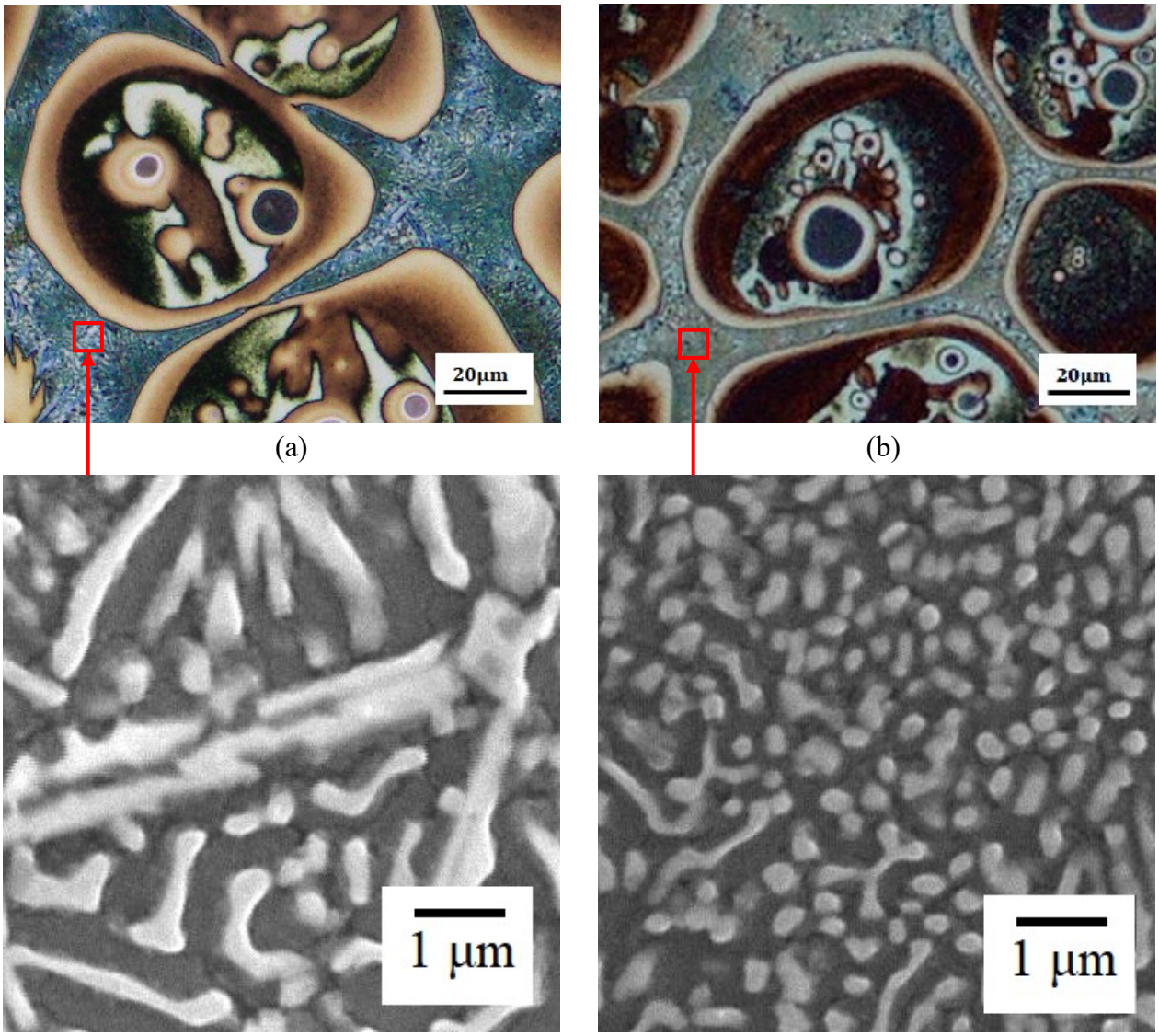


Fig. 4-5. (a) and (b): Optical micrographs of the etched microstructure by Weck's reagent of the quenched large specimen and small specimen from 588°C. (c) and (d): SEM image of the quenched liquid region showing the eutectic solidified structure.

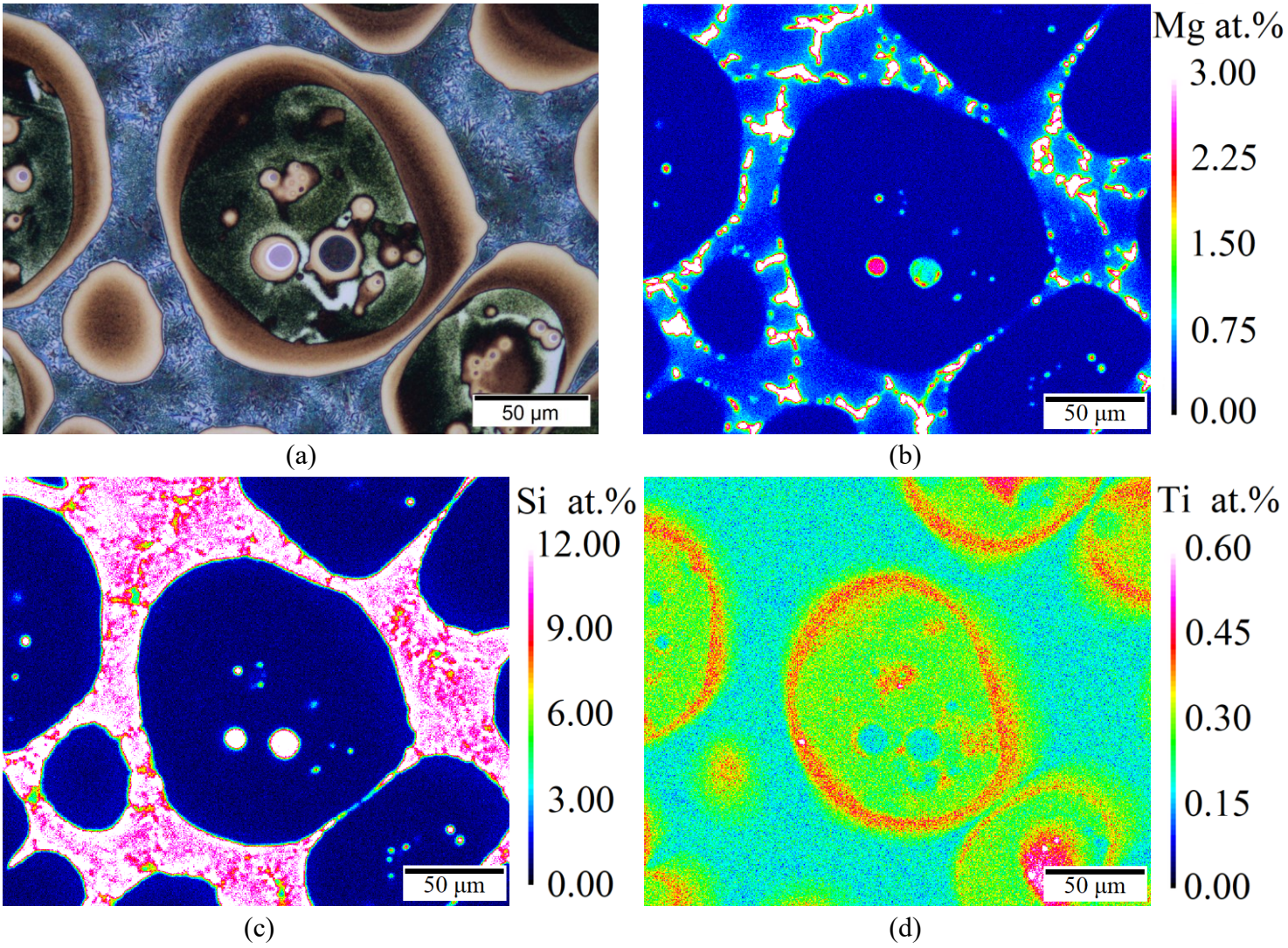
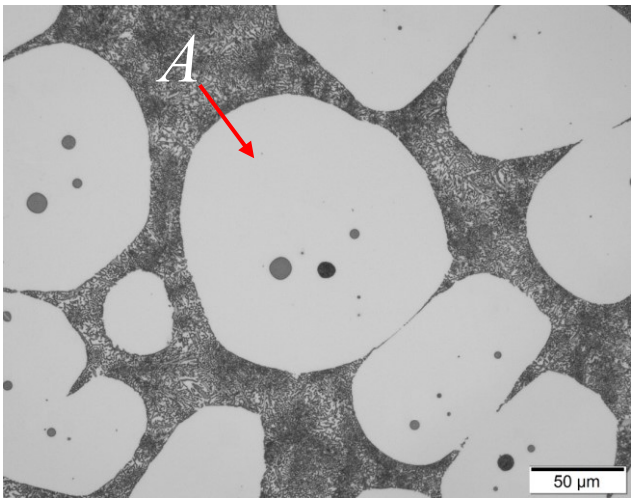
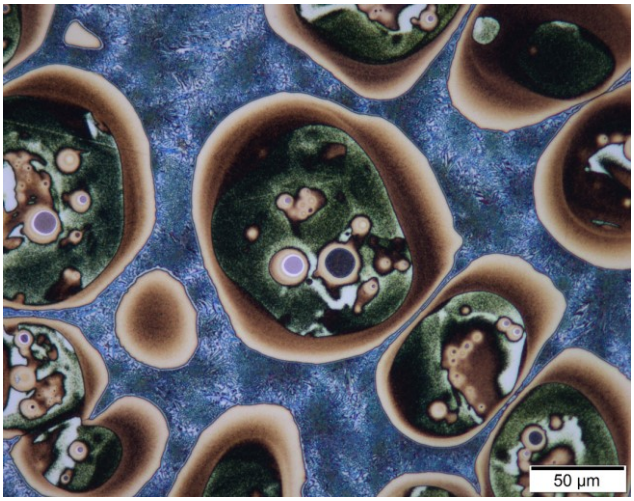


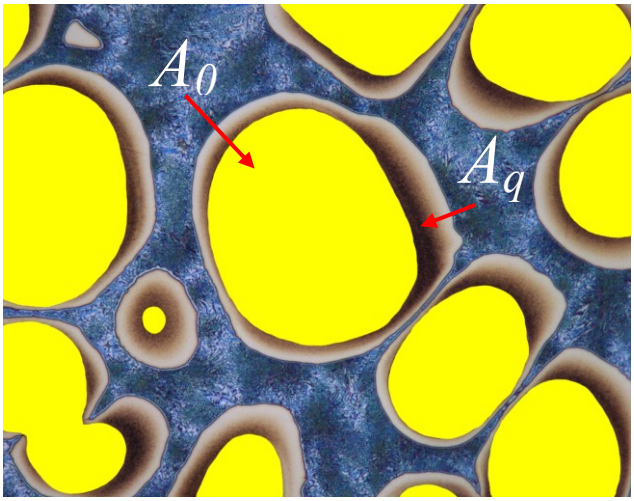
Fig. 4-6. Optical micrograph of the specimen etched by Weck's reagent (a) and results of EPMA analysis, (b) Mg, (c) Si, (d) Ti.



(a)

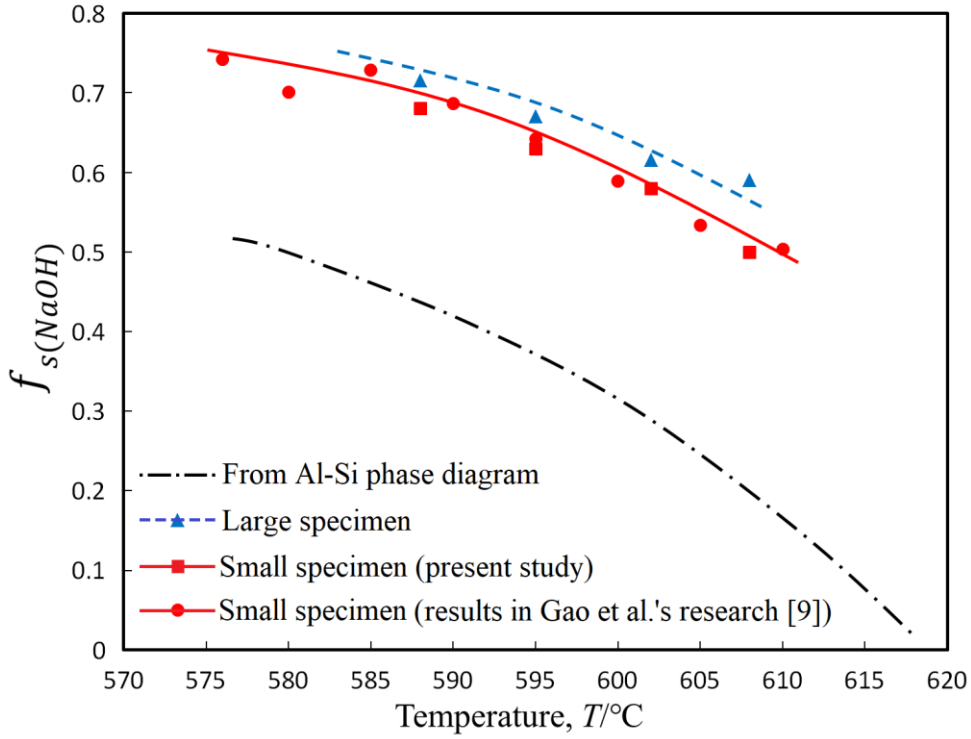


(b)

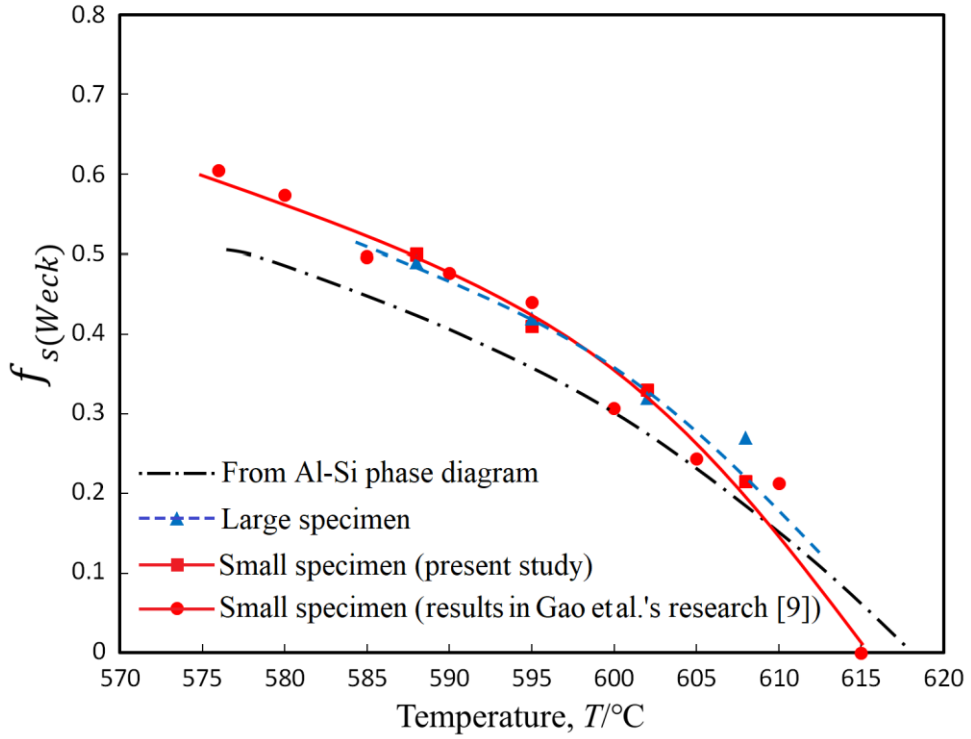


(c)

Fig. 4-7. Microstructures of the large specimen hold at and quenched from 588°C (a) etched by NaOH, A: the area of solid, (b) etched by Weck's reagent, (c) the original solid phase eliminating solid growth during water quenching, A consists of A_0 (original solid area) and A_q (solid growth during water quenching).

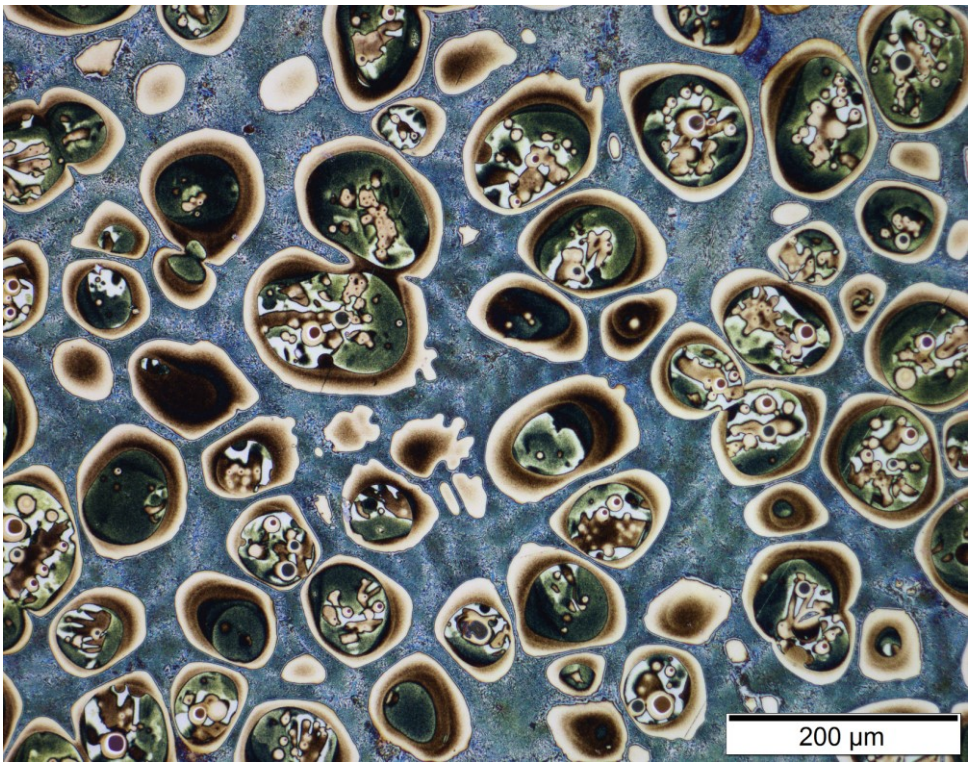


(a)

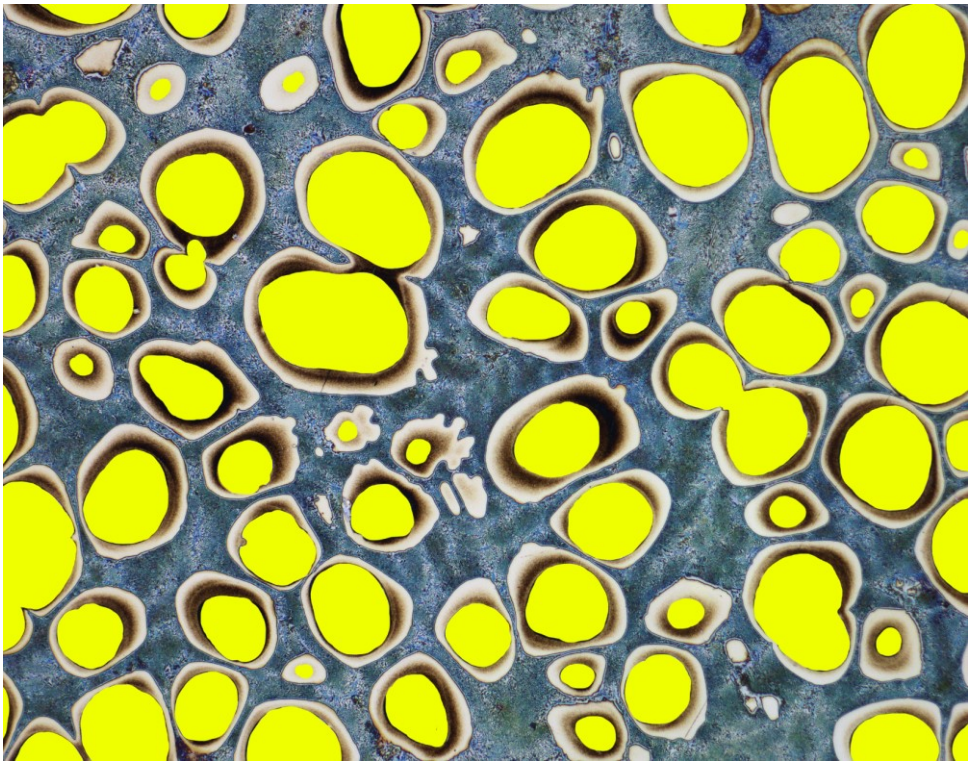


(b)

Fig. 4-8. Solid fraction evaluated by using two methods. (a) Conventional metallography etching method by using NaOH water solution. (b) Color metallography etching method by using Weck's reagent.

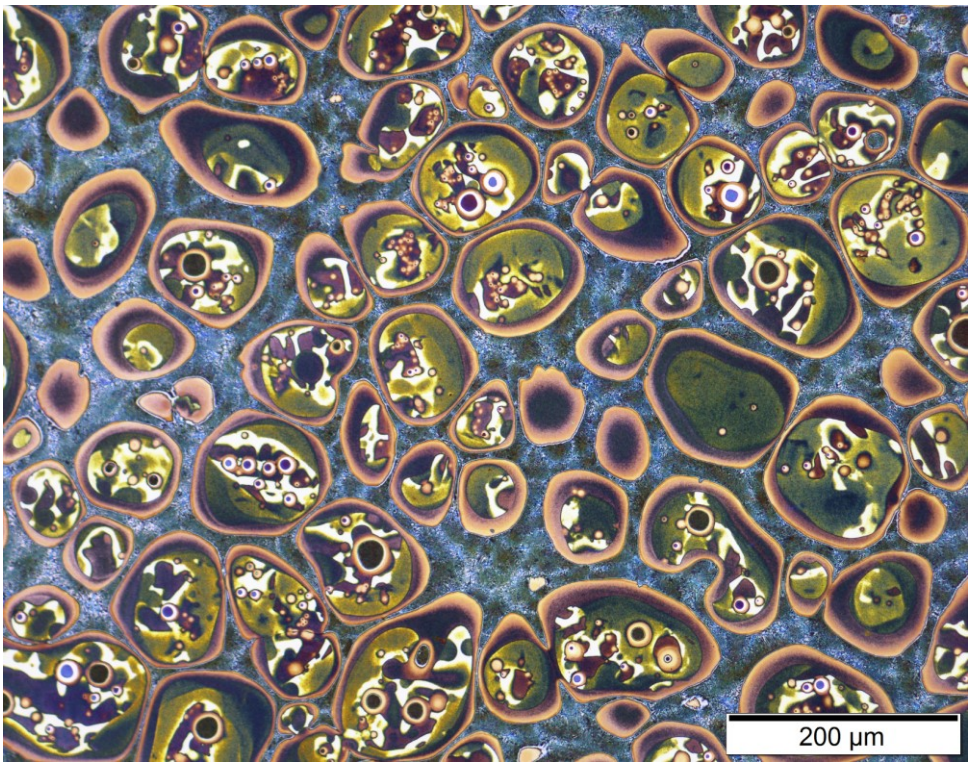


(a)

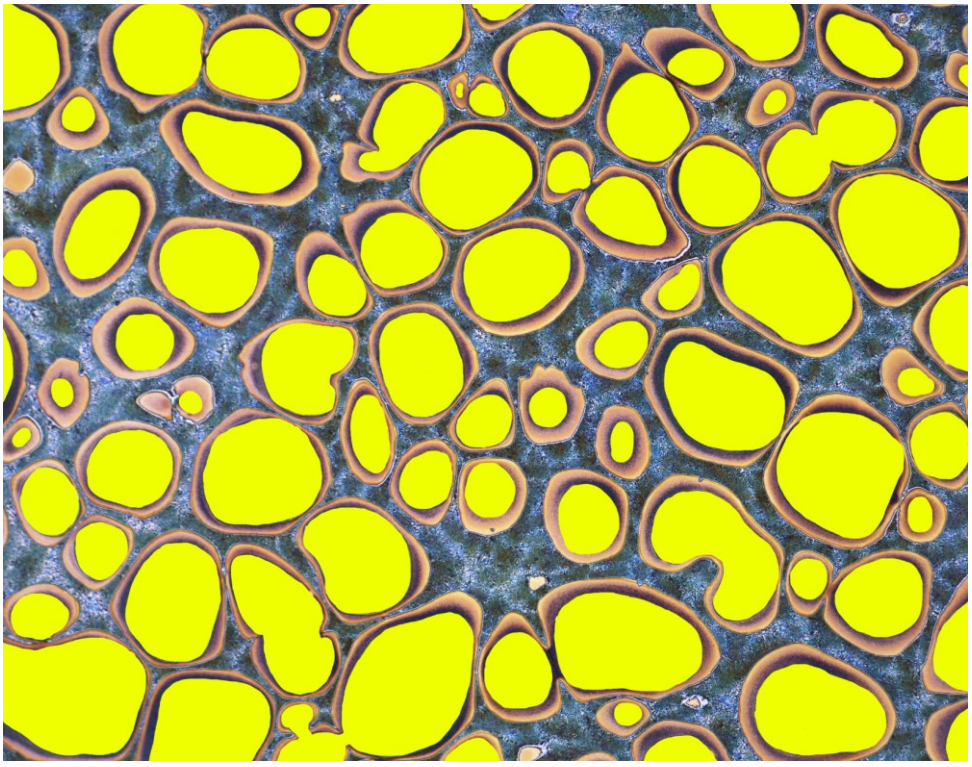


(b)

Fig. 4-9. The optical micrograph of the quenched specimens and the painted area representing the original solid phase before quenching. (a) and (b): The location with lower local solid fraction (about 35%). (c) and (d): The location with higher local solid fraction (about 50%).



(c)



(d)

Continued

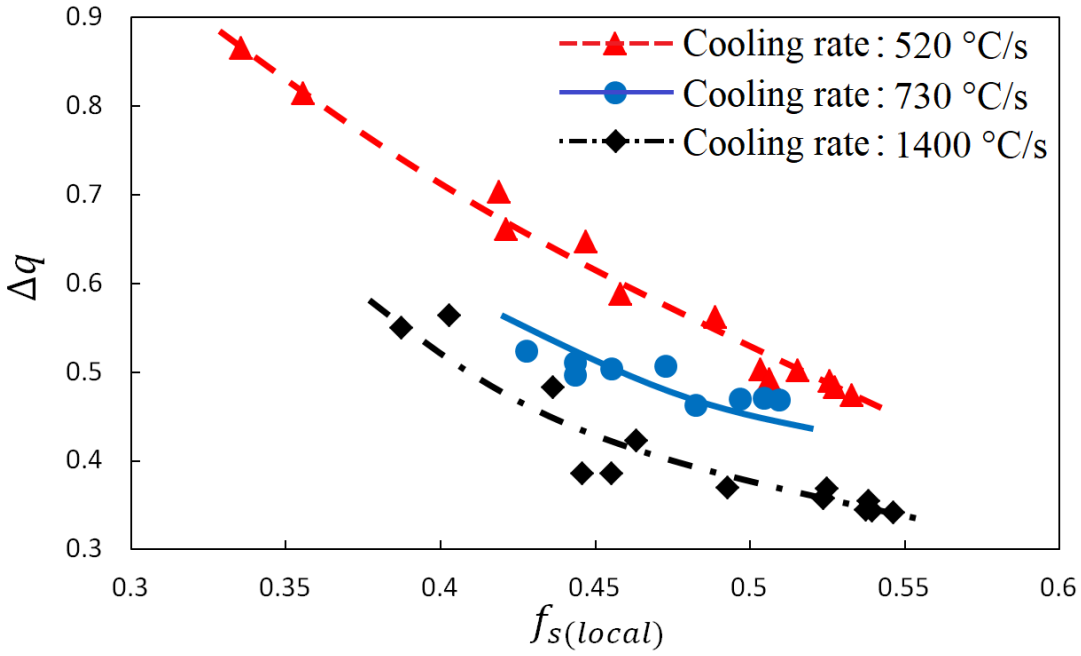


Fig. 4-10. Quantitative analysis result of the amount of grain growth during water quenching, Δq, under the different local solid fractions.

Chapter 5

Summary and general conclusions

The present thesis is entitled “Microstructure analysis of A356 aluminum alloy by color metallography using Weck’s reagent”. This research was carried out to investigate the unsolved subjects in this research field and establish the color metallography by using Weck’s reagent as a useful tool for microstructure analysis of semi-solid processed A356 aluminum alloy.

In Chapter 1, the background of color metallography was briefly reviewed and the etchant called Weck’s reagent was introduced. The recent research concerning the applications and coloring mechanism of Weck’s reagent were explained. Serval subjects which were still left unsolved in this research field were shown, and the purpose of this study was discussed.

In Chapter 2, the color etching behavior of semi-solid die-cast A356 aluminum alloy by using Weck’s reagent was examined. The etching behavior of the eutectic solidified region was intensively investigated. Various characterization methods were applied to understand more about the manganese dioxide film formed during etching process in terms of the

topography of interface between manganese dioxide film and substrate.

Aluminum and silicon in the eutectic solidified region exhibited different color in as-cast condition. SEI observation found that they exhibited different height. The cross-sectional observation and compositional analysis by using STEM and EDS revealed that only aluminum matrix reacted with Weck's reagent and the film was formed by the conversion coating mechanism proposed by Gao et al. No film formation was observed on the silicon phase. Difference in color contrast is considered to depend on the lamellar morphology of the eutectic solidified region. Therefore, the morphological change of silicon phase in the eutectic solidified region, from needle-like morphology to spheroidal morphology, caused the change in color contrast in the solution-treated condition.

A peculiar network structure was observed in solution-treated condition. Cross-sectional observation of the film revealed that the peculiar network morphology may result from local morphological change of the film tracing the boundaries or sub-boundaries of the recrystallized grains due to the solution treatment.

In Chapter 3, the influence of etching conditions on the color contrast revealed by Weck's reagent was examined. As-cast and solution-treated specimens were etched by Weck's reagent with different

etching conditions and the change in surface topography of the etched specimens was also characterized by SEI observation. The color contrast revealed by Weck's reagent was very sensitive to both etching time and etchant temperature. The as-cast specimen was etched at 15 to 30 °C for 8 to 16 s. The best color contrast was the etching time of 12 s and the etchant temperature of 25 °C. The solution-treated specimen was etched at 10 to 25 °C for 12 s. The best etching condition to obtain the best color contrast was the etching time of 12 s and the etchant temperature of 15 °C.

The surface topography is in strong correlation with the color difference revealed by Weck's reagent. This means that the morphology of the manganese dioxide film formed during etching corresponds to the etching depth and roughness of the etched aluminum substrate.

The best coloring condition changes depending on the micro-segregation in the aluminum substrate since the thickness and morphology of the manganese dioxide film are controlled by the local distribution of the solute elements.

In Chapter 4, the applicability of Weck's reagent for accurate evaluation of solid fractions with different cooling rates was focused. Semi-solid processed specimens with different cooling rates were etched by Weck's reagent to visualize the grain growth during water quenching.

The semi-solid slurry of A356 alloy with different volume of various solid fractions were fabricated and water quenched to freeze the morphology of the Al grain in the semi-solid state. Optical microstructure observation was carried out by using Weck's reagent to visualize the inner microstructure of spheroidal aluminum grains, with a focus on the solid growth during water quenching of each spheroidal aluminum grain.

A ring-shaped pale color contrast region was observed around the spheroidal aluminum grain, and this region corresponded to the solid growth during water quenching from the original spheroidal aluminum grain surface. The amount of solid growth during quenching Δq, increased as decreasing the cooling rate. It was found that Δq of each spheroidal aluminum grain also increased when the local solid fraction decreased. These results suggest that the present color metallography is effective for the correct evaluation of solid fraction of the A356 alloy slurry.

Color metallography using Weck's reagent has been known for about 35 years. However, the understanding of this color etching method was not enough, and the application of this method was very limited, either. However, resently, Gao et al. studied the coloring mechanism of Weck's reagent and demonstrated serval applications in the microstructure analysis of A356 aluminum alloy. In the present study,

serval critical subjects left untouched by Gao et al. were taken up as the research targets, and a series of studies were carried out to understand the etching behavior of Weck's reagent more deeply and confirm the applicability of this etching method for color metallography of A356 aluminum alloy. The influence of etching conditions on the color contrast was investigated and the most suitable etching condition was proposed. In addition, the applicability of color etching by Weck's reagent was confirmed for accurate evaluation of solid fraction in the semi-solid processed A356 aluminum alloy.

Acknowledgements

First and foremost, I would like to express my deepest appreciation to my advisor Professor Dr. Shinji Kumai. I would like to thank you for your consideration and generous help for my whole overseas career in Japan. It is my pleasure to study in your laboratory and I enjoyed it very much. You taught me to think and find novel point by myself, and you have always helped me to solve the issues that I met. I am especially grateful for your help with my research.

Then, I would like to thank Associate Professor Dr. Shinji Muraishi, who has been dedicated to our laboratory and has always helped me deal with many formalities to study in Japan. Please allow me to give the special thanks to you.

Also, my sincere appreciation also goes to Assistant Professor Dr. Yohei Harada. You have guided me through most of the usage of experimental instruments in my research. We always discussed about my research contents and we conducted a lot of experiments together. In addition, you always supervise and urge my research, for which I would like to express my deepest gratitude to you.

All my lab mates have given me great help. I would like thank all of you. Mr. Rui Li offered his selfless support for living in Japan, you are my best coordinator. Mr. Li Gao, Mr. Junto Nishiwaki, Mr. Yusuke

Takayama and Mr. Kamolwat Prapasajchavet as my seniors had assisted me a lot with the learning and experimental methods. Mr. Shingo Kimura helped me a lot with my experiments. I really appreciate all the things you have done for me.

Not only people in my laboratory, but also students from other laboratory showed me a lot of support. Mr. Yuanru Yang and Mr. Xuanliang Chen helped me a lot both in life and research. We always discussed academic problems together and faced the difficulties in life together. You are my best friends in Japan.

Finally, I would like to deeply thank my parents for supporting me these years. When I was confused, you were always enlightening me. When I was lost, you always encouraged me. You always support me unconditionally. I would like to dedicate this work to you.

雷斯敏

2021.8.24